The effects of different control methods on human biomechanics during exoskeleton walking

Master Thesis

By

Willem Friso de Boer

In partial fulfilment of the requirements for the degree of

Master of Science
Mechanical Engineering

at Delft University of Technology,
to be defended on Friday October 20, 2017 at 12:00

Student number:	1521721
Supervisor & chairman:	Prof. dr. ir. H. van der Kooij
Thesis committee:	ir. K.E. Rodriguez Hernandez
	Prof. dr. I. Horvath

TU Delft

Acknowledgement

Graduation was a long journey for me. It all started around two years ago after I finished my last exams. During my internship earlier that year at the Biorobotics institute in Pontedera, Italy, I learned about soft robotics, a technology that is still in its infancy. Intrigued by the applications and advantages of soft robotics I wanted use the knowledge I gained to develop a soft exoskeleton and why not do it as a graduation project? This led me to Prof. Dr. Ir. Herman van der Kooij, who is specialized in exoskeletons, among other things. During my literature study I found that my first idea, designing and building a soft exoskeleton, was too ambitious given the complexity of such a device. I struggled to come up with a new assignment, but eventually, after some months, I ended up at the University of Twente, where I could use the Achilles exoskeleton to study the effects of different control methods on human subjects. I would like to thank Herman for this opportunity and for bringing me into contact with the right people in Enschede.

During my time in Enschede I got a ton of help while preparing and conducting my experiments from students and staff of the department of biomechanical engineering. I would first like to thank all fellow students who offered me a workplace at their student room, even though I was officially not allowed, since I was not registered as a student of UT. I had a great time there, lots of laughs during the lunches and coffee breaks. A special thanks to Marjolein de Lange for volunteering many hours in the lab during my pilot studies. Furthermore I would like to thank Annerieke Nijman, Simone Fricke and Gijs van Oort, who showed me around the lab, explained how to use all equipment and were available when I encountered problems during my experiments. A big thank you to all volunteers who participated in my experiments, most of whom were fellow students and some of them even refusing to quit the experiment while they developed blisters on their feet, without them there would not be any results. A huge thanks to Mark Vlutters as well, for providing code and video instructions to process most of my data and getting started with OpenSim. Not having to write all this code saved me weeks or even months, though it still took me a lot of time to process all data and perform the simulations, which I underestimated. From the people in Enschede I would lastly thank assistant professor Edwin van Asseldonk for his advice via email, skype conversations and during the bi-weekly meetings.

Besides the direct help I got in Enschede, I also received indirect support. First and foremost I would like to thank my wife Sanne, who was still my fiancée when I started all this. Back then I promised her to graduate before the wedding and I would like to apologize to her for not making this deadline and for not always focusing on my graduation. Luckily the wedding was still a success and I was able to set aside the work I still had to do on that special day and during the honeymoon that followed. This acknowledgement is not complete without thanking my parents, they will always be there if I need them for anything and they have worked tirelessly at their company and at home to ensure a carefree youth for me and my sisters, I can still learn a thing or two from their work ethic. They have shaped me during my younger years and supported me financially throughout my life and it is now finally time for me, as their third and final child to complete higher education, to find a job and be fully independent of them.

Abstract

Ever since human ancestors picked up rocks and used them as tools, technology has enhanced human capabilities. Over the last decades more and more research has been done in trying to enhance strength and endurance by means of an exoskeleton. Reducing the metabolic cost of human walking using lower extremity exoskeletons is one of the challenges that has been taken on by several research groups. Only recently have some of these groups managed to reduce the metabolic cost of walking with the help of an exoskeleton. Understanding how human walking behavior changes and adapts to these new supportive devices is crucial in the quest to better, more efficient exoskeletons. Effects of two control methods, that were proven to be successful in making human walking more energy efficient, on the biomechanics of human subjects were examined by performing lab experiments and using the collected experimental data to run musculoskeletal simulations to compute muscle mechanics and energetics of six lower extremity muscles. Lab experiments, which were completed by eight out of ten recruited subjects, consisted of treadmill walking with and without the exoskeleton, while EMG, respiratory, kinematic and kinetic data was recorded. Processing of this data, the simulation steps taken and the eventual results are presented in this thesis. It was found that walking with the exoskeleton, while it was not giving any assistance, significantly increased the energy consumption rate of subjects, compared to normal walking. This increase was reduced by one of the two support methods, whereas the other had no significant effect on the total metabolic rate.

Contents

List of Figures

List of Tables

List of Symbols and Abbreviations

α - Angle [rad]
γ - Shape factor
ε - Coupling strength
ε^T - Tendon strain
ε_0^T - Tendon strain at F_0^M
η - Learning constant
τ_{act} - Activation time constant
τ_{deact} - Deactivation time constant
τ_d - Desired torque [N m]
φ - Normalized gait phase
Φ - Gait phase
$\hat{\Phi}$ - Estimated gait phase
ω - Frequency [Hz]
a,b - constants
Act - Muscle activation
BB - Bang-bang
BF - Biceps Femoris
CE - Contractile element
COM - Center of Mass
COP - Center of Pressure
DOF - Degree of Freedom
e - Error
$\dot{E}$ - Metabolic power [W kg^{-1}]
EMG - Electromyography
f^L - active force-length scale factor
f^{PE} - passive force-length scale factor
f^T - force-strain scale factor
f^V - force-velocity scale factor
F - Force [N]
F_{ind} - Force generation ability
F^M - Muscle fiber force [N]
F_0^M - Maximum isometric force [N]
F^T - Tendon force [N]
FF - Foot Flat
GL - Gastrocnemius Lateralis
GM - Gastrocnemius Medialis
GRF - Ground Reaction Force
$\dot{H}$ - Heat rate [J s^{-1}]
$\dot{H}_M$ - Maintenance heat rate [J s^{-1}]
$\dot{H}_s$ - Shortening heat rate [J s^{-1}]
k - Virtual spring stiffness [N m rad^{-1}]
k_* - Shape factor
L^M - Muscle fiber length [m]
L_0^M - Optimum fiber length [m]
L^{MT} - MTU length [m]
L_0^T - Tendon slack length [m]
m - Mass [kg]
MTU - Muscle Tendon Unit
N - Sample size
NE - No exoskeleton
PE - Passive element
P^M - Muscle power [J s^{-1}]
$\boldsymbol{q}$ - Generalized coordinates [rad]
$\dot{\boldsymbol{q}}$ - Generalized velocities [rad s^{-1}]
$\ddot{\boldsymbol{q}}$ - Generalized accelerations [rad s^{-2}]
RF - Rectus Femoris
SEE - Series elastic element
SO - Soleus
T - Torque [N m]
TA - Tibialis Anterior
TO - Toe Off
u - Muscle excitation
$\dot{V}$ - Flow rate [ml s^{-1}]
V^M - Muscle fiber velocity [L_0^M s^{-1}]
V_{max}^M - Maximum shortening rate [L_0^M s^{-1}]
VS - Virtual spring
W^M - Muscle work [J]
ZI - Zero impedance

1

Introduction

Ever since human ancestors used stone tools over 3 million years ago[1], technology has been part of humanity. Tools have enhanced our capabilities immensely since then and made it so that our genus could survive and evolve up until now by hunting for food, defending against predators and surviving ice ages and getting better at surviving with each generation by making better, more efficient tools.

After the Stone Age, Bronze Age, Iron Age and Middle Ages, technology got a real boost by the invention of the printing press. The invention made it possible to mass produce books and share scientific findings with the world so nobody had to reinvent the wheel anymore, instead they could build on previous work done. This led to numerous inventions and a few centuries later to the industrial age with the invention of power-driven machines like the steam engine that could replace human power to drive bigger and heavier machines. During the industrial age quality of life for humans increased dramatically due to the invention of modern medicine, running water and mass production. The acceleration of technologic advancements went on and eventually resulted in the computer, leading to the digital age we are in right now.

Looking at the last couple of decades, computational technology has shrunk in size dramatically. This has made it possible to put computers in the form of smart phones in our pockets and even to wear them as a smart watch or smart glasses. Although the last two have not (yet) been adopted as widespread as the smart phone, one can notice a trend that technology comes closer to the body and the first applications where it is embedded in our clothes and even inside the human body have already been presented; a smart clothing example is project Jacquard (Hill, 2015), a collaboration between Google and Levi's. An example for embedding technology inside the body is the syringe-injectable electronics for monitoring biological activity, developed by Liu et al. (2015).

A particular area of wearable technology that has been the focus of this study is that of exoskeletons and to be more specific lower extremity exoskeletons that try to reduce the metabolic cost of walking. Due to technological advancements making it possible to build lightweight exoskeletons there have been an increasing number of research groups and commercial companies that are getting involved in this field. One can find that many different design paths have been taken to come up with an exoskeleton that makes normal human walking more energy efficient. Although most have failed to reach this goal, as of this writing there have been arguably four groups that have been able to reduce the metabolic cost of walking with their exoskeleton in an experimental environment, arguably four because only two of them were fully autonomous exoskeletons, whereas the other two were tethered to a power source and/or actuator. These four groups took a very different approach towards their exoskeleton design, which will be discussed in section 1.5. We do know from their respective publications what effect each design has on the metabolic cost, kinematics and kinetics of the test subjects. There are however many factors that affect the walking behaviour such as exoskeleton weight, weight distribution and control method. This study tries to isolate one of these factors, the control method, to compare how this influences the human biomechanics.

[1] http://news.sciencemag.org/africa/2015/04/world-s-oldest-stone-tools-discovered-kenya

1.1 Goal

The goal of this study is to get a better understanding of the effects of different control methods on the lower limb biomechanics. Biomechanics is used here as a collective noun for lower limb kinematics, kinetics and muscle mechanics.

The easiest way to accomplish this would be to take experimental results of previously successful exoskeletons and compare these, if it were not for the fact that a different control method was not the only variable in these studies; many other variables in each exoskeleton design play a role, not to mention the experimental differences which include the subjects, testing environment and experimental protocol. So the main challenge here is to come up with an experiment where all variables are the same except for the control methods.

1.2 Background

Exoskeletons today come in many shapes and not all have them serve the same purpose. Before getting into the lower extremity exoskeletons that try to support human walking it is interesting to first get an idea of what is possible with exoskeletons in general and where the idea came from.

1.2.1 History

The idea of enhancing human capabilities to allow individuals to perform (difficult) tasks more easily or let them perform tasks otherwise impossible dates back to the 19th century. The walking aid by Yagn (1890) is often mentioned as the first elaborate exoskeleton design. As can be seen from the illustration (Fig. 1a), it consists of a contraption strapped around the legs of the user and two large leave springs, one for each leg. There is no record of the device ever being build, but we do see similar concepts that have been built recently, such as the single and multiple leaf spring exoskeleton by Grabowski and Herr (2009). This modern exoskeleton uses long leaf springs spanning between the hip and feet, similar to Yagn's exoskeleton, and has proven to be effective in reducing metabolic cost during hopping.

After Yagn patented his concept it took over seven decades before the first powered exoskeletons were actually build. Some notable pioneering exoskeletons from the late 60s and early 70s are the "Hardiman" (Mosher, 1967) and the "Complete exoskeleton" (Vukobratovic et al., 1974), shown in Fig. 1b and 1c respectively. Both of these used hydraulic actuators, but they served a different purpose; Hardiman was supposed to give users superhuman strength while the complete exoskeleton was intended to make paraplegics walk again. The main problem back then was that the state of motor, sensor, battery and computer technology did not allow for fully functioning, lightweight and portable exoskeletons. This lack of proper technology resulted for the Hardiman in a design weighing 680 kg, about 30 times as much as its modern day equivalents, such as the Hybrid Assistive Limb or "HAL" (Sankai, 2011). The complete exoskeleton is reported to weigh 12 kg, but this did not include a power source nor a computer which it had to be tethered to for power and control.

The creators of the devices mentioned were the pioneers in the field of exoskeletons and planted a seed for future research. The ones that followed are too many to mention but they have all build on the works of these pioneers and progressed the exoskeleton technology to what it is at the present. Today, about half a century after the first powered exoskeletons were build, computers and other necessary technology has been improved and their size has shrunk dramatically due to exponential technological growth. This, together with previous work done in the field of exoskeletons, made it possible to build fully autonomous exoskeletons. Some examples of these state of the art exoskeletons will be presented on the following pages.

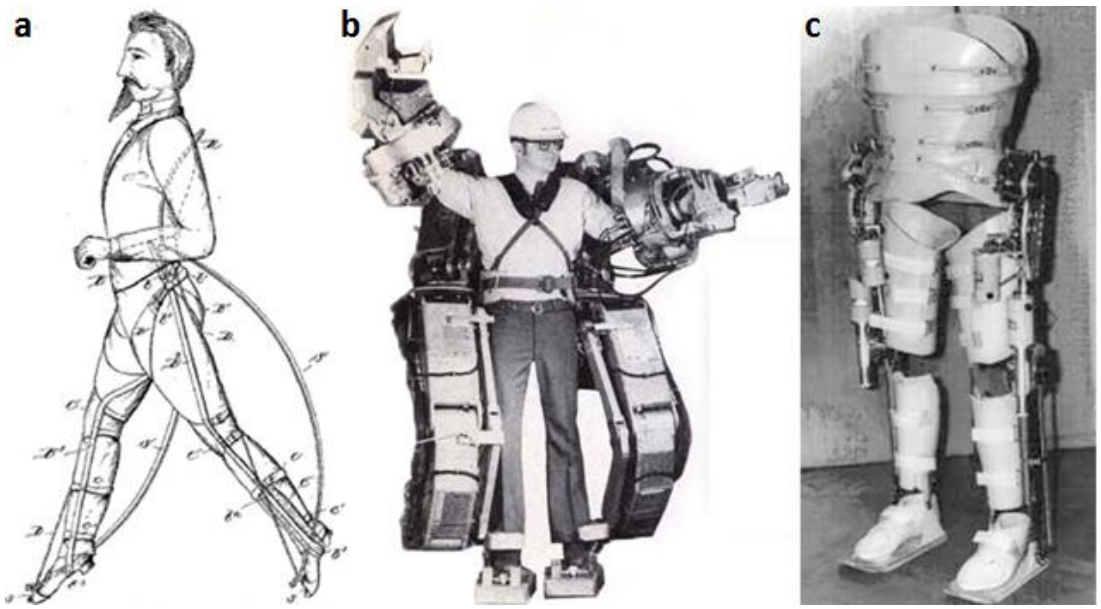

Fig. 1a: Walking aid by Yagn (1890) b: Hardiman (Fick and Makinson, 1971) c: Complete exoskeleton (Vukobratovic et al., 2012)

1.2.2 Exoskeletons in general

Besides modern equivalents of the Hardiman and Complete exoskeleton, we nowadays see exoskeletons serve many other purposes. Researchers came up with various applications for exoskeletons, an overview of these is shown in Fig. 2. Some of the more notable applications will be discussed here.

Currently there is no cure for spinal cord injury, even though a lot of research is done trying to find a method to regenerate the broken circuits in the spinal cord using stem cells. For now paraplegics have to rely on engineering solutions for their mobility, generally a wheelchair. Despite the idea of using exoskeletons to replace wheelchairs being around since the earlier mentioned Complete Exoskeleton, we recently see exoskeletons with the same purpose become a more viable solution. With current technology we see commercial companies such as Ekso Bionics (Fig. 2a) and suitX bring fully autonomous exoskeletons to market. Although these exoskeletons are still mostly used in medical rehabilitation centers, there is a good chance that with ongoing technological advances the price tag of these exoskeletons will drop and that they will replace wheelchairs for paraplegics in their everyday life, unless we see a breakthrough in neuro-regeneration before that.

While the formerly mentioned exoskeletons for paraplegics are being used in medical rehabilitation centers or under the supervision of a medical worker, they will not be able to make these patients learn how to walk on their own again, since the spinal cord injury is not cured. There are however exoskeletons for rehabilitation purposes, though these are currently meant for stroke patients and not for paraplegics. Examples of such exoskeletons are LOPES (Veneman et al., 2007), shown in Fig. 2b, and ALEX (Banala et al., 2009). Scientific evidence has shown that it is possible for stroke survivors to regain their walking ability that they have lost by performing intensive training. Normally physio therapists have to assist with these trainings, which can be physically challenging, not only for the patient but also for the therapist. The aim of these rehabilitation exoskeletons is to relief the therapist from this intensive labour.

The previous examples have shown that exoskeletons can be helpful for impaired humans. Exoskeletons can however also be beneficial for healthy humans that have labour intensive jobs, such as construction workers, nurses or military soldiers. Having superhuman strength could mean the difference between having to retire early due to back problems or easily being able to perform the job until the age of 67 or even beyond that in the future. Commercially available exoskeletons

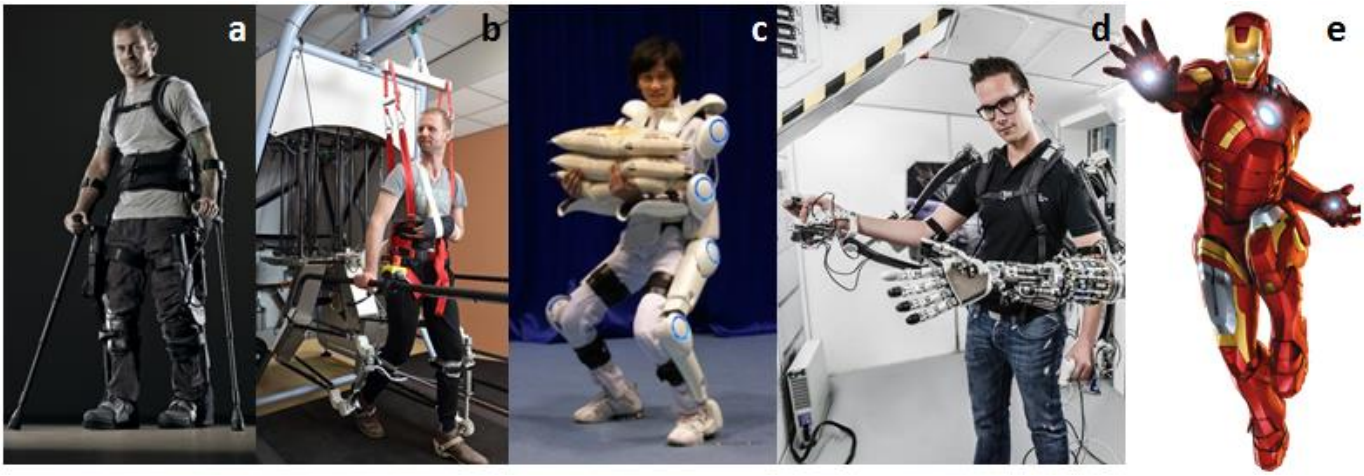

Fig. 2 Variety of exoskeletons with different applications

that try to alleviate heavy labour are HAL (Sankai, 2011), shown in Fig. 2c, and FORTIS (Lockheed Martin, n.d.) among others.

Another application that suits exoskeletons well is teleoperation. In teleoperation a master device, i.e. a human operated controller, controls from a certain distance a slave device, which usually is some form of a robotic arm. Generally these slave devices are deployed in an environment that is hazardous to humans, such as a radioactive environment like the area around Fukushima or in the vacuum of space, around the ISS. For easy tasks a relatively simple robotic arm with only a few degrees of freedom (DOFs) could suffice, such an arm could be operated with one or two joysticks. However for more complex tasks and more complex robotic arms, which can grab varying objects in a way a human would, a joystick would not be sufficient. This is where exoskeletons like ESA's EOVest (ESA-telerobotics) and CAPIO (Mallwitz et al., 2015), shown in Fig. 2d, come in. Such an exoskeleton can, as a master device, register any hand or arm gesture done by the user and transfer them to a complex human-like robotic arm, but also give the user haptic feedback when the slave device touches anything. In particular this feedback gives exoskeletons an edge over technology that can only capture the motion of the user, like the Microsoft Kinect or more advanced equivalents.

The examples mentioned here are just a taste to give a sense of what is currently possible with exoskeletons. There are of course numerous other interesting exoskeletons being developed or already on the market, but including all of them would make this section a very long read. It is important to note that for convenience anytime an exoskeleton is mentioned, in the remainder of this thesis, the word 'exoskeleton' will refer to an ankle exoskeleton that tries to optimize the energy efficiency of human walking, since the main focus will be on these exoskeletons.

1.3 Human gait

Human walking is in nature three-dimensional but for simplicity only forward motion is taken into account, so walking can be analysed as a two dimensional motion of the legs by looking at it from the sagittal plane. Human walking is a cyclic task. One cycle, from heel strike (0%) to heel strike (100%), can be divided in a stance phase and a swing phase which can be subdivided in the initial double support, single limb stance and second double support for the stance phase and initial swing, mid swing and terminal swing for the swing phase. These phases are illustrated in Fig. 3, taken from the book Human Walking (Rose and Gamble 2006). Usually parameters of gait, such as muscle activity and joint angles, are expressed in terms of the gait cycle percentages as shown in Fig. 3. The numbers shown, such as toe off at 62%, are based on averages of healthy humans and may vary slightly between subjects.

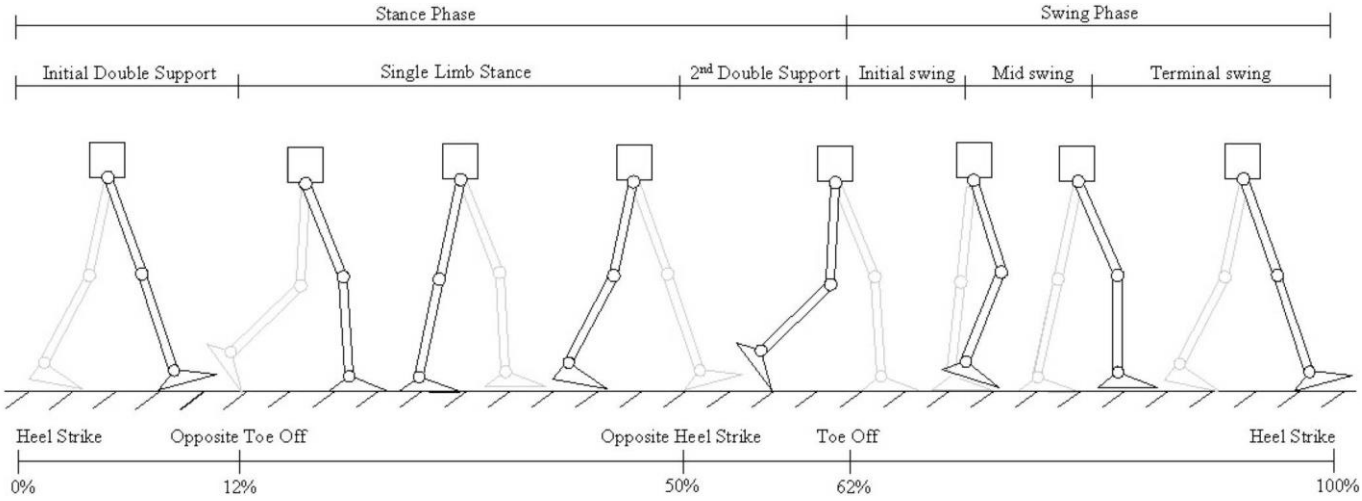

Fig. 3. All phases of a walking cycle

In a frictionless world, horizontal motion does not require any power input since the center of mass of the object in motion stays at the same height and therefore the gravitational potential energy stays the same, only an initial force has to put the object in motion. This theory also holds for the inverted pendulum like motion of walking and has led to passive dynamic walking robots that use this inverted pendulum motion to move horizontally. These passive walkers only need an initial push and will continue to walk by consuming a tiny amount of power to overcome the losses due to friction. An example of such a passive walker is the passive-dynamic walking robot by Collins et al. (2001) that consumes only 1.3W in the form of gravitational power by being placed on a 3.1° slope. Human walking is similar to these passive walkers and is often described as a motion of two coupled pendulums (Kuo et al., 2005). The difference with the passive-dynamic walker mentioned is that in humans the center of mass shifts during the transition from one leg to the other. This means that the center of mass has to accelerate and decelerate from left to right and right to left if seen from the frontal or coronal plane. From Newton's second law we know that accelerating a mass requires a force, thus the shift requires mechanical work and is therefore a major determinant of the metabolic cost of walking (Donelan et al., 2002; Kuo et al., 2005).

1.4 Influencing walking behavior

From experience we, as humans, know that our walking behaviour can be influenced by numerous factors. One can think of a walking stick or crutches which enable elderly or impaired people to walk more easily. Another example that can influence the way we walk are the type of shoes we wear; hiking shoes help to support one's feet during long distance walking, sports shoes give us more grip on the sports field, custom made orthotics embedded inside a shoe can give the wearer a better posture and high heels let women walk more elegantly, after some practice. These are just a few examples that can be beneficial to our walking behaviour, there are however also many elements that make walking more difficult. As already mentioned, shoes can be beneficial in the right circumstances, but wearing inappropriate footwear can make certain tasks much harder, think of walking a long distance on sneakers which will lead to painful blisters or sore muscles. Something that we experience on a regular basis is walking while carrying a load; it is common knowledge that carrying grocery bags, a backpack or a child makes you burn more calories and the heavier the load the faster you fatigue.

We encounter the examples mentioned regularly in everyday life, therefore everyone should agree on them being true. Although we know which factors are beneficial while walking and which ones are not, it is hard to quantify how good or bad they are and that is where science comes in. With the right scientific experiments one can quantify the influence of something by measuring for example the change in energy expenditure in different conditions. Other measures that are often used are muscle activity, kinematics and kinetics. Over the last decades researchers have been able to quantify how human locomotion is influenced under certain conditions. Some of these studies

focused on the effect of exoskeletons on human walking behaviour. The most relevant results regarding exoskeleton walking will be discussed.

1.4.1 Added mass

From Newton's second law, $\mathbf{F} = m\mathbf{a}$, we know that the force ($\mathbf{F}$) required to accelerate an object is proportional to the mass (m) of the object. Furthermore, from basics physics we know that the amount of work (W) done is the product of the force that is applied on an object and the displacement (s) of this object: $W = Fs$. From these equations it is clear that it takes more energy to get a heavier object into motion. For humans this is no different, an obese person uses a lot more energy doing everyday tasks compared to a healthy weighing person. That is also the reason why someone who lost 10 kg on a diet will regain this if he goes back to his old diet, unless he compensates this with more physical activity.

Adding mass to a free moving body will have an effect on the force required to accelerate it, but the human body is a bit more complex given that it consists of several body parts. To quantify the effect of adding mass to these different body parts, and in particular the lower limbs, Browning et al. (2007) performed an empirical study by simply strapping weights at different locations on the lower extremities of human subjects and letting them walk while measuring their metabolic cost. The study found that the total metabolic cost of walking would increase with 14.8, 5.6, 5.6 and 3.3 W for every kg added to the ankle, shank, thigh and waist respectively.

Mass and mass distribution are one of the most important determinants in whether an exoskeleton is successful in reducing metabolic cost of walking or not and although this study is about controlling an exoskeleton and not about designing one, it is still meaningful to understand how the weight of the exoskeleton might affect the results of this study.

1.4.2 Adaptation

Whenever a human interacts with a device, i.e. another dynamical system, they need to get used to it. For Dutch citizens cycling is their second nature, however we all had to learn how to ride at some point in our lifetime. No human can ride a bicycle when sitting down on one for the first time; they will need to learn how to balance, while also turning the pedals to put themselves in motion. After some practice anyone will master to ride their bike. However if one tries a different bike than he or she is used to, for instance a mountain bike that is balanced differently and has a different suspension, compared to their old city bike, he or she has to adapt to the handling of this new vehicle. For exoskeletons this is no different; although a healthy adult has mastered walking, this person will have to get used to a device that is interacting with him or her while walking. This adaptation, of a human to an exoskeleton, has been studied by Sawicki and Ferris (2008) and Kao et al. (2010). Both studies found that subjects who were not fully adapted to the exoskeleton they were wearing had an increased metabolic rate during walking compared to when they had some more practice and were used to it, as one would expect. Between studies there were however differences in the adaptation time, the time it takes to get used to something, these may be attributed to factors such as the amount of assistance provided by the exoskeleton.

The adaptation effects in these studies were examined by letting healthy subjects, who had no prior experience with exoskeleton walking, walk multiple 30 minute sessions on a treadmill. Main difference between these studies was that Sawicki and Ferris let the subjects perform three walking sessions, whereas Kao et al. opted to only perform two walking sessions. It was found by Kao et al. that after their two 30 minute sessions only six out of the eleven subjects reached a steady state in their muscle activation patterns, meaning that the other five were not fully adapted and could improve with more training. Sawicki and Ferris came to roughly the same conclusion in that they found that the mean metabolic power of their group improved, i.e. it was lower, in the third session.

In contrast to results mentioned a similar study by Gordon and Ferris (2007), the same Daniel Ferris that was involved in the other studies mentioned, that used the same exoskeleton, found that subjects reached steady state after about 15 minutes of walking during the second session. The main difference in these studies was that in the latter the exoskeleton delivered less torque. This suggests that a greater assistance during walking might be harmful for the learning process. Furthermore these results have shown that adaptation is an important factor when performing experiments with inexperienced subjects. It is therefore important that these subjects get sufficient training before doing any evaluation.

1.4.3 Control

Many exoskeletons have been designed over the last decades and they all have to be controlled in some way. The control methods used can be quite different between these exoskeleton designs. The majority of control methods used are based on the gait cycle and rely on some form of gait phase detection. One of the few exceptions to this is the exoskeleton that was used in the adaptation studies mentioned above, they relied on muscle activity to control the torque. How these different control methods influence walking behaviour is not fully understood yet, what is known though will briefly be discussed here.

As already described in the goal of this thesis, the main challenge when comparing control methods is to perform an experiment where all other variables are the same. To the writers knowledge so far only Cain et al. (2007) have performed such an experiment. Cain et al. investigated the different effects of proportional myoelectric control versus footswitch control. They named their control methods to the input signal, i.e. electromyography signals of the soleus muscle and pressure sensors placed under the foot. The output signal for the first method was, as the name suggests, proportional to the processed EMG signal, the control signal for the other method was simply an on-off or ‘bang-bang’ signal, which triggered some time after heel strike, measured by the footswitch.. Cain et al. recruited two groups of six, one group per control method, and measured lower limb EMG and joint kinematics. They found big difference between the two groups; muscle activation was much lower for the proportional myoelectric group compared to footswitch control, furthermore it was found that ankle kinematics of the latter group were perturbed substantially. The on-off method however has been optimized over the last decade and is now a common method to control ankle exoskeletons. The lesson that can be learned from this is that a well-designed control algorithm may be just as important for the success of an exoskeleton as the physical design of it.

To get back to on-off control method; this method has been optimized over the years and to be more specific the timing of the on-off signal. Malcolm et al. (2013) and Wehner et al. (2013) both have studied the effects of the timing and duration of this signal. In both studies the turn on time was variable from anywhere between 10% of the gait cycle, just after heel strike, and 60%, right before toe off. Both Malcolm and Wehner used pneumatically actuated exoskeletons, however their actuators did not have the same properties, therefore they each found a different optimal turn on time. For Malcolm et al. this was 42% and for Wehner et al. 30%. Wehner et al. also found that their subjects performed worst when the turn on time was 20%; an average metabolic power of 438.8 ± 3.4W was found for this turn on time, substantially more than the 386.7 ± 4.4W average at 30% turn on time. This shows that a small change in actuation timing can have a considerable effect on the performance of an exoskeleton.

1.5 Lower extremity exoskeletons

Lower extremity exoskeletons come in all shapes and sizes; some assisting multiple leg joints, while others only deliver an assisting torque around one joint. Three of the four successful exoskeletons as of this writing are ankle exoskeletons. The fourth one can also assist hip extension and flexion, but given that the available exoskeleton for this study cannot do this we will focus on assisting the ankle. Below the four exoskeletons will be discussed briefly.

1.5.1 Active exoskeletons

Three of the four exoskeletons mentioned can be categorized as active exoskeletons. This means that the exoskeletons use a power source to power actuators that deliver an assistive torque around a joint, in this case the ankle joint.

The first to achieve a reduction in metabolic rate during walking compared to normal walking were Malcolm et al. (2013), this result was accomplished during the study about actuation timing mentioned above. Their exoskeleton, shown in Fig. 4a, used McKibben actuators, which can be described as pneumatic artificial muscles. The main problem with this type of actuator is that it uses compressed air to contract and therefore has to be tethered to a compressed air supply, which makes it impractical for portability. This problem has to be considered when evaluation the results of Malcolm et al. Nonetheless their test subjects did show a reduction in metabolic cost during exoskeleton walking compared to walking without an exoskeleton and is therefore considered the first to achieve this feat.

The second active exoskeleton that has recently shown it can reduce the metabolic cost of walking is the soft exosuit by Asbeck et al. (2013 & 2015), shown in Fig. 4b. In short, this exoskeleton is made of flexible materials, this not only makes the exoskeleton more comfortable because of its compliance, but the textiles are also more lightweight than stiff metal materials which are often used for exoskeleton designs. Another difference, compared to the other three exoskeletons, is that this exoskeleton can assist hip extension and flexion, as already mentioned, in addition to assisting ankle plantarflexion. For assisting these joints the soft exosuit uses Bowden cables to transfer forces generated by an actuator module which is carried like a backpack, this backpack-like system also includes a computer and batteries and weighs 10.6 kg, whereas the cloth of the exosuit only weighs 1.1 kg. This weight distribution, where most of the weight is worn on the torso, close to the wearer's center of mass, has the least impact on the increase of metabolic cost, as already discussed in section 1.4.1. More details on the exoskeleton design can be found in the papers mentioned (Asbeck et al., 2013; 2015). A more recent paper by Ding et al. (2017) describes the biomechanical evaluation of the soft exosuit. They found that an average metabolic reduction up to 14.6% for multi-joint assistance, for hip extension assistance the reduction was 4.6%, suggesting that ankle joint assistance plays a big role in the 14.6% reduction. This study was done without wearing the 10.6 kg actuation system, but with wearing a 23.8 kg backpack during all walking conditions. However, by doing some back of the envelop calculations one can find that, using the empirical results of Browning et al. (2007) discussed in 1.4.1, adding the extra 10.6 kg would still result in a reduction of the metabolic cost of walking and that further improvements, i.e. reducing the weight of the actuator system, will result in larger reductions, given that the exosuit is still a prototype.

The last active exoskeleton to be discussed here is the autonomous exoskeleton by Mooney et al. (2014a; 2014b). It is the first exoskeleton to reduce the metabolic cost of walking during autonomous experiments, so without being tethered to an external power source or actuator system. The exoskeleton, shown in Fig. 4c, consists of winch actuators strapped to the shank. This actuator can pull two struts, which act as lever arm extensions of the feet, to generate a plantar flexion torque. The struts and actuators weigh a little over one kilogram per leg, with the actuator being 0.87 kg and the two struts 0.19 kg combined. Motor controllers and batteries that are worn around the waist add another 1.48 kg, making the exoskeleton have a total mass of 3.6 kg. The exoskeleton has been tested in load carriage (Mooney et al., 2014a) and normal (Mooney et al., 2014b) walking conditions. A similar reduction of the metabolic cost of walking was found in both experiments; a reduction of 36 ± 12 W or 8 ± 3% during load carriage and 35 ± 13 W or 10 ± 3% during normal walking. As a percentage the reduction is larger for the latter condition, but this experiment was done with a slightly improved version of the exoskeleton. The studies show that a lightweight autonomous exoskeleton can achieve a reduction in the metabolic cost of walking, even if an additional load is being carried.

What these active exoskeletons have in common is that they all use an on-off or 'bang-bang' control method to assist ankle plantar-flexion. They provide positive power during walking by

producing a torque about the ankle right before push-off, based on gait phase estimation. It is important to note that the control methods tested during this study were based on the work done by Malcolm et al. and Mooney et al. since these were published prior to the start of the experiments, whereas the evaluation of the soft exosuit, done by Ding et al., was published after this.

1.5.2 Passive exoskeletons

Instead of providing positive power using actively controlled actuators it is also possible to use passive elements, such as springs, to assist during walking. These passive devices do not have a power source, but they can provide positive power as long as the net power is equal to or lower than zero. This is done by getting energy out of the system and storing it, i.e. negative power, after which this energy can be released when it is needed. Think of it as a regenerative braking system in electric vehicles.

Collins et al. (2015) are the first and, for now, only to have successfully demonstrated that a passive exoskeleton can be used to lower the walking metabolic rate. The passive exoskeleton, which is shown in Fig. 4d, has a support structure similar to that of the pneumatic exoskeleton used by Malcolm et al., also consisting of a shell around the lower leg and one placed inside a shoe. These two parts are connected via an ankle aligned hinge, about which they can rotate separately from one another. A spring, that is attached to a lever arm extension of the foot part and the back of the lower leg part, is able to store kinetic energy of the user in the form of elastic potential energy. The absence of a power source, motors and controllers means the whole exoskeleton weighs an order of magnitude less than most active exoskeletons; only 0.4-0.5 kg, depending on the length of the user.

The assistance of the exoskeleton works by having an engagement system hold the spring during stance, starting at ‘foot flat’, this is when the foot is flat on the ground shortly after heel strike, in this position the foot is at maximum plantar flexion during early stance and the distance between both attachment points of the spring is shortest. After foot flat and spring engagement the wearer will dorsiflex, due to his or her forward motion, this will stretch the spring and thus resist the dorsiflexion motion, resulting in the conversion of kinetic energy to elastic energy. This elastic energy is released after the maximum dorsiflexion angle is reached, in this position the spring is stretched the most. After push off the spring is disengaged, to prevent the spring from hindering the swing motion. Resisting the motion to lower the energetic cost of walking might seem counterintuitive, but this is exactly what happens biologically; the calf muscles and the Achilles tendon have the same working principle during walking, the Achilles tendon stores elastic energy similar to the spring and the muscles are holding the tendon by contracting isometrically (Alexander & Bennet-Clark, 1977). This negative work does however require metabolic energy (Ryschon et al., 1997), so by mimicking mucle-tendon behaviour, Collins et al. not only try to assist plantar flexion during push off but also try to reduce the negative work that has to be performed by the user during stance, to relieve isometric muscle contraction.

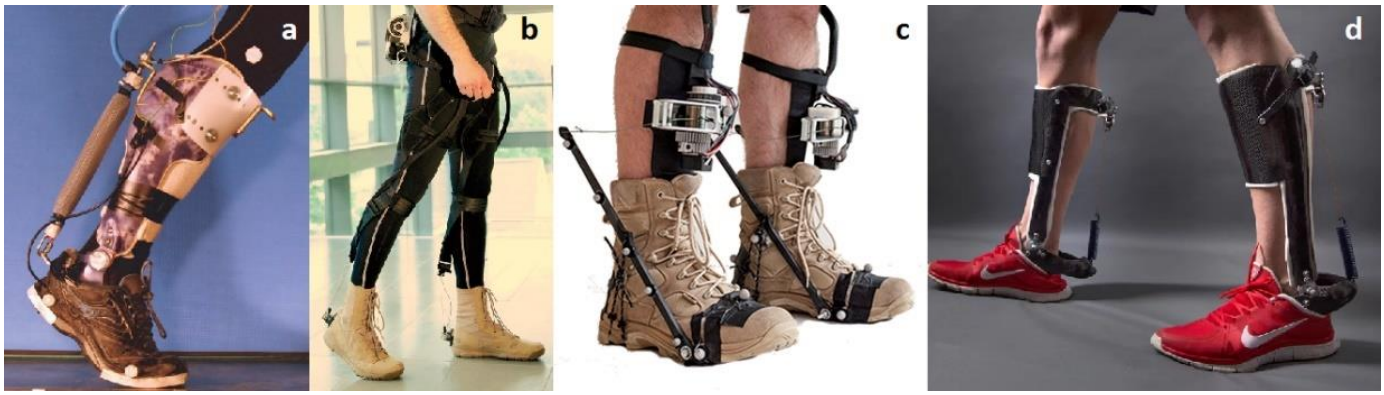

Fig. 4a: Pneumatic exoskeleton (Malcolm et al., 2013) b: Soft exosuit (Asbeck et al., 2013) c: Ankle exoskeleton (Mooney et al., 2014) d: Passive ankle exoskeleton (Collins et al., 2015)

2

Materials and methods

2.1 Achilles Ankle Exoskeleton

The exoskeleton available for this study was the Achilles ankle exoskeleton, which is shown in Fig. 5a. Details about the design were published by Meijneke et al. (2014). To summarize, Achilles is an autonomous exoskeleton consisting of two lightweight support frames, weighing 1.5 kg each, which are strapped around the shank and foot, and a backpack, with a mass of 6 kg, containing a computer and power source, for a total weight of 9 kg. The weight of the leg parts is equivalent to approximately one third of the total mass of the foot and shank, given that a foot and shank of a person weighing 75 kg have a mass of 1 and 3.4 kg respectively (de Leva, 1996). Achilles can assist with ankle flexion by generating a torque around the ankle. The torque is generated by a linear actuator that is connected in series with a leaf spring, which acts as a lever-arm.

2.2 Controllers

This section describes the high level control, which regulates the desired support torque, that was implemented in order to mimic the control methods used by the exoskeletons mentioned in section 1.5. These high level control algorithms were programmed in Matlab and Simulink (version R2014b, Mathworks, Natick, MA, US).

2.2.1 Phase detection

Malcolm et al. (2013) and Wehner et al. (2013), as discussed in 1.4, have shown the importance of actuation timing and duration when using on-off control. As is common with exoskeleton control, this timing is based on a percentage of one gait cycle, as described in 1.3. Since humans vary, not every cycle is the same length in time, even a single person shows slight differences between steps. For an accurate actuation timing it is therefore important to have a reliable phase detection method to get a good estimation of where the person is in their walking cycle (Fig. 3).

There are many parameters that can be used to estimate gait phase detection, examples are the ground reaction force (GRF) and angular acceleration or velocity of lower limbs. Although inertial measurement units (IMUs) were available, the more convenient choice of using GRFs and ankle rotation for phase detection was made, since these parameters were already being measured to study the possible changes in kinematics and kinetics for each subject.

During treadmill walking GRFs were used to divide each stride in four phases: 1. Double stance, left foot in front of right (LIFOR) 2. Single stance left (SSL) 3. Double stance, right foot in front of left (RIFOL) and 4. Single stance right (SSR). The single stance phases are simply determined by using the vertical component of the reaction forces (F_z) of the left and right force plates as input: if F_z of one of the plates is above a certain threshold value and the other one is below this value then the gait phase (Φ) corresponds to either 2. SSL or 4. SSR. During double stance the F_z of both plates will be above the threshold. To determine which foot is in front the y components of the center of pressure (COP_y) are compared. This can all be summarized in the following algorithm:

$$\Phi = \begin{cases} 1 \\ 2 \\ 3 \\ 4 \end{cases} \quad if \quad \begin{matrix} F_{zR} \geq F_{trsh}\ and\ F_{zL} \geq F_{trsh}\ and\ COP_{yL} - COP_{yR} > 0 \\ F_{zR} < F_{trsh}\ and\ F_{zL} \geq F_{trsh} \\ F_{zR} \geq F_{trsh}\ and\ F_{zL} \geq F_{trsh}\ and\ COP_{yL} - COP_{yR} \leq 0 \\ F_{zR} \geq F_{trsh}\ and\ F_{zL} < F_{trsh} \end{matrix} \tag{1}$$

Subscripts L and R refer to left and right and F_{trsh} is a constant threshold value of 3.

The resulting staircase waveform of Φ was used as input for an adaptive frequency oscillator (AFO) (Gams et al., 2009) to learn the walking frequency of the subject. By doing so a normalized sawtooth waveform was created, i.e. a periodic signal with a value between 0 and 1, where 0 is the start of a stride and 1 the end of it. This allows for an accurate actuation timing. The normalized gait phase (φ) was continuously updated during walking trials, to account for changes in walking speed (speed changes only occurred during training) and step length.

AFOs are, as the name suggests, oscillators, e.g. a sinusoidal function, that can adapt their frequency to match the frequency of a certain input or teaching signal, in this case Φ. The frequency (ω) is learned by making changes to parameters in the initial oscillator function and updating it, this updating is repeated for as long as there is a teaching signal. A sinusoidal function, with a variable amplitude (a) and offset (b), was used as an AFO to estimate Φ:

$$\widehat{\Phi} = b + a \cdot \sin(2\pi \cdot \varphi) \tag{2}$$

The error between the teaching signal and the estimation can now be written as:

$$e = \Phi - \widehat{\Phi} \tag{3}$$

The estimation was updated by the following set of differential equations:

$$\begin{aligned} \dot{\omega} &= \varepsilon \cdot e \cdot \cos(2\pi \cdot \varphi) \\ \dot{\varphi} &= 2\pi(\omega + \dot{\omega}) \\ \dot{a} &= \eta \cdot e \cdot \sin(2\pi \cdot \varphi) \\ \dot{b} &= \eta \cdot e \end{aligned} \tag{4}$$

Where the coupling strength ε, which determines the speed of convergence, and the learning constant η had, after some manual tuning, values of 2 and 0.4 respectively.

2.2.2 On-off or 'bang-bang' control

The on-off or 'bang-bang' controller is based on the control method used by the active exoskeletons of Malcolm et al. and Mooney et al., mentioned in 1.5. This controller is very straightforward in that it simply provides an assistive plantar flexion torque during late stance. Based on the work done by Malcolm et al. (2013) the onset time (φ_{on}) of the desired torque (τ_d) was chosen to be 43% of the stride cycle, with the offset time (φ_{to}) at toe off or 63% of the stride cycle. Mooney et al. (2014a) use the same timing. The controller is described by the following algorithm:

$$\tau_d = \begin{cases} T & if \quad \varphi_{on} < \varphi(t) \leq \varphi_{to} \\ 0 & otherwise \end{cases} \tag{5}$$

The torque was proportional to the weight of the user and was equal to 0.4 N m kg^{-1}, this resulted in a normalized peak power of approximately 2 W kg^{-1}, given that maximum ankle angular velocity was around 5 rad s^{-1} for this control method during pilot experiments. The torque value was chosen for two reasons; it is roughly the same as the maximum support torque used by Malcolm et al. (2013). Mooney et al., reported a 15% larger normalized peak power of 2.3 W kg^{-1} for the unloaded condition, the reason for not providing larger assistance is that the maximum power that could be exerted by the exoskeleton had to be considered. The actuation system of the Achilles exoskeleton can theoretically provide up to 192 W of power (actuator and spring power combined) according to simulations done by Van Dijk et al. (2017). Benchtop tests, described in the same paper, found

a peak power that was only 85.9% of the theoretical maximum, scaling the whole actuation power with this percentage leads to a maximum power of 165W. This means that with a normalized peak power of 2 W kg^{-1}, subjects up to 82.5 kg can be tested, increasing the normalized peak power would make it harder to find suitable test subjects.

2.2.3 Virtual spring control

The virtual spring controller is based on the passive exoskeleton by Collins et al. (2015). The virtual spring engages during foot flat (φ_{ff}) and disengages after toe off (φ_{to}). For every stride the maximum plantar flexion during early stance, as measured by the encoders, is used to determine foot flat, furthermore the ankle angle in this position (α_{ff}) is recorded and used to determine how much the virtual spring stretches after engagement; this is done by subtracting the current ankle angle (α_{aj}). Multiplying the difference between α_{ff} and α_{aj} by the spring stiffness (k) yields the desired torque:

$$\tau_d = \begin{cases} k \cdot (\alpha_{ff} - \alpha_{aj}) & if \quad \varphi_{ff} < \varphi(t) \leq \varphi_{to} \\ 0 & otherwise \end{cases} \tag{6}$$

For determining the spring stiffness it is, by simple reasoning, easy to understand that a spring with very low spring stiffness, e.g. a rubber band, cannot store merely enough energy to provide useful assistance during late stance, whereas a spring with nearly infinite stiffness can store a lot of energy but is impossible to stretch. The ideal stiffness has to be somewhere in between and this is what Collins et al. have been trying to find. By testing five different springs they found that the ideal rotational stiffness is 180 N m rad^{-1}. The resulting normalized average exoskeleton torque was 0.1 N m kg^{-1}, with a peak of 0.29 N m kg^{-1}. This torque was used as starting point during pilot studies to determine k. It was found that a k of 80 N m rad^{-1} for a subject weighing 67 kg resulted in a similar torque and power profile. During experiments the stiffness was adjusted according to the weight of the subject.

2.3 Human experiments

2.3.1 Subjects

Ten healthy participants without any walking impairments were recruited for this study. Eight (6 male, 2 female, age = 25y9m ± 2y5m, height = 1.80 ± 0.08 m, mass = 75.4 ± 9.1 kg, mean ± s.d.) out of those ten completed all trials. Technical issues with the exoskeleton prevented the other two subjects from completing the experiment. The experiment was approved by the Human Research Ethics Committee of the Technical University of Delft. All subjects were given written and verbal information prior to the experiments and all gave written informed consent to participate.

2.3.2 Kinematic and kinetic data

Kinematic data was recorded at 100 Hz using a Visualeyez II motion capture system (Phoenix Technologies Inc., Vancouver, Canada). Due to technical problems only two VZ4000v trackers were used, otherwise three would have been used for more redundancy. One tracker was placed in front of the treadmill and the other on the side, to track eight marker clusters, each containing three LED markers. These clusters were placed on the feet, lower legs, upper legs, pelvis and sternum of the subject. Prior to measurements, a probe was used to determine anatomical landmarks for each of these body parts, i.e. noticeable bony parts on the body like the calcaneus for the foot and the 7th cervical vertebra for the torso. This probing was done to be able to reconstruct the position of each body part relative to their respective cluster after measurements are done. All anatomical landmarks and their position relative to the COM of the corresponding body part are listed by Dumas et al. (2007).

Ground reaction forces and moments were collected at 1000 Hz using a dual-belt instrumented treadmill (M-gait, Motekforce Link, Amsterdam, The Netherlands). Biological joint moments can

be determined by combining these ground reaction forces with kinematic data and using inverse dynamics.

Motor stroke $x_m(t)$ and joint angle $q_j(t)$ were measured using, respectively, two SCH24-200-D-03-64-3-B incremental encoders (Scancon, Allerod, Denmark) and two RMB20SC13BC absolute encoders (RLS-Renishaw, Ljubljana, Slovenia). These are recorded to work out the spring deflection and exoskeleton torque $T_j(t)$ (Fig. 5a).

2.3.3 Surface electromyography

A Delsys Bagnoli system (Delsys Inc., Boston, MA, US) collected EMG data at 1000 Hz. To evaluate the effect on the ankle flexor muscle activity, wired bipolar surface electrodes were placed following SENIAM guidelines on the Gastrocnemius Medialis (GM), Gastrocnemius Lateralis (GL), Soleus (SO) and Tibialis Anterior (TA). Additional electrodes were placed on the knee flexor Rectus Femoris (RF) and knee extensor Biceps Femoris (BF), this was done to verify Collins' assumption that knee muscle activity is likely affected by altered ankle mechanics, this was suggested in the supplementary information of their paper (Collins et al., 2015). It was decided to only measure muscle activity of the left leg, since this would reduce the amount of preparation time significantly and reduced the amount electrodes and wires needed.

2.3.4 Metabolism

Oxygen intake and carbon dioxide production was measured using the Oxycon Mobile (CareFusion – Becton, Dickinson and Company, Franklin Lakes, NJ, US), a portable breath-by-breath cardiopulmonary stress testing system. The system consists of a mask, covering the nose and mouth, which is attached to sensors measuring the flow rate and composition of the inhaled and exhaled air. Data is wirelessly transmitted to a host computer, additional to this a back-up of the data is saved on the measuring device worn by the subject, in case the wireless connection is lost. All data including the flow rate of oxygen ($\dot{V}_{O_2}$) and carbon dioxide ($\dot{V}_{CO_2}$), necessary to compute metabolic rate, is averaged and saved every five seconds. Resting metabolic rate was measured while subjects were standing for 6 minutes prior to the measurements.

2.3.5 Experimental protocol

Four different walking conditions, all at 1.25 m s^{-1}, were evaluated:

1. Without the exoskeleton (NE)
2. With the exoskeleton in Zero Impedance mode (ZI)
3. With Bang-Bang support (BB)
4. With Virtual Spring support (VS)

The trials with the support conditions, BB and VS, lasted 12 minutes. The base conditions, NE and ZI, had a duration of 6 minutes. The subjects had to complete all four trials in a quasi-randomized order, with the NE condition always as the first or last condition, reason for this is the hassle of subjects getting out of and in to the exoskeleton in between trials. At least 15 minutes of rest was given in between trials, this together with the randomization was done to minimize the effects of fatigue. Prior to the measurement trials participants got the opportunity to familiarize with the exoskeleton during training sessions. The training session consisted of 6 and 12 minute walking trials similar to the measurement trials, only difference being is that the participants could self-select a treadmill speed, where they felt comfortable with, for the first half of each trial, for the second half the speed was increased to 1.25 m s^{-1}. Preparations for taking measurements, such as placing markers and EMG electrodes as described above, were done between training and measurements, this usually took at least 1.5 hours giving the subjects enough rest.

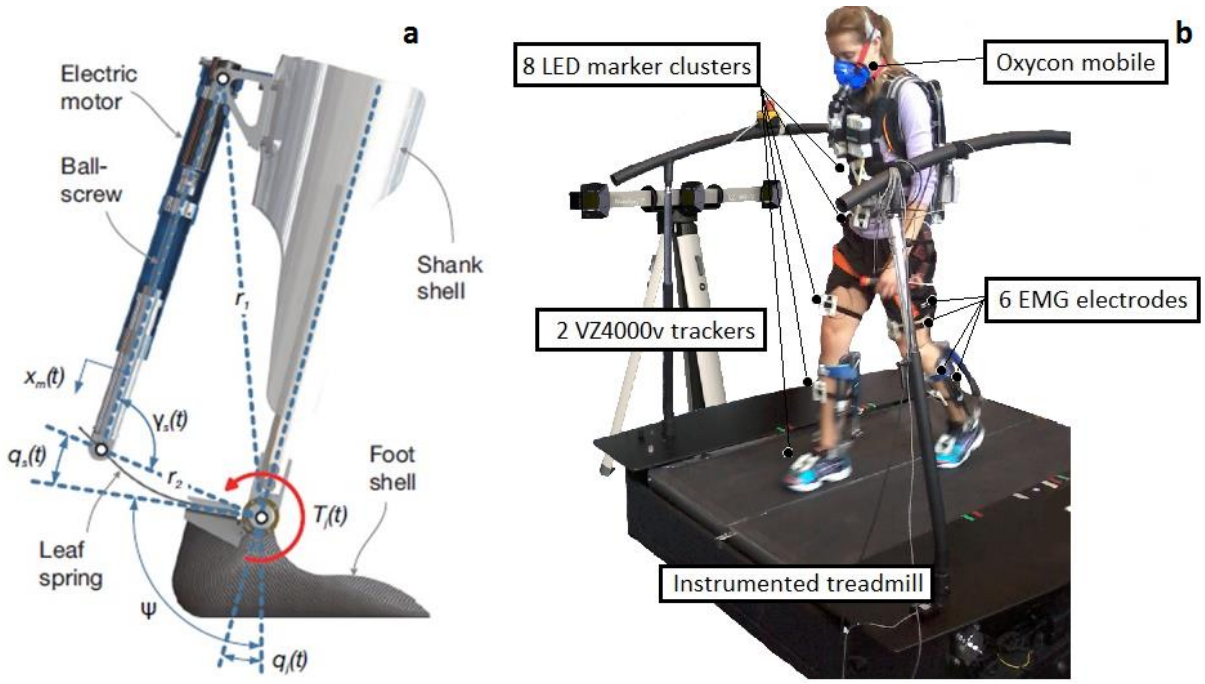

Fig. 5a: CAD model of Achilles leg part (Meijneke et al., 2014) b: Experimental setup (only 1 tracker is shown)

2.4 Data processing

2.4.1 Kinematic and kinetic data

Some individual LED markers were not tracked perfectly due to two issues, the first was that the wireless marker clusters depend on small batteries, which not always make good contact resulting in flickering LEDs and the second issue was that the line of sight between some markers and both trackers was occasionally obscured by loose cloths, straps or cables. This missing data was reconstructed using cubic spline interpolation. Marker data was then low-pass filtered using a second-order zero-phase Butterworth filter with a cut-off frequency of 6 Hz. The orientation of each cluster was used to reconstruct the position of the corresponding anatomical landmarks that were probed prior to measurements. These processing steps were done in Matlab (version R2014b, Mathworks, Natick, MA, US). Inverse kinematics and inverse dynamics were performed to compute lower extremity kinematics and kinetics, i.e. joint angles and joint torques. This was done using OpenSim v3.3 (Delp et al., 2007) and will be discussed in more detail in section 2.5.

2.4.2 Surface electromyography

The raw EMG data was processed by first removing the DC offset, this was done using a second-order high-pass zero-phase Butterworth filter with a cut-off frequency of 10 Hz. After that it was full-wave rectified, i.e. taking the absolute value, and finally the data was passed through a second-order low-pass zero-phase Butterworth filter with a cut-off frequency of 6 Hz. Processed data for each subject's individual muscle was normalized to the maximum value found across all steps and conditions for that particular muscle.

2.4.3 Metabolism

The normalized metabolic rate $\dot{E}$ [W kg^{-1}] can be estimated using the following formula, derived from Brockway (1987):

$$\dot{E} = \frac{16.48\dot{V}_{O_2} + 4.48\dot{V}_{CO_2}}{m_{sub}} \quad (7)$$

Where $\dot{V}_{O_2}$ and $\dot{V}_{CO_2}$ are the flow rate of respectively oxygen and carbon dioxide in ml s^{-1} and m_{sub} is the weight of the subject in kg. The mean resting metabolic rate, as measured during the six minutes of standing still, was subtracted in order to find the net metabolic energy used for walking with and without the exoskeleton.

2.5 Musculoskeletal simulations

Generally in human movement experiments kinematic, kinetic and EMG data is collected to characterize effects on the movement during a specific task, e.g. in this case walking with an exoskeleton. The walking experiments performed here are no different, apart from the additional metabolic data that was measured. This information gives a broad description of the changes that happen, yet it does not tell how each individual muscle has contributed to this change, although the EMG signals give an idea how the activity of an individual muscle changes it does not tell how much muscle force was generated. To study the underlying muscle mechanics one has to perform musculoskeletal simulations.

As a guide for these simulations two publications (Arnold et al., 2013a; Farris et al., 2014a) and their supplementary material, including a webinar by Dominic Farris and Gregory Sawicki (Farris et al. 2014b), were consulted. In short, the study by Arnold et al. (2013a) involves trained subjects walking and running on a treadmill at eight different speeds ranging from 1.0 to 5.0 m s^{-1}. During these trials kinematic and kinetic data was collected, as well as EMG data from eleven lower limb muscles. This data drove musculoskeletal simulations to compute muscle mechanics for these eleven muscles. The study by Farris et al. (2014a) used a similar approach to computing the muscle mechanics. The main difference was that their study involved an exoskeleton and a different locomotion, namely hopping with and without the exoskeleton.

For this study OpenSim V3.3 was used to perform simulations. OpenSim is open-source software that allows users to recreate movements using musculoskeletal models that are either developed by the user or (modified versions of) existing models. The simulations are driven by experimental data. The program contains several analysing tools to compute kinematics, kinetics and muscle mechanics among others. A schematic overview of all simulation steps taken is shown in Fig. 7. Details about the tools, their underlying models and the musculoskeletal model that were used will be discussed below.

2.5.1 Musculoskeletal model

The Gait2354 model (Thelen et al.) was used as the base model. This model is a three-dimensional 23-DOF model of the human musculoskeletal system, shown in Fig. 6. The unscaled model has a length of about 1.8 m and weight of 75.15 kg. Inertial properties of each body segment are based on anthropomorphic data from five subjects (Anderson & Pandy, 1999). It contains 54 muscle-tendon units (MTU), which are represented by a single red fiber (Fig. 6) and are governed by a Hill-type muscle model (Thelen, 2003), details about this muscle model and the muscle properties used will be discussed hereafter. More details about the Gait2354 model can be found in the OpenSim documentation online ("Gait 2392 and 2354 Models," n.d.).

For this study the Gait2354 model was simplified by removing the muscles that were not of interest. The muscle gastrocnemius lateralis was added to the model, since it was not present in the original model. Muscle properties for gastrocnemius lateralis, including origin and insertion points, were adapted from the musculoskeletal model used by Arnold et al. (2013b). Arnold et al. (2013b) introduced a massless body, shown in blue in Fig. 6, in their model to wrap both gastrocnemius lateralis and medialis around, to give them a more natural path. Gastrocnemius medialis was modified to also wrap around this body. Lastly the head, torso and right lower extremities were removed for a faster simulation time (Fig. 6).

For simplicity the Achilles exoskeleton was modelled as a massless rotational actuator placed at the ankle joint. Exoskeleton torque data was used to prescribe the torque exerted by this actuator.

A scaled version of the modified Gait2354 model was made for each subject using the scale tool available in OpenSim. Scaling of body segments was done using anatomical landmarks, shown as pink dots in Fig. 6, which were defined by using a probe as described in 2.4. The calcaneus and first caput metatarsale landmarks were used to scale the foot; epicondylus lateralis and trochanter major for scaling the femur; and malleolus lateralis and caput fibula for scaling the tibia.

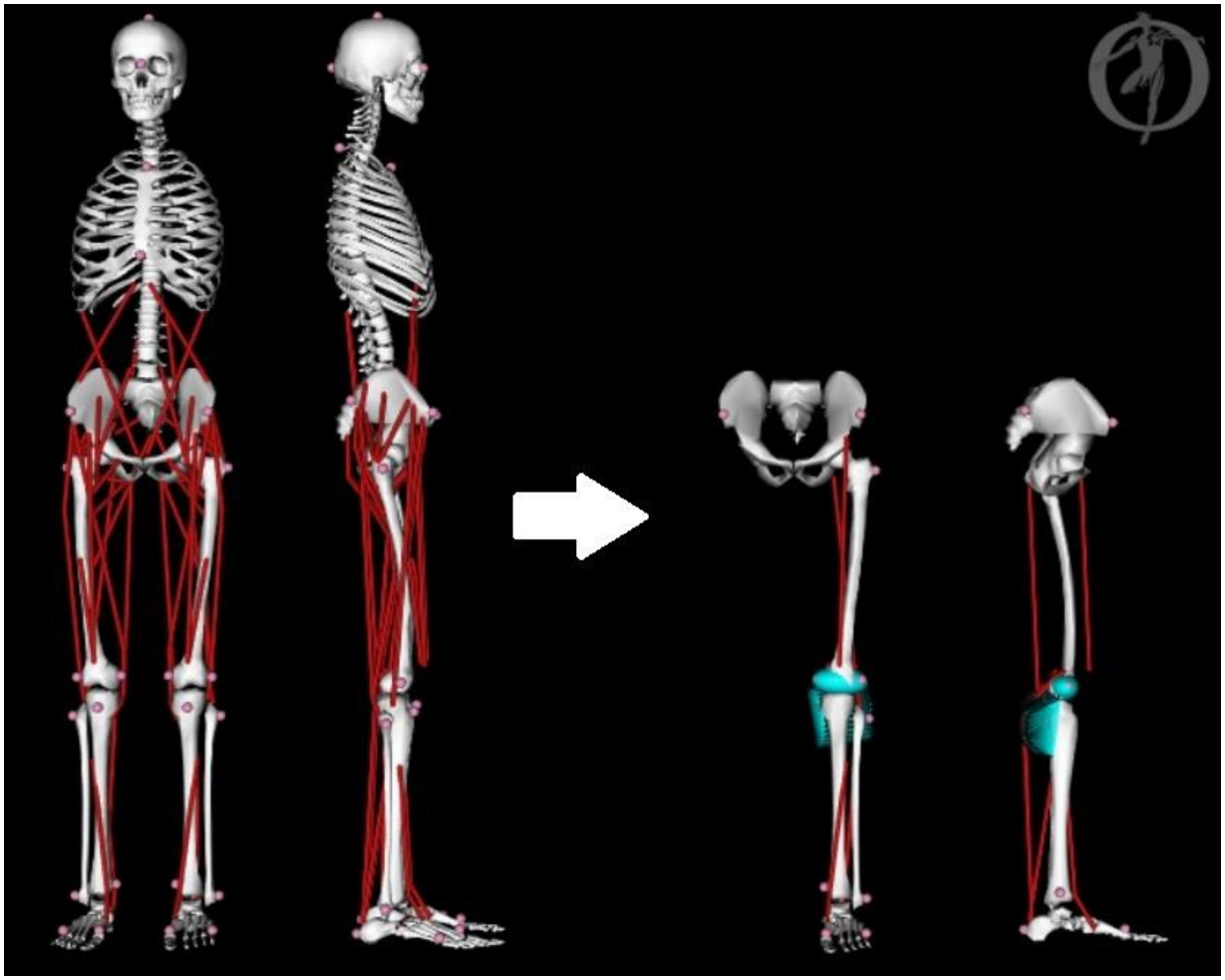

Fig. 6 Left: Original unscaled Gait2354 musculoskeletal model by Thelen et al. Right: Simplified version used for this study. Pink dots represent bony landmarks, they are used for scaling the model and performing inverse kinematics by assigning them recorded motion capture data. Each red fiber represents one MTU. The simplified version includes a massless body, shown in blue, around which the gastrocnemius lateralis and medialis are wrapped, to give them a more natural path.

2.5.2 Inverse kinematics and dynamics

The inverse kinematics tool of OpenSim was used to compute the generalized coordinates, i.e. each joint angle. Input for this tool were the positions over time of each experimental anatomical landmark marker. For every time step each experimental marker is matched to a virtual marker on the musculoskeletal model, represented as a pink dot in Fig. 6. At least three markers are required per body segment to compute the position and orientation of each segment.

Inevitably there will be errors between experimental and virtual markers, given that the musculoskeletal model is not perfectly modelled after the subject and some of its DOFs have been constraint, e.g. the knee has been modelled as a single DOF revolute joint, while a normal functioning knee joint has 6 DOFs, although the range of motion is small for all but flexion-extension. A weighted least square equation is used to minimize these marker errors ("How Inverse Kinematics Works", n.d.):

$$\min_{\mathrm{q}} \left[\sum_{i \in markers} w_i \left\| \boldsymbol{x}_i^{exp} - \boldsymbol{x}_i(\boldsymbol{q}) \right\|^2 + \sum_{j \in coords} \omega_j \left(q_j^{exp} - q_j \right)^2 \right] \tag{8}$$

Where $\boldsymbol{x}_i^{exp}$ and $\boldsymbol{x}_i(\boldsymbol{q})$ are the positions of the i^{th} experimental and virtual marker, respectively. $\boldsymbol{q}$ is the vector with generalized coordinates that the equation is being solved for. w_i is the marker weight for the i^{th} marker, these weights can be designated a certain value based on how confident one is of the measurement of a specific marker, e.g. the motion capture system used for this study

relied on marker clusters attached to different body segments, with some clusters being more prone to displacing due to the motion of a subject, meaning that the position of the markers corresponding to these clusters is less reliable, thus a lower weight would be assigned to these. q_j^{exp} and q_j are the experimental and computed values of the j^{th} coordinate, this part of the equation can be used if one has measured coordinates during their experiment. The exoskeleton used for this study has built-in encoders to measure the ankle angle, this is an example of how one could measure a coordinate experimentally and this could have been used as q^{exp} for the ankle plantar-/dorsiflexion coordinate, however only marker data was used for inverse kinematics given that no ankle coordinate could be recorded during the no exoskeleton condition.

Joint moments were computed by solving the equations of motion:

$$\boldsymbol{M}(\boldsymbol{q})\ddot{\boldsymbol{q}} + \boldsymbol{C}(\boldsymbol{q}, \dot{\boldsymbol{q}}) + \boldsymbol{G}(\boldsymbol{q}) + \boldsymbol{F} = \boldsymbol{\tau} \tag{9}$$

Where, $\boldsymbol{q}, \dot{\boldsymbol{q}}$ and $\ddot{\boldsymbol{q}}$ are vectors containing the generalized coordinates, velocities and accelerations, which have been computed using inverse kinematics. $\boldsymbol{M}(\boldsymbol{q})$ is the mass matrix, this has been scaled to each subject. $\boldsymbol{C}(\boldsymbol{q}, \dot{\boldsymbol{q}})$ is the vector containing Coriolis and centrifugal forces, $\boldsymbol{G}(\boldsymbol{q})$ the vector with gravitational forces and $\boldsymbol{F}$ contains additional applied forces. The equations of motion are solved for $\boldsymbol{\tau}$, the unknown generalized forces, i.e. the moments acting on each joint. The inverse dynamics tool in OpenSim contains all equations of motion and only requires inverse kinematic data and a scaled musculoskeletal model to compute $\boldsymbol{\tau}$. Additional ground reaction forces, measured by the force plates in the treadmill, and exoskeleton torque were provided as external loads acting on the foot and around the ankle, respectively. Exoskeleton torque, which was measured by sensors integrated in the Achilles exoskeleton, was subtracted from the total ankle moments found through inverse dynamics to calculate the biological contribution to this moment.

2.5.3 Forward dynamics

The goal of this study was to not only find kinematic, kinetic and metabolic changes due to different control methods during exoskeleton walking but also to investigate the underlying muscle mechanics that may explain these changes. The same method Farris et al. (2014a; 2014b) used to perform a muscle-tendon analysis was adopted. A schematic overview of this method is shown in Fig. 7. The activation dynamics (Thelen, 2003; Winters, 1995), contraction dynamics (Thelen, 2003; Zajac, 1989) and energetics model (Farris et al., 2014a; Lichtwark and Wilson 2005a; Woledge et al., 1985) shown in the figure are explained below.

The same equations of motion (eq. (9)) are used in the forward dynamics tool. The main difference is that the forward tool takes muscle excitation, which is converted to muscle activation through a first-order activation dynamics model (2.5.5), as an input to determine the generalized forces ($\boldsymbol{\tau}$) and, based on these forces and moments, solves the equation for $\ddot{\boldsymbol{q}}$. The tool, apart from solving for $\ddot{\boldsymbol{q}}$, which is not of interest since it was already known from inverse kinematics, also includes modules for analyzing muscle properties. The problem with the forward tool is that the excitation data (EMG) of six muscles is insufficient as input to drive the forward simulation, it will result in inaccurate and even non-physiological motions as Farris et al. (2014b) show in their webinar. The solution to this is to prescribe the motion to the musculoskeletal model. This was done for each subject by taking the corresponding scaled musculoskeletal model and assigning the generalized coordinates of each trial, found through inverse kinematics, to a copy of this scaled model.

From this prescribed motion the length and velocity of each MTU (L^{MT}, V^{MT}) over time is known, since the origin and insertion of each muscle are defined in the musculoskeletal model. The muscle mechanics are then computed, using Act and L^{MT}, through a contraction dynamics model. The muscle fiber force (F^M), length (L^M) and velocity (V^M) that come out of this, along with Act, are used in an energetics model to find the muscle metabolic power ($\dot{E}^M$).

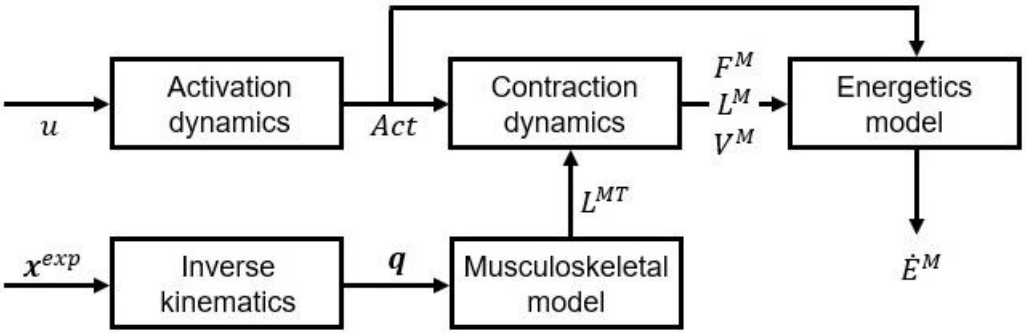

Fig. 7 Schematic overview of the simulation steps taken to find the muscle mechanics. Generalized coordinates ($\boldsymbol{q}$) are obtained by solving inverse kinematics, using the positions of experimental marker data ($\boldsymbol{x^{exp}}$). With the origin and insertion of each MTU defined in the musculoskeletal model, the length of each MTU ($\boldsymbol{L^{MT}}$) is known for any given position or motion. A first-order activation dynamics model is used to convert muscle excitation ($\boldsymbol{u}$) to activation ($\boldsymbol{Act}$). $\boldsymbol{Act}$, along with $\boldsymbol{L^{MT}}$, are used as input for a contraction dynamics model to compute muscle fiber force ($\boldsymbol{F^M}$), length ($\boldsymbol{L^M}$) and velocity ($\boldsymbol{V^M}$), which in turn can be used, with $\boldsymbol{Act}$, to compute muscle metabolic power ($\boldsymbol{\dot{E}^M}$).

2.5.4 Thelen muscle properties

Musculotendon models can be divided in two groups: cross-bridge models (e.g. Eisenberg et al., 1980 and Zahalak & Ma, 1990) and Hill-type models (e.g. Zajac, 1989 and Thelen, 2003). Hill-type models (Fig. 8a), named after the late English physiologist Archibald Hill, are widely used in muscle-driven simulations, including the simulations done by Arnold et al. (2013) and Farris et al. (2014a). The focus here will be on the muscle mechanics model by Darryl Thelen (Thelen, 2003), one of two muscles models included in OpenSim, the other being a more recent model by Matthew Millard (Millard et al., 2013). Fig. 8a shows a schematic representation of this Hill-type musculotendon model. The muscle consists of a contractile element (CE) and a passive element (PE) that run parallel to each other. The tendon is described as a series elastic element (SEE) to the muscle. The tension developed in a MTU is the sum of active force, due to the CE, and passive force due to the stiffness of the PE and SEE (eqs. (12) and (13)).

Farris et al. (2014a) have shown that simulation results using this musculotendon model agreed with experimentally measured results. For the muscle properties the default settings were used with only the optimum fiber length L_0^M of the GL and GM being modified due to their longer path. An overview of the properties is shown in table 1.

2.5.5 Activation dynamics

Force generation and relaxation in muscles does not happen instantaneously. Between the firing of motor units, i.e. muscle excitation, and the actual force generation through muscle activation there is a delay, the same has been observed when a muscle relaxes after being excited. The relationship between muscle activation and muscle excitation can be described by this first-order dynamic model (Thelen, 2003; Winters, 1995; "First-Order Activation Dynamics", n.d.):

$$\frac{dAct}{dt} = \frac{u - Act}{\tau(Act, u)} \tag{10}$$

where u is the excitation and Act the activation signal. Both u and Act have a value between 0 and 1, where 0 represents no excitation and no contraction, whereas 1 relates to maximum excitation and full contraction, respectively. Processed EMG signals were used as excitation signal. The variable time constant $\tau(Act, u)$ depends on whether the muscle activation level is increasing ($u > Act$) or decreasing ($u \leq Act$):

$$\tau(Act, u) = \begin{cases} \tau_{act}(0.5 + 1.5Act) & : u > Act \\ \tau_{deact}/(0.5 + 1.5Act) & : u \leq Act \end{cases} \tag{11}$$

where τ_{act} and τ_{deact} are time constants for activation and deactivation respectively. The default time constants of 0.01 and 0.04 were used for this study (Table 1).

	Biceps femoris	Rectus femoris	Gastroc. Lat.	Gastroc. Med.	Soleus	Tibialis anterior
$\boldsymbol{F_0^M}$ (N)	2700	1169	606	1308	4000	1375
$\boldsymbol{V_{max}^M}$ ($\boldsymbol{L_0^M}$ s^{-1})	10	10	10	10	10	10
$\boldsymbol{L_0^M}$ (m)	0.109	0.114	0.081	0.090	0.050	0.088
$\boldsymbol{L_0^T}$ (m)	0.33	0.31	0.39	0.40	0.25	0.22
$\boldsymbol{\varepsilon_0^T}$ (%)	3.3	3.3	3.3	3.3	3.3	3.3
τ_{act}	0.01	0.01	0.01	0.01	0.01	0.01
τ_{deact}	0.04	0.04	0.04	0.04	0.04	0.04

Table 1 Muscle properties of the unscaled model. All values are from the original Gait2354 model by Thelen et al., only the optimum fiber length, $\boldsymbol{L_0^M}$, and the tendon slack length, $\boldsymbol{L_0^T}$, of gastrocnemius lateralis and medialis have been modified. $\boldsymbol{F_0^M}$, maximum contractile force; $\boldsymbol{V_{max}^M}$, maximum shortening rate; $\boldsymbol{L_0^M}$, optimum fiber length; $\boldsymbol{L_0^T}$, tendon slack length; $\boldsymbol{\varepsilon_0^T}$, tendon strain at $\boldsymbol{F_0^M}$; τ_{act} and τ_{deact}, time constants for activation and deactivation.

2.5.6 Contraction dynamics

The Hill-type model, shown in Fig. 8a, was used for performing simulations. The model relies on four parameters to compute muscle force (F^M) and tendon force (F^T): muscle activation (Act), normalized muscle length ($\bar{L}^M$), muscle velocity ($\bar{V}^M$) and tendon length ($\bar{L}^T$) or strain (ε^T) (an overline indicates normalized parameters). These equations are used to compute muscle and tendon forces:

$$F^M = F_0^M\left(Act\, f^L(\bar{L}^M)\, f^V(\bar{V}^M) + f^{PE}(\bar{L}^M)\right) \tag{12}$$

$$F^T = F_0^M\, f^T(\varepsilon^T) \tag{13}$$

Where F_0^M is the maximum isometric contractile force a muscle can generate and f^L, f^V, f^{PE} and f^T are scale factors defined by the curves shown in Fig. 7b-d and detailed as functions of the four aforementioned parameters by equations (18-23) below.

From Newton's third law, assuming muscle mass is negligible, it follows that muscle force and tendon force should cancel each other out for the system to be in equilibrium:

$$F^M \cos\alpha - F^T = 0 \tag{14}$$

where α is the pennation angle between the muscle fibers and tendon.
Substituting eqs. (12) and (13) into (14) yields:

$$F_0^M\left(Act(t)\, f^L(\bar{L}^M)\, f^V(\bar{V}^M) + f^{PE}(\bar{L}^M)\right)\cos\alpha - F_0^M\, f^T(\varepsilon^T) = 0 \tag{15}$$

The equation can be solved for $f^V(\bar{V}^M)$ to get:

$$f^V(\bar{V}^M) = \frac{f^T/\cos\alpha - f^{PE}(\bar{L}^M)}{Act(t)\, f^L(\bar{L}^M)} \tag{16}$$

Fiber velocity is computed by inverting the force-velocity curve, f^V:

$$\bar{V}^M = f^{V^{-1}}\left\{\frac{f^T/\cos\alpha - f^{PE}(\bar{L}^M)}{Act(t)\, f^L(\bar{L}^M)}\right\} \tag{17}$$

Integrating (17) simulates the contraction dynamics (Thelen, 2003; Zajac, 1989; "Thelen 2003 Muscle Model", n.d.).

2.5.7 Fundamental muscle and tendon relationships

The force being developed by a MTU is a complex process between active and passive elements as discussed above. The muscle and tendon force (eqs. (12) and (13)), depend on muscle length, velocity and tendon strain. The relationships between these will be outlined here.

The maximum active force that can be generated during isometric muscle contraction, i.e. contraction when muscle length (L^M) does not change, depends on the normalized length of the muscle and peaks at a muscle length equal to the optimum fiber length (L_0^M). This non-linear relationship was approximated by Thelen (2003) using the following equation:

$$f^L = e^{-\left(\bar{L}^M-1\right)^2/\gamma} \tag{18}$$

where γ is a shape factor with a value of 0.5. The resulting force-length curve is shown in Fig. 8b.

Force generated during non-isometric muscle contraction varies with the rate of shortening or lengthening. Hill's equation (Hill, 1938) is, after almost 8 decades, still considered to be a good approximation for the force-velocity relation (Fig. 8c) when it comes to muscle shortening:

$$(F^M + a)(V^M + b) = (F_0^M + a)b \tag{19}$$

where F^M and V^M are the muscle force and velocity, respectively. F_0^M is the isometric force, i.e. at zero velocity. And a and b are two experimentally defined constants. The maximum shortening rate, V_{max}^M, is defined as the velocity at which no force is generated, from eq. (19) follows that $V_{max}^M = F_0^M b/a$ for $F^M = 0$. Rewriting eq. 19 in a normalized form gives:

$$f^V = \frac{(1+\bar{a})\bar{b}}{\bar{V}^M + \bar{b}} - \bar{a} \tag{20}$$

where $f^V = F^M/F_0^M$, $\bar{V}^M = V^M/V_{max}^M$, $\bar{a} = a/F_0^M$ and $\bar{b} = b/V_{max}^M$. The following values were taken for parameters $\bar{a}$ and $\bar{b}$ to plot the curve in Fig. 8c:

$$\begin{pmatrix}\bar{a}\\ \bar{b}\end{pmatrix} = \begin{cases}\begin{pmatrix}0.25\\ 0.25\end{pmatrix} & : \bar{V}^M \geq 0\\ \begin{pmatrix}-1.8\\ -0.16\end{pmatrix} & : \bar{V}^M < 0\end{cases} \tag{21}$$

values for shortening ($\bar{V}^M \geq 0$) were taken from McMahon (1984), the value $\bar{a}$ for lengthening is equal to the maximum normalized muscle force that can be achieved during lengthening ($\bar{F}_{len}^M$)(Thelen, 2003) and $\bar{b}$ was chosen such that there was a continuity of slopes at the transition between lengthening and shortening. It is important to note that this is an approximation of the force-velocity curve and not the actual curve used by Thelen (2003). No equation was given but it is likely that Thelen used Hill's equation for muscle shortening given the hyperbolic shape shown in his paper.

In addition to the active force generated by the muscle there will also arise a passive force when the muscle is stretched beyond its optimum fiber length. This spring-like behaviour is described using the passive muscle force-length relation (Fig 8b)(Thelen, 2003):

$$f^{PE} = \frac{e^{k_{PE}(\bar{L}^M-1)/\varepsilon_0^M} - 1}{e^{k^{PE}} - 1} \tag{22}$$

where k_{PE} is an exponential shape factor set to 4 in the default model. ε_0^M is the muscle strain due to maximum isometric force, which decreases with age (Brown et al., 1999). It was set to 0.6 (Thelen, 2003; Winters, 1995), a value associated to young adults, which all subjects were.

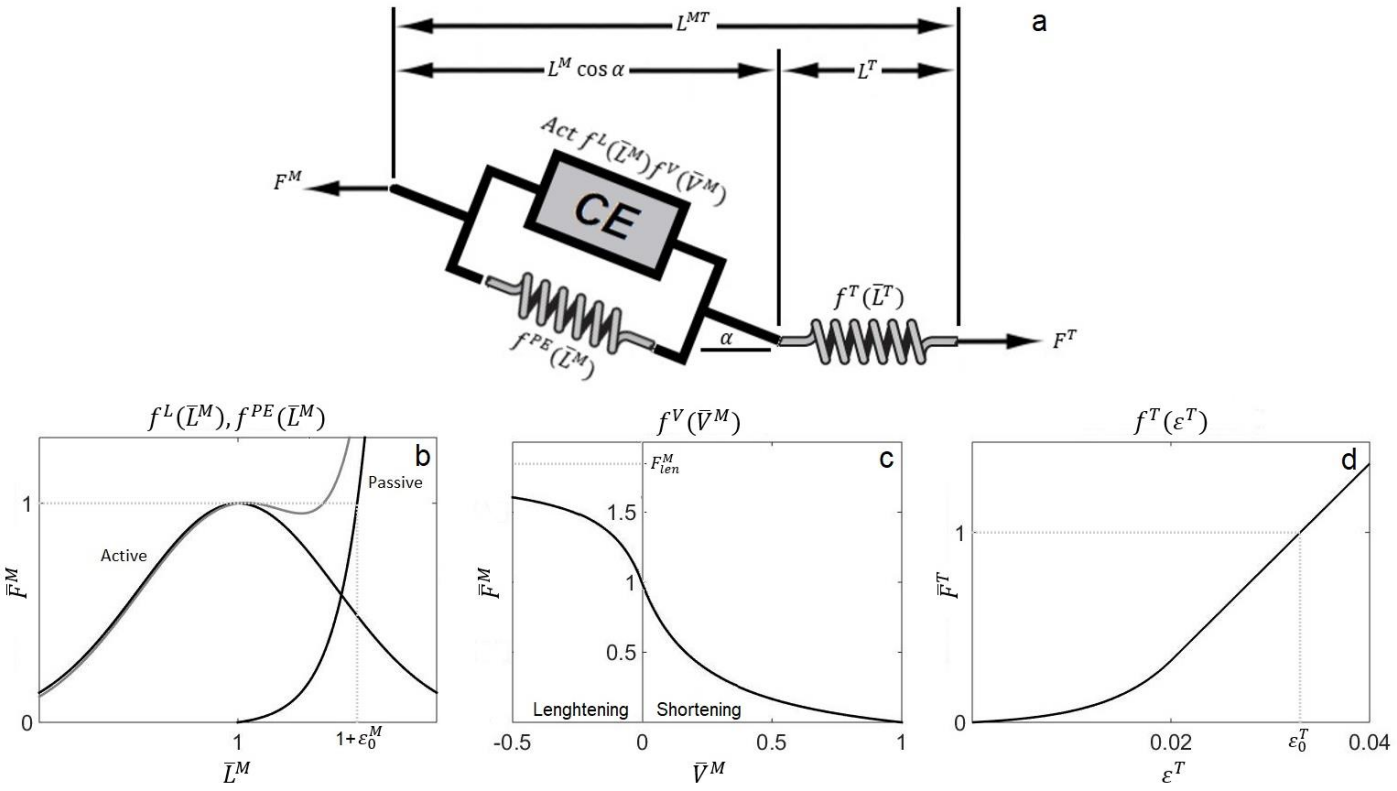

Fig. 8a: A Hill-type model describes the contraction mechanics of a MTU. The muscle is modelled as a contractile element with a parallel spring. The tendon is modelled as a spring in series with the muscle. b: Active and passive force-length curve. c: force-velocity curve. d: force-strain curve. Force generated by the contractile element is defined as the product of the maximum isometric force ($\boldsymbol{F_0^M}$), Activation ($\boldsymbol{Act}$), an active force-length multiplier ($\boldsymbol{f^L(\bar{L}^M)}$), defined by the active force-length curve (eq. (18)), and a force-velocity multiplier ($\boldsymbol{f^V(\bar{V}^M)}$), defined by the force-velocity curve (eq. (20)). Force generated by the passive element, through stretching of the muscle, is defined by the product of $\boldsymbol{F_0^M}$ and a passive force-length scale factor ($\boldsymbol{f^{PE}(L^M)}$), defined by the passive force-length curve (eq. (22)). Force developed by stretching of the tendon is defined by the product of $\boldsymbol{F_0^M}$ and a force-strain multiplier ($\boldsymbol{f^T(\varepsilon^T)}$), defined by the force-strain curve (eq. (23)).

The final element to be discussed is the series elastic element or tendon. Tendons are made of fibrous tissue that connects the muscle to the bone. Initial elongation of the tendon produces a non-linear tensile force with respect to change in length and is described by a toe region in the force-strain curve. After this initial stretch, the stiffness of the tendon is increased and tension will develop linear with further elongation. This behaviour is described by the tendon force-strain relationship (Fig. 8d)(Thelen, 2003):

$$f^T = \begin{cases} \dfrac{\bar{F}^T_{toe}}{e^{k_{toe}} - 1}\left(e^{k_{toe} \cdot \varepsilon^T / \varepsilon^T_{toe}} - 1\right) & : \varepsilon^T \le \varepsilon^T_{toe} \\ k_{lin}(\varepsilon^T - \varepsilon^T_{toe}) + \bar{F}^T_{toe} & : \varepsilon^T > \varepsilon^T_{toe} \end{cases} \tag{23}$$

where ε^T is the tendon strain, ε^T_{toe} the strain at the transition from linear to non-linear behaviour. $\bar{F}^T_{toe}$ is the normalized tendon force above which the tendon behaves linearly. k_{toe} and k_{lin} are exponential and linear shape factors, respectively. Default values as they were implemented in OpenSim and described by Thelen (2003) were used for each parameter: $\bar{F}^T_{toe} = 0.33$ and $k_{toe} = 3$, this results in $\varepsilon^T_{toe} = 0.609\varepsilon^T$ and $k_{lin} = 1.712/\varepsilon^T$ to make sure the linear region is tangent to the toe region at ε^T_{toe}.

2.5.8 Force generation ability

A method of evaluating the potential of a muscle to generate a certain force is described by Arnold et al. (2013a). The index of force producing ability (F_{ind}), as Farris et al. (2014a) call it, is determined by dividing the active force that is produced along the tendon (F_{act}^{T}) by the muscle activation (Act) and the maximum isometric force (F_0^M) that muscle can generate:

$$F_{ind} = \frac{F_{act}^{T}}{Act \cdot F_0^M} \tag{24}$$

Active force along the tendon can be derived from the equilibrium equation (eq. (14)) and eq. (12) by simply omitting the contribution of the passive element:

$$F_{act}^{T} = Act \cdot F_0^M \cdot f^L(\bar{L}^M) \cdot f^V(\bar{V}^M) \cdot \cos\alpha \tag{25}$$

dividing both sides of the equation by activation and maximum isometric force yields:

$$\frac{F_{act}^{T}}{Act \cdot F_0^M} = f^L(\bar{L}^M) \cdot f^V(\bar{V}^M) \cdot \cos\alpha \tag{26}$$

From eq. (24) it can be seen that:

$$F_{ind} = f^L(\bar{L}^M) \cdot f^V(\bar{V}^M) \cdot \cos\alpha \tag{27}$$

which can be calculated using the pennation angle (α), normalized fiber length ($\bar{L}^M$) and velocity ($\bar{V}^M$) found through simulations. This was done for each subject, condition, muscle and stride at the moment active force along the corresponding tendon peaked. The average value for each subject, condition and muscle was computed by taking the mean of all strides of the concurrent subject, condition and muscle. Differences found between conditions indicate that a different activation level is required to produce the same force, i.e. a higher F_{ind}-value means less activation is needed.

2.5.9 Energetics model

The final muscle property to be investigated is the muscle metabolic rate ($\dot{E}^M$), which is the sum of heat production rate ($\dot{H}$) and muscle power (P^M). This can give insight into how each muscle contributed to the increase or decrease of total metabolic cost of walking. Net mechanical work done by a muscle (W^M), i.e. the sum of positive and negative mechanical work, is determined by integrating muscle power (P^M) over time and muscle power is computed by the product of muscle fiber force (F^M) and velocity (V^M):

$$W^M = \int P^M \, dt = \int F^M \cdot V^M \, dt \tag{28}$$

The muscle mechanics, found through the activation and contraction dynamics models described above, were used for this. The applied energetics model to determine the heat production is the same one used by Farris et al. (2014a) and is described in more detail by Lichtwark and Wilson (2005a; 2007). The main components are described here briefly.

The total heat production rate ($\dot{H}$) can be split into two terms: the maintenance heat rate ($\dot{H}_M$) and the shortening heat rate ($\dot{H}_s$) (Note that dot notation is used, so $\dot{H} = dH/dt$). The maintenance heat can be considered as the base energetic cost when a muscle contracts isometrically; it is defined as the minimum heat rate necessary for isometric force production at any given activation level. Maintenance heat rate is proportional to activation level and fiber length, and depends on

whether the muscle is shortening ($V^M > 0$) or lengthening ($V^M \leq 0$). At maximum activation and optimum fiber length the maintenance heat rate is approximated by the following equations (Lichtwark and Wilson, 2005; Woledge et al., 1985):

$$\dot{H}_M = \begin{cases} \Gamma\left(\frac{V^M_{max}}{G^2}\right) & : V^M > 0 \\ 0.3\left(\Gamma\left(\frac{V^M_{max}}{G^2}\right)\right) + 0.7\left(\Gamma\left(\frac{V^M_{max}}{G^2}\right)\right) e^{-7V^M_{max}\left(f^V(\bar{V}^M)-1\right)} & : V^M \leq 0 \end{cases} \quad (29)$$

where Γ is a constant of 1.5, V^M_{max} is the maximum shortening rate, defined in table 1. $f^V(\bar{V}^M)$ is the force-velocity curve (eq. (20)) and G has a value of 4, based on Hill's force-velocity constants (eqs. 19-21). The shortening heat is added on top of the maintenance heat and accounts for the heat production due to muscle shortening and lengthening. During shortening this heat term increases linearly with the muscle fiber velocity (V^M), normalized by the optimum fiber length (L^M_0), and for lengthening it was found experimentally that half of the work done can be attributed to heat production. This yields the following equations to govern the heat output due to shortening (Constable et al., 1997; Hill, 1938; Lichtwark and Wilson, 2007 (suppl. mat.)):

$$\dot{H}_s = \begin{cases} \frac{V^M}{G} & : V^M > 0 \\ -0.5 f^V(\bar{V}^M) \cdot V^M & : V^M \leq 0 \end{cases} \quad (30)$$

The total heat rate is defined as the sum of maintenance and shortening heat rate, scaled by activation (Act) and the fraction of bound cross-bridges (X):

$$X = Act \cdot f^L(\bar{L}^M) \quad (31)$$

$$\dot{H} = 0.3Act\left(\dot{H}_M\right) + 0.7X\left(\dot{H}_M\right) + X\left(\dot{H}_s\right) \quad (32)$$

where $f^L(\bar{L}^M)$ is the maximum force that can be generated based on the muscle fiber length (L^M) defined by the force-length curve (eq. (18)). The total metabolic power is simply determined as the sum of heat rate and muscle power:

$$\dot{E}^M = \dot{H} + P^M \quad (33)$$

2.6 Data reduction & statistics

Each trial was split into individual steps. The algorithm for this used the recorded gait phases (see 2.2.1) to determine heel strike and toe off. Each stride was normalized to 1001 evenly spaced data points. Experimentally measured variables (i.e. metabolism, kinematics, kinetics and EMG) were calculated for each step taken during the second half of each trial, assuming subjects needed the first minutes of each trial to adapt to the different condition. Simulation variables (i.e. muscle mechanics and energetics) were computed for the last minute of each trial, to keep simulation time manageable. Variables were averaged across all steps within a subject. These individual averages were used to come up with the group average. Metabolic results, including muscle energetics, were normalized to body mass. Muscle mechanics were normalized to their respective maximum activation, maximum isometric force (F^M_0) or optimum fiber length (L^M_0)(table 1).
Student's paired *t*-tests were performed to find significant ($P < 0.05$) differences between normal walking and each of the exoskeleton conditions. Paired *t*-tests were also done to find differences between the zero impedance condition and each of the two support conditions.

3

Results

3.1 Metabolism

Results for net metabolic cost of walking at 1.25 m s^{-1}, i.e. measured metabolic rate minus resting metabolic rate, are shown in Fig. 9. Values are normalized by body mass. An overview of individual results can be found in appendix A (table 7).

The results show a significant increase for all exoskeleton conditions compared to normal walking. The net metabolic rate increased from 3.39±0.14 W kg^{-1} (mean ± sem), during normal walking, to 4.70±0.26 W kg^{-1}, when walking with the exoskeleton in zero impedance mode, an increase of 39±8% (P = 0.00003). Metabolic cost increased 30±10% (P = 0.0006) and 36±11% (P = 0.0004) compared to no exoskeleton for the 'bang-bang' (4.40±0.31 W kg^{-1}) and virtual spring condition (4.60±0.35 W kg^{-1}), respectively. The bang-bang support condition reduced metabolic cost of walking by 6.3±3.4% compared to the zero impedance condition (P = 0.0086), whereas the virtual spring condition did not reduce the metabolic cost of walking significantly (P = 0.29). An earlier evaluation of the Achilles exoskeleton by van Dijk et al. (2017) also saw metabolic increases when walking with the exoskeleton, more on this in the discussion.

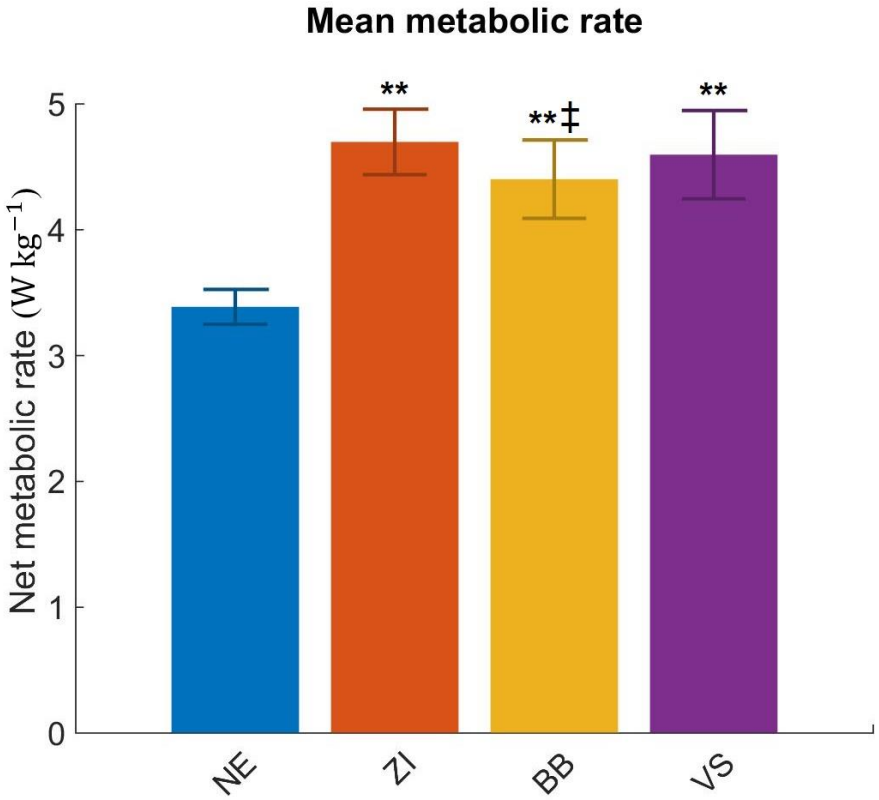

Fig. 9 Group mean (± s.e.m. 95% confidence interval) metabolic rate (N=8). The blue bar represents the no exoskeleton condition (NE), orange bar represents walking with the exoskeleton in zero impedance mode (ZI), yellow bar represents the bang-bang condition (BB) and purple bar represents the virtual spring condition (VS). **Statistically significant difference compared to no exo condition (P < 0.01). ‡Statistically significant difference compared to zero impedance condition (P < 0.05).

3.2 Kinematics & kinetics

The average stride time, which was calculated using force plate data from seven subjects, increased significantly when walking with the exoskeleton, compared to normal walking (table 2). This difference in stride time did not lead to significant changes in toe off timing.

A visual representation of the knee and ankle kinematics, kinetics and power is shown in Fig. 10, alongside the torque and power generated by the exoskeleton and the ankle angle and angular velocity as measured by the encoders on the exoskeleton. Group mean kinematics and kinetics were based on four subjects, the reason for this is explained in the discussion. Likely due to this low sample size there were no significant changes in ankle kinematics found, although there was a trend towards decreased plantarflexion after toe off for the zero impedance condition and a decreased dorsiflexion during late stance for both support conditions (BB and VS), compared to normal walking (Fig. 10A). Maximum knee flexion did increase significantly from 1.12±0.02 rad (mean±sd) during normal walking to 1.19±0.03 rad during the bang-bang support condition (Fig. 10B, P=0.03). Peak ankle angular velocity, before toe off, was significantly lower for all exoskeleton conditions, compared to normal walking (Fig. 10D), though the difference was reduced during the bang-bang support condition. For knee angular velocity there was also a significant difference between wearing and not wearing the exoskeleton; peak extension velocity during swing phase was higher for normal walking (Fig. 10E).

Peak biological ankle moment (Fig. 10G), i.e. the difference between total ankle moment, found through inverse dynamics, and exoskeleton torque, was significantly lower during the BB support condition (0.86±0.09 Nm kg^{-1}), compared to the NE (1.29±0.14 Nm kg^{-1}, P=0.004) and ZI conditions (1.46±0.08 Nm kg^{-1}, P=0.0003). The difference between NE and ZI was insignificant (P=0.07). Mean biological ankle moment was also significantly lower during BB support. The peak knee moment (Fig. 10H) between 40 and 50% of the stride was significantly higher for the ZI condition (0.48±0.10 Nm kg^{-1}) compared to NE (0.37±0.10 Nm kg^{-1}, P=0.04) and BB (0.33±0.05 Nm kg^{-1}, P=0.03). Besides this difference, there was a significantly lower knee moment between 10 and 20% of the stride cycle during the BB condition (-0.48±0.21 Nm kg^{-1}), compared to the no support condition (-0.38±0.21 Nm kg^{-1}, P=0.04) and also a significant difference between these conditions when comparing the average knee moment (0.00±0.09 vs 0.06±0.09 Nm kg^{-1}, P=0.009).

Peak ankle power (Fig. 10J) was found the be significantly lower with BB support (1.60 W kg^{-1}) compared to normal walking (2.11 W kg^{-1}). There was no significant difference in net ankle power between conditions, despite this there was an increase in mean negative power for all exoskeleton conditions compared to normal walking; mean negative power was -0.26 W kg^{-1}, -0.29 W kg^{-1} and -0.25 W kg^{-1} for respectively the ZI, BB and VS conditions and -0.11 W kg^{-1} for normal walking. There were no significant differences in peak negative power for the knee (Fig. 10K) around toe off. Also net mean knee power did not change. Mean positive knee power did change and was smaller for BB (0.23 W kg^{-1}) compared to no exo (0.33 W kg^{-1}, P=0.01). For mean negative power the VS condition (-0.37 W kg^{-1}) was significantly smaller compared to all other conditions; BB (-0.57 W kg^{-1}), NE (-0.52 W kg^{-1}) and ZI(-0.49 W kg^{-1}).

When observing the ankle angles and angular velocities there is a notable difference between the exoskeleton kinematics and those found through inverse kinematics. The most striking differences are found for the support conditions. Possible explanations for these deviations are described in the discussion.

Condition	Stride time (s)	Toe off (% gait cycle)
No Exoskeleton	1.12±0.07	63.5±1.3
Zero Impedance	1.16±0.06*	63.5±1.3
Bang Bang	1.16±0.07**	64.2±1.4
Virtual Spring	1.15±0.06**	63.9±1.5

Table 2 Stride time and toe off timing. Values are mean±s.d. (N=7). *Statistically significant difference compared to NE condition (P < 0.05). **Statistically significant difference compared to no exo condition (P < 0.01).

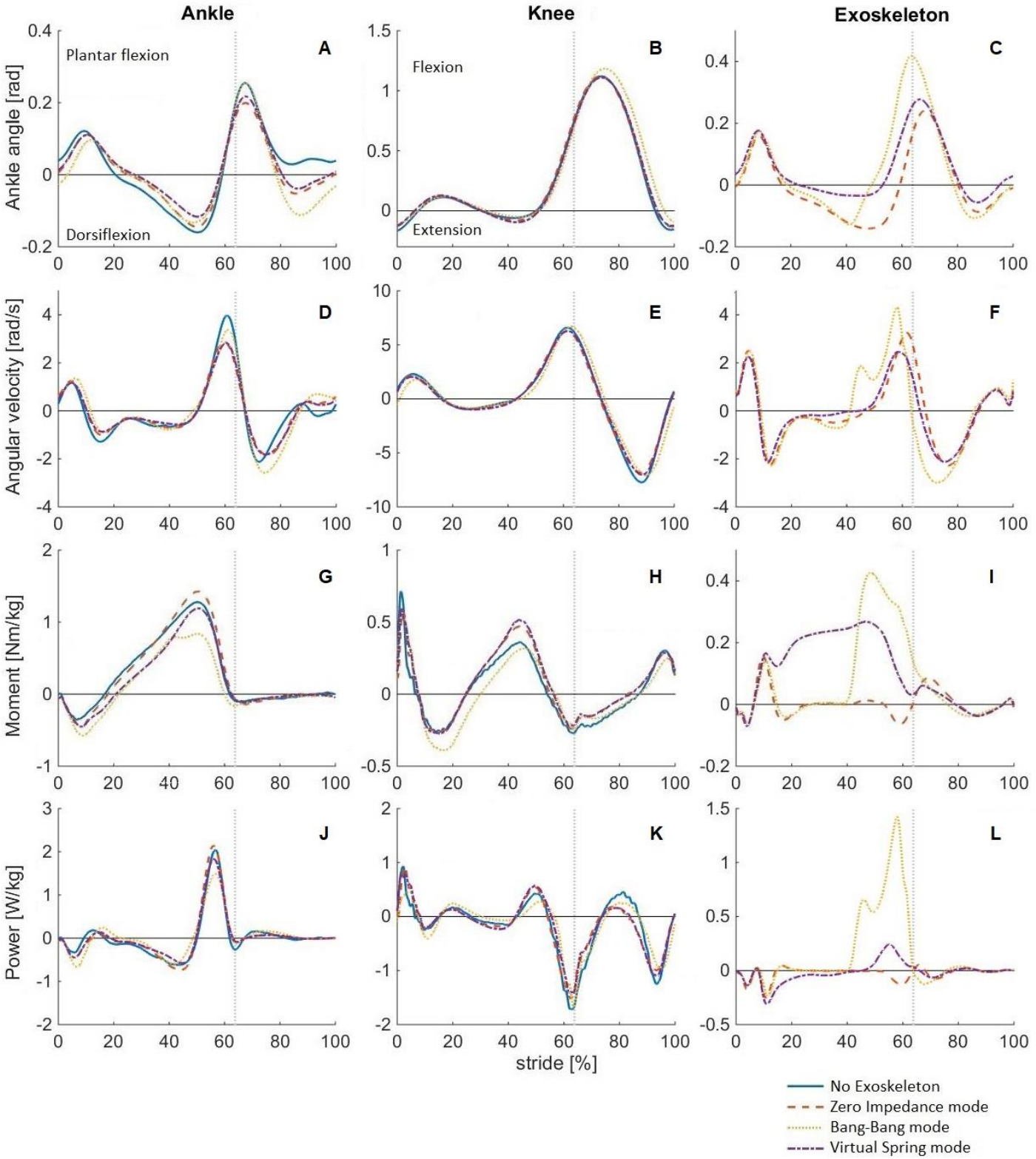

Fig. 10 Group mean knee, ankle and exoskeleton kinematics and kinetics (*N*=4). (A,B) Ankle and knee angles, (C) ankle angle as measured by an encoder on Achilles, (D-F) angular velocities, (G-I) moments, (J-L) power. Solid blue lines represent the no exoskeleton condition (NE), orange dashed lines represent walking with the exoskeleton in zero impedance mode (ZI), yellow dotted lines represent the bang bang condition (BB) and purple dash-dotted lines represent the virtual spring condition (VS). Data are normalized to stride cycle time (0-100%), with 0% representing heel strike and the grey dotted vertical lines representing the average toe off (63.8%).

3.3 Muscle activity

Processed EMG signals for all muscles measured are shown in Fig. 11. Average processed EMG signals were significantly higher during all exoskeleton conditions for BF, SO and TA, when comparing to normal walking. For RF and GM the signals were also higher during exoskeleton walking, but for RF this increase was insignificant during the VS condition and for GM it was insignificant for the BB condition. For SO and TA the EMG decreased when support was on. Peak EMG signals saw less significant differences; GM had an increased peak value for the VS condition compared to normal walking, SO had a significant increase during the ZI and VS conditions, and the BB support lowered the peak EMG during exoskeleton walking. More details about the muscle activation, which is a function of EMG (eq. 10), are presented on the following pages.

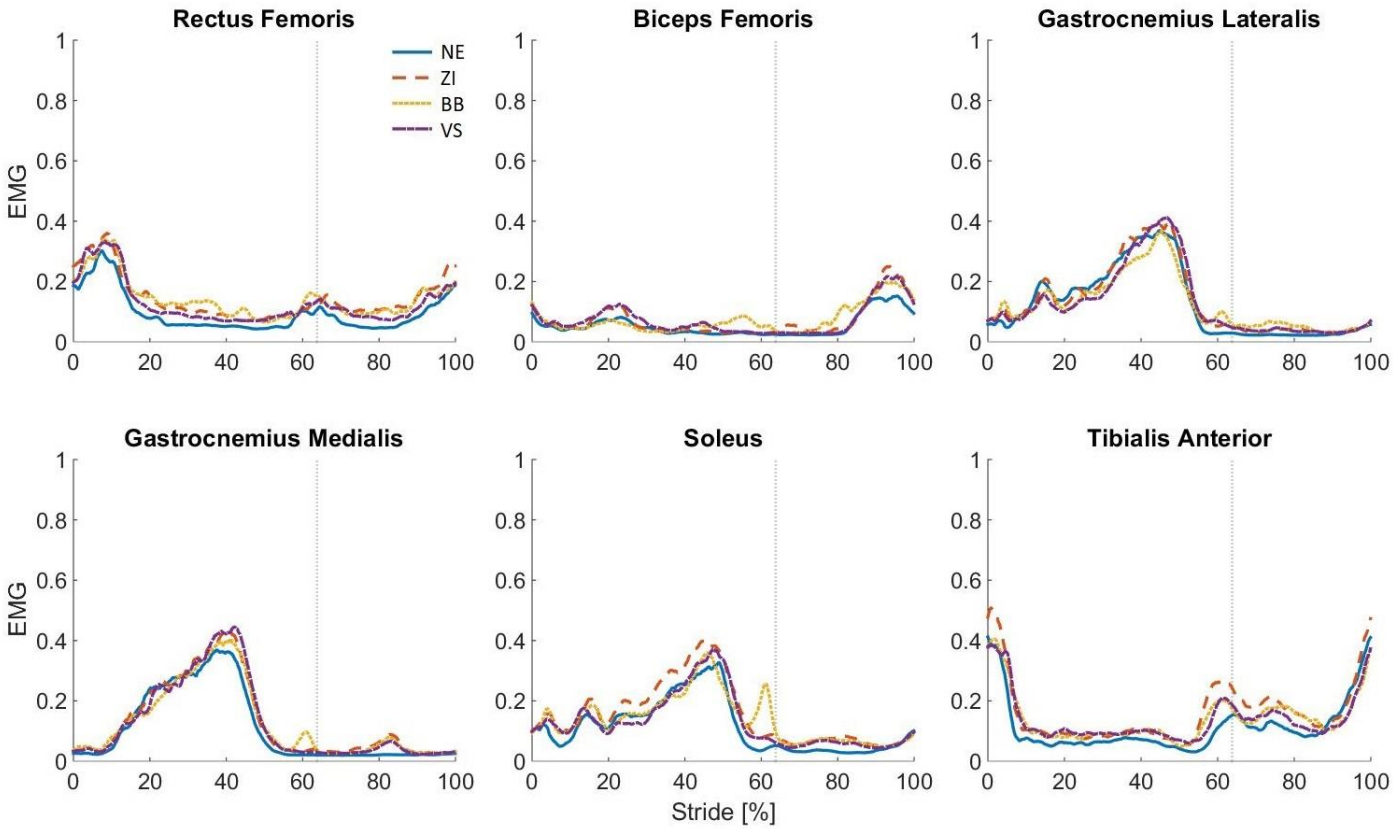

Fig. 11 Group mean plots of processed EMG for subjects walking with and without the Achilles exoskeleton (*N*=4 for RF and BF; *N*=5 for GL, GM and SO; *N*=6 for TA). Surface EMG was collected for six lower extremity muscles: RF, BF, GL, GM, SO and TA. The raw signal was high-pass filtered (10 Hz), rectified and finally low-pass filtered (6 Hz). For each subject the processed EMG signals of each muscle were normalized to the maximum value detected for that muscle across all four conditions. Solid blue lines represent the no exoskeleton condition (NE), orange dashed lines represent walking with the exoskeleton in zero impedance mode (ZI), yellow dotted lines represent the bang bang condition (BB) and purple dash-dotted lines represent the virtual spring condition (VS). Data are normalized to stride cycle time (0-100%), with 0% representing heel strike and the grey dotted vertical lines representing the average toe off (63.8%).

	Rectus Femoris				Biceps Femoris			
	NE	ZI	BB	VS	NE	ZI	BB	VS
Normalized peak activation	0.33±0.04	0.39±0.08	0.40±0.04	0.39±0.10	0.21±0.05	0.31±0.09*	0.28±0.08*	0.27±0.08
Normalized mean activation	0.12±0.01	0.17±0.03*	0.17±0.02*	0.15±0.03	0.07±0.02	0.09±0.03*	0.10±0.03*	0.09±0.03*
Peak fiber shortening velocity ($\mathbf{L_0^M\ s^{-1}}$)	3.1±0.1	3.1±0.2	3.2±0.3	3.1±0.2	1.0±0.2	1.0±0.2	1.1±0.2	1.1±0.1
Mean fiber velocity† ($\mathbf{L_0^M\ s^{-1}}$)	0.99±0.06	0.88±0.06	0.96±0.06‡	0.99±0.12	0.23±0.17	0.25±0.15	0.37±0.08	0.27±0.22
Mean fiber length† ($\mathbf{L^M\ L_0^{M^{-1}}}$)	0.88±0.08	0.86±0.08	0.84±0.08**	0.86±0.06*	1.01±0.10	1.04±0.10	1.04±0.09*	1.04±0.08
Peak fiber force ($\mathbf{F^M\ F_0^{M^{-1}}}$)	0.48±0.05	0.51±0.07	0.57±0.07	0.53±0.12	0.33±0.05	0.44±0.12	0.42±0.11	0.40±0.10
Mean fiber force ($\mathbf{F^M\ F_0^{M^{-1}}}$)	0.15±0.01	0.18±0.02*	0.19±0.03*	0.18±0.03	0.06±0.01	0.09±0.02*	0.09±0.03*	0.08±0.02*
Force producing ability (F_{ind})	1.22±0.05	1.12±0.06	1.21±0.13	1.22±0.12	1.35±0.16	1.27±0.08	1.35±0.11	1.34±0.14
Pos. fiber work (J kg^{-1} stride^{-1})	0.030±0.01	0.039±0.01**	0.045±0.01*	0.034±0.01	0.053±0.03	0.082±0.04	0.068±0.03	0.081±0.04*
Neg. fiber work (J kg^{-1} stride^{-1})	-0.27±0.07	-0.30±0.06	-0.32±0.03	-0.33±0.08	-0.27±0.06	-0.35±0.10	-0.45±0.19	-0.37±0.11
Net fiber work (J kg^{-1} stride^{-1})	-0.24±0.06	-0.26±0.06	-0.28±0.03	-0.30±0.07	-0.22±0.07	-0.27±0.08	-0.38±0.19	-0.29±0.10
Pos. MTU work (J kg^{-1} stride^{-1})	0.034±0.01	0.041±0.00	0.047±0.01	0.038±0.01	0.067±0.03	0.100±0.05	0.083±0.03	0.099±0.04*
Neg. MTU work (J kg^{-1} stride^{-1})	-0.27±0.06	-0.30±0.06	-0.33±0.03	-0.34±0.08	-0.29±0.06	-0.37±0.10	-0.47±0.18	-0.39±0.11
Net MTU work (J kg^{-1} stride^{-1})	-0.24±0.06	-0.26±0.06	-0.28±0.03	-0.30±0.07	-0.22±0.07	-0.27±0.08	-0.38±0.19	-0.30±0.10
Energy consumption (J kg^{-1} stride^{-1})	0.05±0.03	0.15±0.04	0.15±0.06	0.08±0.06	0.08±0.11	0.14±0.11	0.06±0.14	0.13±0.10

Table 3 Group mean (± s.d.) metrics of muscle mechanics for walking during four different conditions; No exoskeleton (NE), Zero impedance mode (ZI), Bang Bang mode (BB) and Virtual Spring mode (VS). †These variables were calculated during periods of highest muscle activity. *Statistically significant difference compared to no exo condition ($P < 0.05$). **Statistically significant difference compared to no exo condition ($P < 0.01$). ‡Statistically significant difference compared to zero impedance condition ($P < 0.05$). ‡‡Statistically significant difference compared to zero impedance condition ($P < 0.01$).

3.4 Muscle mechanics

Results of the muscle mechanics analysis are presented here in different forms; first the group averages of peak and mean muscle mechanic and energetic variables are shown in tables 3, 4 and 5, values marked grey represent results that show no significant difference compared to the no exoskeleton nor the zero impedance condition. Fig. 12 shows barplots of average fiber force, activation, fiber velocity, fiber length, index of force producing ability and rate of metabolic energy consumed. Then a visual representation of mean muscle power and normalized muscle force, length and velocity is given in Fig. 13 and 14. Lastly the effects of changes in operating muscle length and peak velocity on the ability to produce a force are illustrated in Fig. 15 and 16.

In all tables and figures, an asterix (*) represents a statistically significant difference between the corresponding condition and the no exoskeleton condition with a *P*-value below 0.05, a double asterix represents a significance with a *P*-value below 0.01. A double dagger (‡) and double double dagger indicate a significant difference between the zero impedance condition and either the bang-bang condition or the virtual spring condition. Notable results will be, apart from being presented by these tables and figures, mentioned for each muscle under 3.4.1-3.4.6.

3.4.1 Rectus Femoris

Muscle mechanics for RF were computed for four subjects, the reason for this is explained in the discussion, this low sample size led to mostly insignificant changes in muscle mechanics. Increases in muscle activation, however, were large enough to show a significant effect between the NE condition and the ZI and BB condition (table 3, Fig. 12). Since active force changes proportional with activation (eq. 25), the average fiber force is also shown to be a significantly larger for these same conditions, compared to normal walking (table 3, Fig. 12, Fig. 13), despite the average fiber length, for the BB condition, deviating further from the optimum length. This deviation from the optimum fiber length, which was also a significant change in the VS condition, means the force producing capability decreases (eq. 18, Fig.15). Increased fiber force, in combination with no significant changes in fiber velocity, resulted in a significant rise in positive fiber work (table 3).

3.4.2 Biceps Femoris

Results of four subjects were used to compute group averages for BF muscle mechanics and energetics, similar to RF. Activation levels and fiber force for this muscle increased for all exoskeleton conditions (table 3, Fig. 12). The increased force led to increases in fiber and MTU work, but these changes were only significant for positive work during the VS condition (table 3).

	Gastrocnemius Lateralis				Gastrocnemius Medialis			
	NE	ZI	BB	VS	NE	ZI	BB	VS
Normalized peak activation	0.44±0.09	0.47±0.091	0.41±0.08	0.48±0.08	0.41±0.03	0.49±0.05	0.45±0.05	0.48±0.03**
Normalized mean activation	0.15±0.04	0.16±0.04	0.15±0.05	0.16±0.04	0.13±0.02	0.16±0.02*	0.16±0.01*	0.16±0.02**
Peak fiber shortening velocity ($\mathbf{L_0^M\ s^{-1}}$)	2.8±0.2	2.6±0.4	2.9±0.4‡	2.6±0.3*	2.4±0.4	2.1±0.5*	2.3±0.4	2.0±0.4*
Mean fiber velocity† ($\mathbf{L_0^M\ s^{-1}}$)	-0.26±0.06	-0.29±0.06	-0.25±0.05	-0.23±0.05	-0.22±0.06	-0.23±0.06	-0.20±0.04	-0.18±0.04
Mean fiber length† ($\mathbf{L^M\ L_0^{M-1}}$)	1.00±0.02	0.99±0.02*	1.00±0.02‡	1.00±0.03	1.00±0.01	0.99±0.01*	1.00±0.02	1.00±0.02
Peak fiber force ($\mathbf{F^M\ F_0^{M-1}}$)	0.50±0.11	0.52±0.09	0.46±0.08	0.53±0.09	0.49±0.05	0.57±0.08	0.53±0.07	0.55±0.04*
Mean fiber force ($\mathbf{F^M\ F_0^{M-1}}$)	0.16±0.05	0.17±0.05	0.16±0.06	0.16±0.04	0.15±0.03	0.18±0.03*	0.17±0.02*	0.17±0.03**
Force producing ability (F_{ind})	1.03±0.04	1.02±0.04	1.02±0.03	1.01±0.01	1.07±0.04	1.05±0.04	1.06±0.03	1.04±0.04**
Pos. fiber work (J kg^{-1} stride^{-1})	0.009±0.00	0.014±0.00**	0.013±0.00	0.013±0.00*	0.016±0.00	0.027±0.01*	0.033±0.01*	0.026±0.01*
Neg. fiber work (J kg^{-1} stride^{-1})	-0.035±0.01	-0.041±0.01	-0.048±0.02	-0.036±0.01	-0.09±0.02	-0.13±0.03*	-0.13±0.03*	-0.12±0.02*
Net fiber work (J kg^{-1} stride^{-1})	-0.026±0.01	-0.027±0.01	-0.033±0.02	-0.023±0.01	-0.075±0.02	-0.11±0.04*	-0.099±0.03	-0.093±0.03
Pos. MTU work (J kg^{-1} stride^{-1})	0.013±0.00	0.018±0.00*	0.016±0.00	0.017±0.00**	0.015±0.00	0.024±0.01*	0.030±0.01*	0.023±0.01*
Neg. MTU work (J kg^{-1} stride^{-1})	-0.039±0.01	-0.044±0.02	-0.049±0.02	-0.039±0.01	-0.09±0.02	-0.13±0.03**	-0.13±0.03*	-0.12±0.02**
Net MTU work (J kg^{-1} stride^{-1})	-0.026±0.01	-0.027±0.01	-0.033±0.02	-0.023±0.01	-0.075±0.02	-0.11±0.04*	-0.099±0.03	-0.093±0.03
Energy consumption (J kg^{-1} stride^{-1})	0.09±0.02	0.10±0.02	0.09±0.02‡	0.10±0.02	0.25±0.03	0.30±0.07	0.31±0.07	0.29±0.04*

Table 4 Group mean (± s.d.) metrics of muscle mechanics for walking during four different conditions; No exoskeleton (NE), Zero impedance mode (ZI), Bang Bang mode (BB) and Virtual Spring mode (VS). †These variables were calculated during periods of highest muscle activity. *Statistically significant difference compared to no exo condition ($P < 0.05$). **Statistically significant difference compared to no exo condition ($P < 0.01$). ‡Statistically significant difference compared to zero impedance condition ($P < 0.05$). ‡‡Statistically significant difference compared to zero impedance condition ($P < 0.01$).

All other changes found were insignificant, besides a small but significant increase in operating fiber length during the BB condition (table 3, Fig. 12, Fig. 15).

3.4.3 Gastrocnemius Lateralis

The sample size for all variables which are independent off activation levels (i.e. fiber length and velocity) was seven, for all activation-dependent variables it was five. GL did not show a significant increase in muscle activation. Mean fiber velocity and fiber force were not affected either (table 4, Fig. 12). Despite this there was a significant increase in positive fiber and MTU work (table 4), though this accounts for only a small part of the total energy consumption, which only saw a significant difference between the ZI and BB conditions (table 4). Other significant changes found for this muscle were an increased peak shortening velocity during the BB condition, compared to the no support condition (table 4, Fig. 13, Fig. 16), a decreased peak shortening velocity during the VS condition, compared to normal walking (table 4, Fig. 13, Fig. 16), and a small change to the fiber length during the ZI condition, compared to NE and BB.

3.4.4 Gastrocnemius Medialis

Sample size was seven for activation-independent variables, otherwise it was five. For this plantar-flexor mean muscle activation increased for the ZI and VS conditions (table 4, Fig. 12), also peak activation was increased for the latter condition. Fiber force consequently increased for these conditions as well as for the BB condition (table 4, Fig. 12). Again, since work is defined by integrating the product of force and velocity over time and mean fiber velocity did not change, there is an increase found in the amount of positive and negative work done by the muscle fibers and MTU (table 4). This increase is seen for all exoskeleton conditions. Net work done, however, did not show a significant change for the support conditions (BB and VS), due to the effects on positive and negative work cancelling each other out to some extent. It was furthermore found that the force producing index (F_{ind}), which is calculated for the moment active force peaked, was slightly but significantly reduced during VS support (table 4, Fig. 12), this indicates a higher activation is needed to produce the same peak force (eq. 24), it can be seen, however, that peak fiber force was not the same but significantly higher for this condition (table 4, Fig. 14), meaning even more muscle activation is required at this instant during the gait cycle. Lastly there is a decline in the peak shortening velocity found during the ZI and VS conditions (table 4, Fig. 14), this causes a shift to the left on the force-velocity curve (Fig. 16), though it can be seen in Fig. 14 that this should have no effect on the muscle activation given that fiber force was close to zero during peak shortening.

	Soleus				Tibialis Anterior			
	NE	ZI	BB	VS	NE	ZI	BB	VS
Normalized peak activation	0.35±0.06	0.44±0.05*	0.44±0.12	0.40±0.07**	0.45±0.13	0.54±0.07	0.43±0.04‡	0.43±0.05
Normalized mean activation	0.14±0.02	0.19±0.02**	0.17±0.02**‡	0.16±0.02**‡‡	0.14±0.04	0.20±0.03**	0.18±0.02*‡	0.17±0.03*‡
Peak fiber shortening velocity ($\mathbf{L_0^M\ s^{-1}}$)	2.7±0.4	2.1±0.6**	2.7±0.7‡	2.2±0.4**	1.1±0.2	0.9±0.2	1.3±0.3‡‡	0.9±0.2
Mean fiber velocity† ($\mathbf{L_0^M\ s^{-1}}$)	-0.12±0.08	-0.17±0.09	-0.20±0.11	-0.14±0.08	0.57±0.12	0.47±0.12*	0.61±0.13‡	0.52±0.11
Mean fiber length† ($\mathbf{L^M\ L_0^{M^{-1}}}$)	0.89±0.04	0.89±0.04	0.89±0.04	0.89±0.04	0.93±0.06	0.91±0.07*	0.90±0.06**	0.90±0.06*
Peak fiber force ($\mathbf{F^M\ F_0^{M^{-1}}}$)	0.48±0.11	0.58±0.07	0.48±0.07	0.54±0.10**	0.55±0.14	0.69±0.13	0.55±0.07‡	0.55±0.05
Mean fiber force ($\mathbf{F^M\ F_0^{M^{-1}}}$)	0.17±0.03	0.21±0.03**	0.19±0.03*‡	0.18±0.02*‡‡	0.14±0.03	0.19±0.02**	0.17±0.01*‡	0.17±0.02*‡
Force producing ability (F_{ind})	1.00±0.03	0.96±0.03	0.98±0.04	0.96±0.05	1.19±0.04	1.24±0.03*	1.20±0.06	1.16±0.14
Pos. fiber work (J kg^{-1} stride^{-1})	0.032±0.01	0.066±0.02**	0.080±0.02**	0.052±0.01**‡	0.042±0.02	0.054±0.01*	0.050±0.02*	0.050±0.02*
Neg. fiber work (J kg^{-1} stride^{-1})	-0.17±0.03	-0.20±0.05	-0.23± 0.05*	-0.18±0.02	-0.15±0.04	-0.22±0.06	-0.21±0.03*	-0.18±0.03*
Net fiber work (J kg^{-1} stride^{-1})	-0.14±0.04	-0.14±0.05	-0.15±0.06	-0.12±0.03	-0.11±0.02	-0.17±0.05	-0.16±0.03*	-0.13±0.02
Pos. MTU work (J kg^{-1} stride^{-1})	0.050±0.01	0.085±0.02*	0.096±0.02**	0.070±0.01**	0.044±0.02	0.059±0.02*	0.053±0.02*	0.053±0.02**
Neg. MTU work (J kg^{-1} stride^{-1})	-0.19±0.03	-0.22 0.07	-0.25±0.06*	-0.19±0.03	-0.15±0.04	-0.22±0.06	-0.21±0.04*	-0.19±0.04*
Net MTU work (J kg^{-1} stride^{-1})	-0.14±0.04	-0.14±0.05	-0.16±0.06	-0.12±0.03	-0.11±0.02	-0.17±0.05	-0.16±0.03*	-0.13±0.02
Energy consumption (J kg^{-1} stride^{-1})	0.29±0.04	0.41±0.05*	0.41±0.09*	0.35±0.04*‡	0.15±0.06	0.21±0.07**	0.19±0.06**‡	0.19±0.07**‡

Table 5 Group mean (± s.d.) metrics of muscle mechanics for walking during four different conditions; No exoskeleton (NE), Zero impedance mode (ZI), Bang Bang mode (BB) and Virtual Spring mode (VS). †These variables were calculated during periods of highest muscle activity.*Statistically significant difference compared to no exo condition ($P < 0.05$). **Statistically significant difference compared to no exo condition ($P < 0.01$). ‡Statistically significant difference compared to zero impedance condition ($P < 0.05$). ‡‡Statistically significant difference compared to zero impedance condition ($P < 0.01$).

3.4.5 Soleus

Sample size was seven for activation independent variables, otherwise it was five. Similar to the other muscles, it was found that mean activation increased significantly during exoskeleton conditions (table 5, Fig. 12). In contrast to the previously mentioned muscles it can be seen that muscle activation was reduced during the support conditions, compared to no support. The same effects can be seen for the mean fiber force (table 5, Fig. 12), since there were no significant changes to fiber length and velocity, thus the ability to produce a force given the muscle activation (F_{ind}) was not changed either. Increases in the fiber and MTU work were similar to the other plantar-flexors and these changes too cancelled each other out, so that the net work done did not change significantly (table 5). Peak fiber shortening did see significant changes (table 5, Fig. 14, Fig. 16), but, as with the other plantar-flexors, this did not have any effect on the muscle activation at that instant.

3.4.6 Tibialis Anterior

Sample size was seven for activation independent variables, otherwise it was six. Mean muscle activation increased for all exoskeleton conditions and, like SO, decreased when comparing the support conditions with the no support condition (table 5, Fig. 12). A significantly lower mean fiber velocity during no support (table 5, Fig. 12), compared to NE and BB, was also seen back in an increased F_{ind}, as a left shift on the force-velocity curve (Fig. 8b) means an increase in force producibility. F_{ind} increased despite the less favorable fiber lengths (table 5, Fig. 12, Fig. 15), which was also significantly shorter for the other exoskeleton conditions. Mean fiber force saw the same differences between conditions as mean activation; an increase for all exoskeleton conditions, compared to normal walking and a decrease for the BB and VS support compared to ZI (table 5, Fig. 12). Positive and negative mechanical work done by the muscle fibers and MTU increased significantly, expect for negative work during the ZI condition (table 5), due to the increased force. The decrease between the support and no support conditions was insignificant, because the lower fiber force during support conditions was compensated by the increased fiber velocity, resulting in a smaller, insignificant difference.

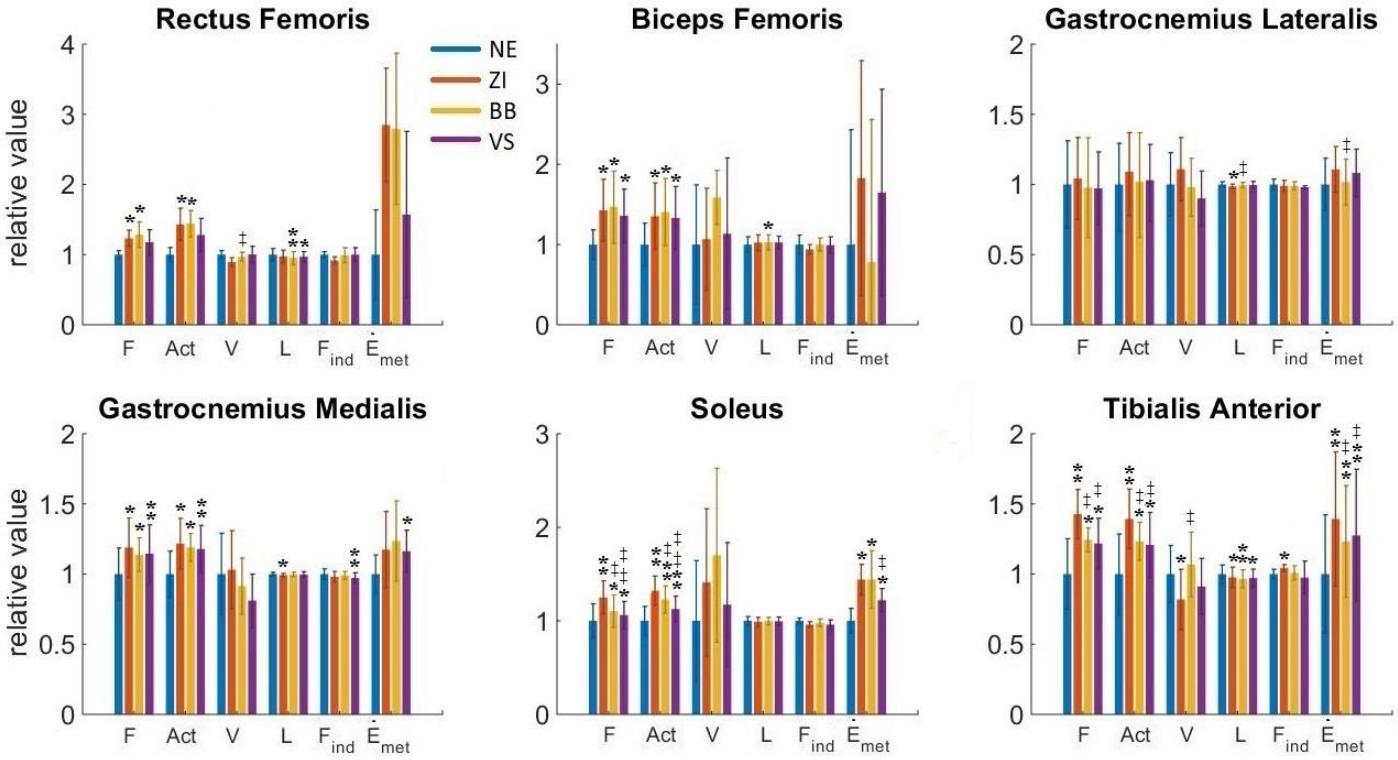

Fig. 12 Group mean (± s.d.) barplots of average fiber force (F), activation (Act), fiber velocity (V), fiber length (L), index of force producing ability (F_{ind}) and rate of metabolic energy consumed ($\dot{E}_{met}$). This figure is a visual representation of the same results presented in tables 3, 4 and 5. Values are normalized to the no exoskeleton condition. Blue bars represent the no exoskeleton condition (NE), orange bars represent walking with the exoskeleton in zero impedance mode (ZI), yellow bars represent the bang bang condition (BB) and purple bars represent the virtual spring condition (VS). *Statistically significant difference compared to no exo condition ($P < 0.05$). **Statistically significant difference compared to no exo condition ($P < 0.01$). ‡Statistically significant difference compared to zero impedance condition ($P < 0.05$). ‡‡Statistically significant difference compared to zero impedance condition ($P < 0.01$).

3.5 Muscle energetics

The simulation results of the metabolic energy rate for both RF and BF did not show a significant change (table 3). When looking at the combined metabolic energy rate of all ankle dorsi- and plantar flexors, shown in table 6, there is a significant increase during all exoskeleton conditions compared to normal walking. It can be seen from tables 4 and 5 that mostly SO and TA contribute to this increase, with both showing significant increases in energy consumption per stride when walking with the exoskeleton, regardless of the support. GM also saw a significant increase during the virtual spring support condition, whereas the other exoskeleton conditions trended towards an increased metabolic rate (both: P=0.10). When comparing the non-support condition to the support conditions, there is significant reduction seen for GL and TA during bang-bang support. For virtual spring support there is a reduction found for SO and TA. The combined energy consumption showed a 7.9±5.3% decrease in the virtual spring condition compared to the no support or zero impedance condition.

Condition	Energy consumption (J kg^{-1} stride^{-1})
No Exoskeleton	0.80±0.09
Zero Impedance	1.03±0.14**
Bang Bang	1.02±0.16*
Virtual Spring	0.95±0.12**‡

Table 6 Combined metabolic energy rate of GL, GM, SO and TA (mean±sd). *Statistically significant difference compared to no exo condition ($P < 0.05$). **Statistically significant difference compared to no exo condition ($P < 0.01$). ‡Statistically significant difference compared to zero impedance condition ($P < 0.05$).

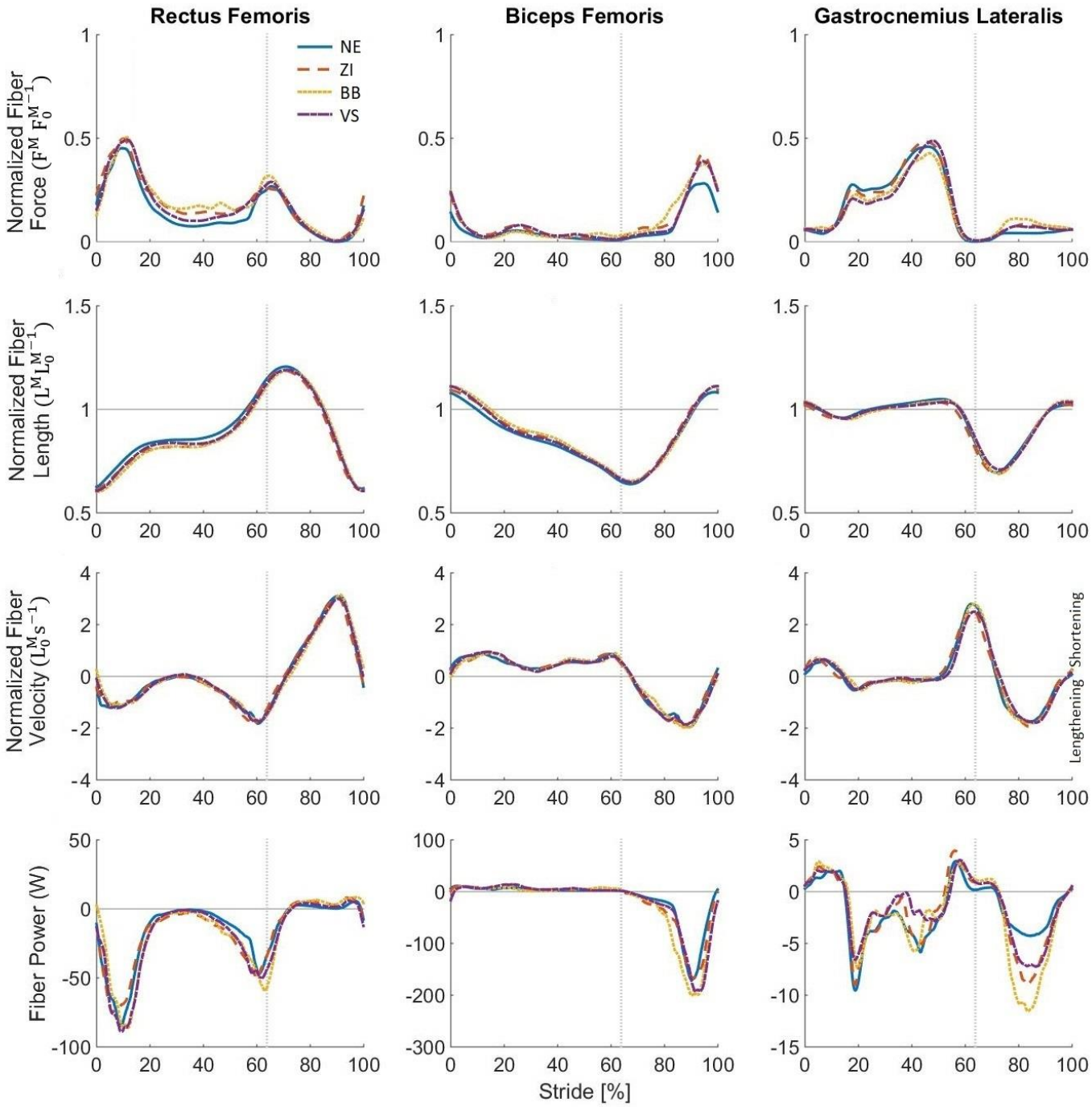

Fig. 13 Group mean plots of normalized fiber force (*N*=4 for RF and BF, *N*=5 for GL) , normalized fiber length (*N*=4 for RF and BF, *N*=7 for GL), normalized fiber velocity (*N*=4 for RF and BF, *N*=7 for GL) and fiber power (*N*=4 for RF and BF, *N*=5 for GL) for rectus femoris, biceps femoris and gastrocnemius lateralis. Positive values for fiber velocity correspond to muscle fiber shortening. Solid blue lines represent the no exoskeleton condition (NE), orange dashed lines represent walking with the exoskeleton in zero impedance mode (ZI), yellow dotted lines represent the bang bang condition (BB) and purple dash-dotted lines represent the virtual spring condition (VS). Data are normalized to stride cycle time (0-100%), with 0% representing heel strike and the grey dotted vertical lines representing the average toe off (63.8%). F, fiber force; F_{max}, maximum isometric force; L, fiber length; L_0, optimum fiber length.

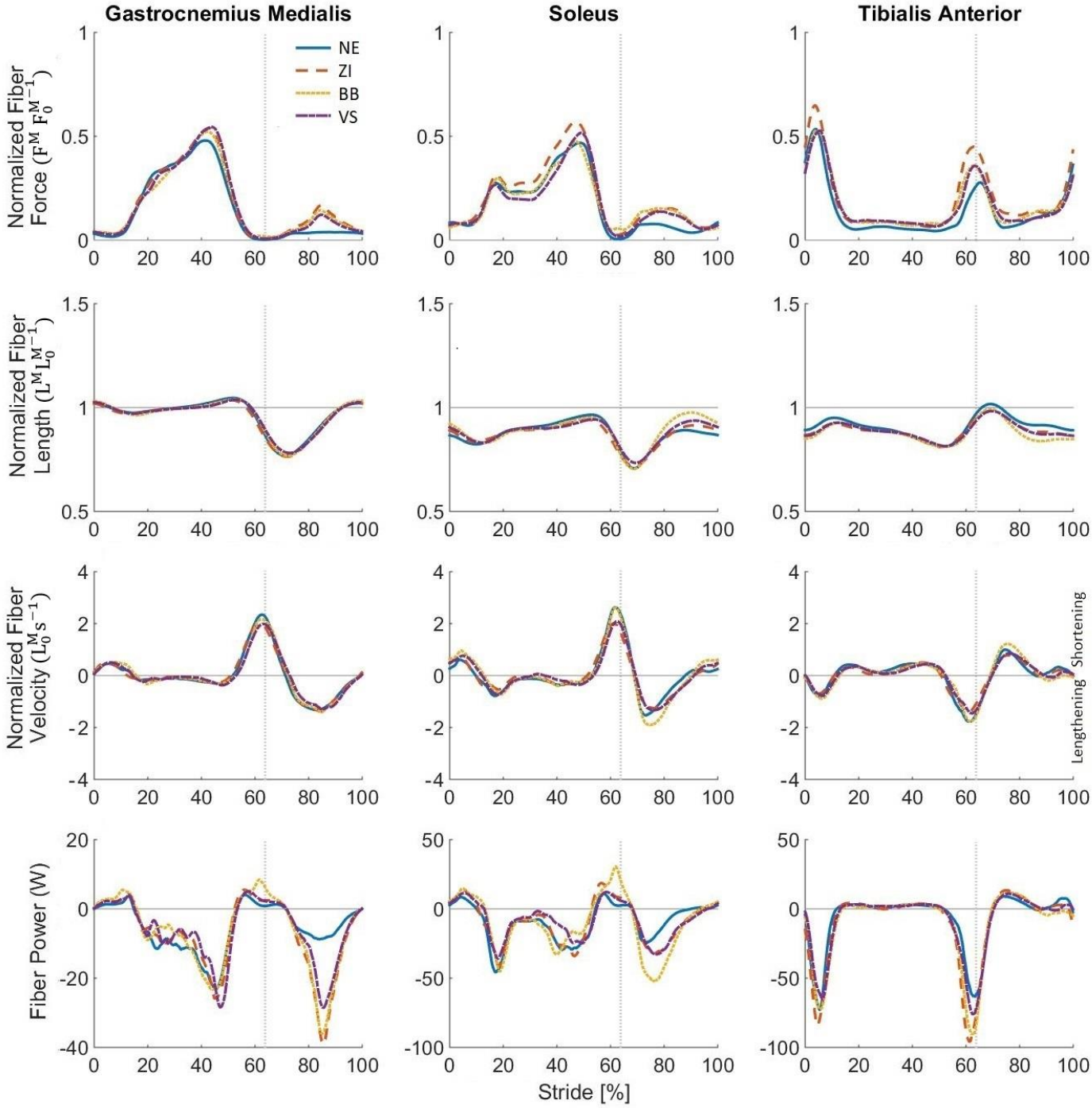

Fig. 14 Group mean plots of normalized fiber force (*N*=5 for GM and SO, *N*=6 for TA), normalized fiber length (*N*=7), normalized fiber velocity (*N*=7) and fiber power (*N*=5 for GM and SO, *N*=6 for TA) for gastrocnemius medialis, soleus and tibialis anterior. Positive values for fiber velocity correspond to muscle fiber shortening. Solid blue lines represent the no exoskeleton condition (NE), orange dashed lines represent walking with the exoskeleton in zero impedance mode (ZI), yellow dotted lines represent the bang bang condition (BB) and purple dash-dotted lines represent the virtual spring condition (VS). Data are normalized to stride cycle time (0-100%), with 0% representing heel strike and the grey dotted vertical lines representing the average toe off (63.8%). F, fiber force; F_{max}, maximum isometric force; L, fiber length; L_0, optimum fiber length.

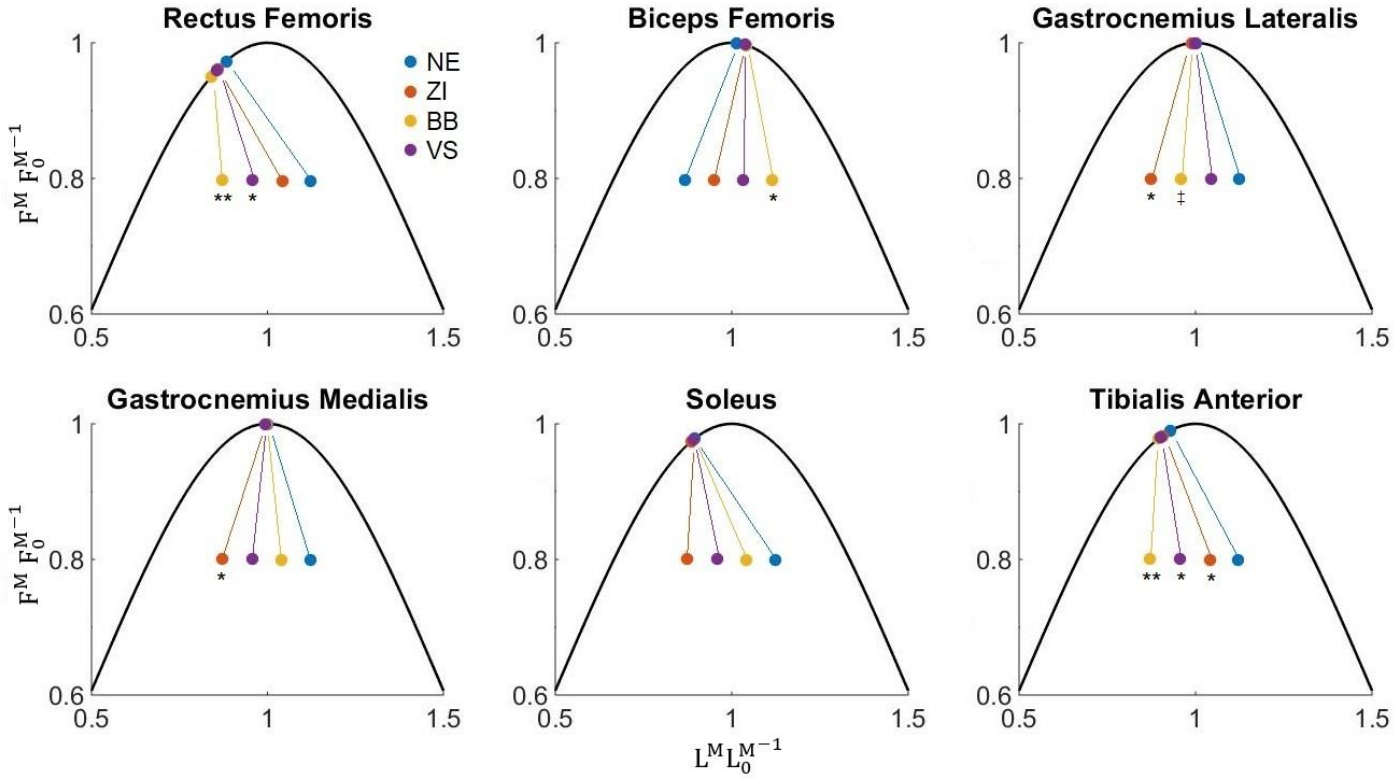

Fig. 15 Force-length curve with the average operating lengths for each muscle during each condition. The curve represents the relationship between muscle force ($\boldsymbol{F^M}$) and muscle fiber length ($\boldsymbol{L^M}$) as described in 2.5. The more a muscle length deviates from the optimum fiber length ($\boldsymbol{L_0^M}$), the less force it can produce for any given activation level. *Statistically significant difference compared to no exo condition ($P < 0.05$). **Statistically significant difference compared to no exo condition ($P < 0.01$). ‡Statistically significant difference compared to zero impedance condition ($P < 0.05$). ‡‡Statistically significant difference compared to zero impedance condition ($P < 0.01$).

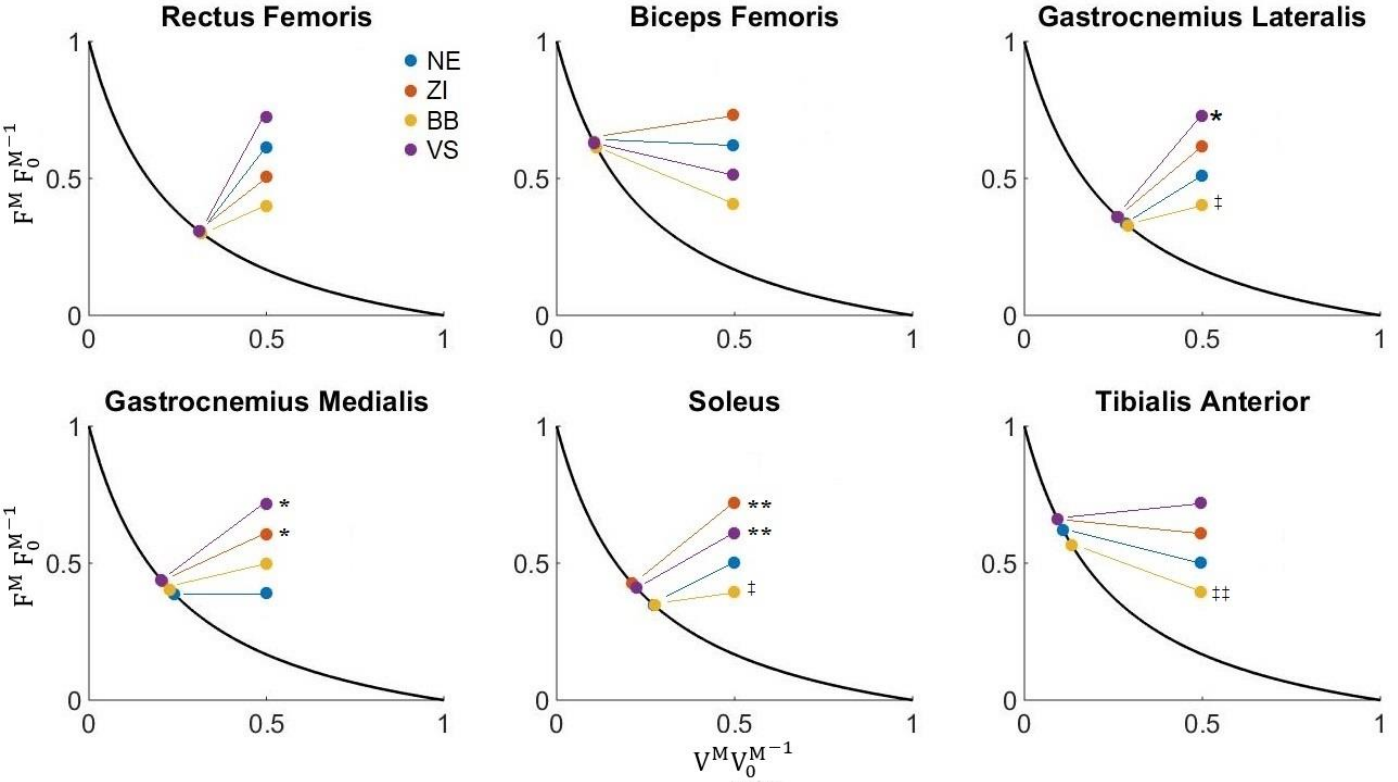

Fig. 16 Force-velocity curve with the peak velocities for each muscle during each condition. The curve represents the relationship between muscle force ($\boldsymbol{F^M}$) and muscle fiber velocity ($\boldsymbol{V^M}$) as described in 2.5. The faster a muscle shortens, the less force it can produce for any given activation level. *Statistically significant difference compared to no exo condition ($P < 0.05$). **Statistically significant difference compared to no exo condition ($P < 0.01$). ‡Statistically significant difference compared to zero impedance condition ($P < 0.05$). ‡‡Statistically significant difference compared to zero impedance condition ($P < 0.01$).

4

Discussion

4.1 Metabolic cost

Metabolic cost increased when wearing the exoskeleton without assistance compared to normal walking. This was expected when looking at previous results with the Achilles (van Dijk, 2015; van Dijk et al., 2017) and given the added weight of the exoskeleton. When using the results of Browning et al. (2007), mentioned in 1.4.1, one would predict an increase of 42W; 6 kg added to the waist, 1.2 kg added to each shank and 0.3 kg added to each foot. While van Dijk found a smaller than expected increase of 22.7W when walking with the exoskeleton at 3.5 km h^{-1}, this study found an increase of 103W (table 7) on average when walking at 4.5 km h^{-1}, more than double the amount of what one would expect. Differences in walking speed might partially be the reason of the differences found between this study and van Dijk's evaluation of the Achilles. It was however found that there was a substantial amount of friction between moving parts, likely due to debris and wear inside the leg parts, that has been accumulated over the years. This friction may be the biggest contributor to the larger than expected metabolic increase.

During measurements with the third subject a ball bearing in one of the actuator parts broke, which is the reason for not using the results of this subject. Note that the order of subject numbers in table 7 is not the order in which measurements were done, e.g. subject number five in table 7 participated as the third volunteer during the experiments. The mean increase of the metabolic rate, when considering the six subjects that were measured after replacement of the ball bearing, was 86W. This is still double the expected increase, but the improvement after replacement of one part suggests that friction, which eventually caused the part to fail, contributes to the bigger than expected increase in metabolic rate. Another contributor to the increased metabolic cost may have been the change in walking kinematics due to the exoskeleton. Although no significant changes were measured, likely due to a small sample size, there was a trend towards decreased plantarflexion after toe off.

Group mean metabolic cost of walking during bang-bang assistance was reduced significantly compared to no assistance. A reduction was expected, considering that the control method is based on multiple ankle exoskeletons that also managed to reduce metabolic cost. It is interesting to note that there was a large variety between individuals (table 7); for one subject the rate increased by 3%, while for the other seven subjects their rate decreased between 2.7% and 13% compared to no support. An explanation for this can be found in two recently published papers by Zhang et al. (2017) and Jackson and Collins (2017). Both papers describe walking experiments with an exoskeleton that has an adaptive controller.

In short, Zhang et al. use an evolution strategy to find an optimal torque pattern at different walking speeds; during walking trials the torque pattern is systematically modified based on a set of control laws by changing one or more of these four parameters: peak torque, timing of peak torque, rise time (time in which peak torque is reached) and fall time. A visual representation of these parameters is shown in Fig. 17a. Results were evaluated in real-time based on respiratory data, the evaluation of one set of control laws forms one generation and the best results of this generation form the basis for the control laws of the next generation. After some generations an optimized torque pattern is reached tailored to a specific subject. With this strategy they managed to lower the metabolic cost of walking by 24.2±7.4% compared to no torque. The parameter values

differed greatly across subjects; the range of torque profiles is shown in Fig. 17b, including the measured torque patterns from this study. When comparing Zhang's study with this one, it can be seen that peak torques were higher in Zhang's study, however it was not possible to reach these peaks with the Achilles. Peak time of the virtual spring and bang-bang control methods occur within the range of peak time found by Zhang. Hypothetically increasing the peak torque of the bang-bang controller should increase the rise time and the total torque pattern should fall within the range of torque profiles found by Zhang et al., this would help in reducing the metabolic cost of walking further but it would not result in the optimal profile for all subjects, which requires a pattern tailored to each individual.

Jackson and Collins, who were also involved in the study by Zhang et al., used the same exoskeleton for their experiment, but implemented an electromyography-based adaptive controller. The torque pattern of this controller was continuously updated based on EMG data of soleus and tibialis anterior, with the aim of taking over the soleus function and reducing muscle activity of the soleus muscle to zero. The metabolic rate of subjects showed a 22% reduction, along with significantly lower soleus activity, after 30 minutes of walking with the adaptive controller, compared to zero torque. As with the study by Zhang et al. there were large variations between final torque patterns and since the patterns were adapted independently for each leg, there was even a variation found between left and right legs.

These two studies emphasize the diversity of human beings and that tailor-made controllers are the way to go when striving for the biggest possible reduction in metabolic cost. They might also explain why the 'one size fits all'-methods used in this study, which only adjusted for body weight, had a better result on some subjects, whereas others hardly decreased their energy consumption rate or even increased it.

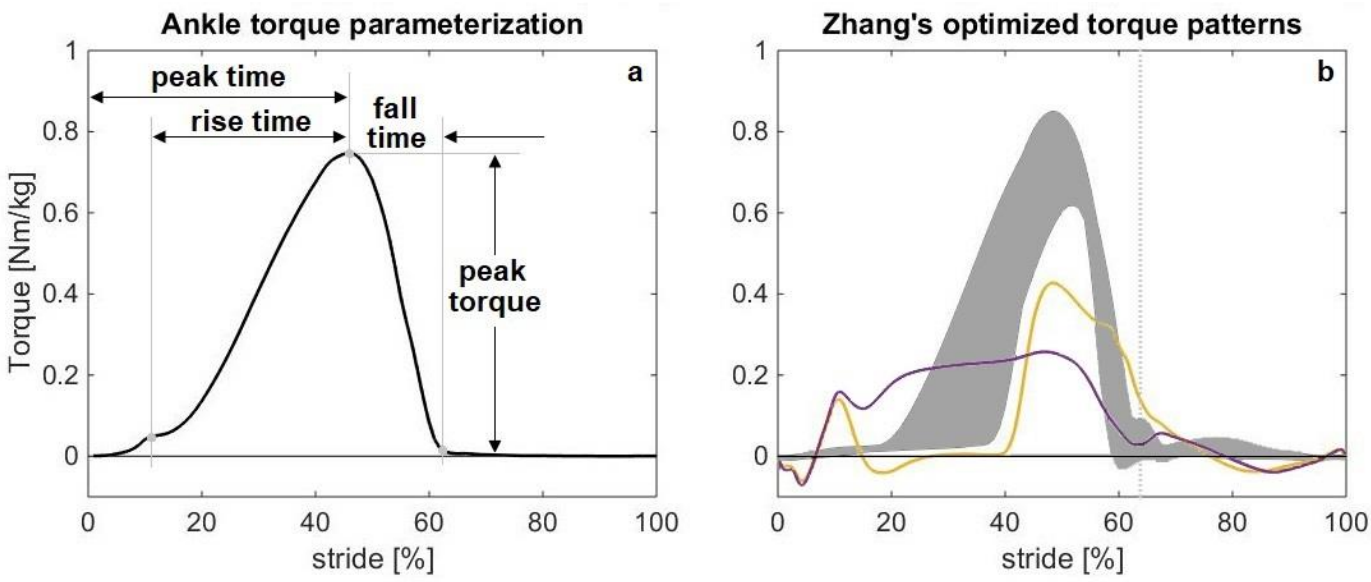

Fig. 17a: The torque profiles used by Zhang et al. (2017) were defined by the parameters shown. b: The grey area depicts the range of optimized torque patterns found by Zhang et al. (2017). Data from Zhang et al. (2017) was used to generate these images. Each of the four parameters shown in 17a was adjusted according to certain control laws to find better torque profiles after each adjustment. The optimized torque profiles differed greatly between subjects, they all fall within the grey area shown in 17b. The yellow and purple line show the mean exoskeleton torque as measured during the bang-bang and virtual spring conditions respectively.

4.2 Kinematics & kinetics

4.2.1 Kinematics

Continuing with the fact that each human is unique, it was found that toe off does not occur at the same time for each subject; some have a longer stance phase and a shorter swing phase. The bang-bang condition was based on heel strike and stride time and did not account for this variability; the onset and offset time were fixed at 43% and 63% of the stride cycle. Again, referring to the previously mentioned study, Zhang et al. (2017) found that optimal values for rise and fall time varied greatly across subjects and this may explain the small shift in toe off timing observed for some subjects (Appendix B, Fig. 21). Individual shifts in toe off timing ranging between -1.2% and 1.4% were observed for the bang-bang condition, compared to normal walking, where a negative shift means toe off occurs earlier during a stride, resulting in a shorter stance phase. However, it should be noted that the virtual spring condition had a similar range (between -1.4% and 1.6%), while this controller relied on ankle angle for timing of assistance.

Apart from the technical issues with two of the four available motion trackers, there was also a problem involving the recording of the motion capture data; not all marker clusters could be fixed properly to each body parts. The legs were not a problem since markers could be placed on bare skin. The ones on the feet, which had to be placed on the shoes, were also less of a problem since these shoes were tightly tied to the feet. The main problem was with the clusters that had to be placed on the pelvis and torso, these had to be placed on top of loose clothes and although most effort was done to ensure the clusters did not move, by using double sided tape and straps that were put tightly around the hip and torso, there were still occasions in between measurements where some displacement of one of the clusters occurred. The resulting shift led to a clear offset of the hip angle for some subjects as the example in Fig. 18 shows. Getting in and out of the exoskeleton increased the likelihood of such displacements, this was one of the reasons that the no-exo condition was always the last condition to be measured, meaning that the subjects only had to get out of the exoskeleton once in between measurements and did not have to get back in it.

It is needless to say that hip angle data affected by this was not used for the computation of muscle properties that relied on this data, which are the upper leg muscles, RF and BF, that have their origin located on the pelvis.

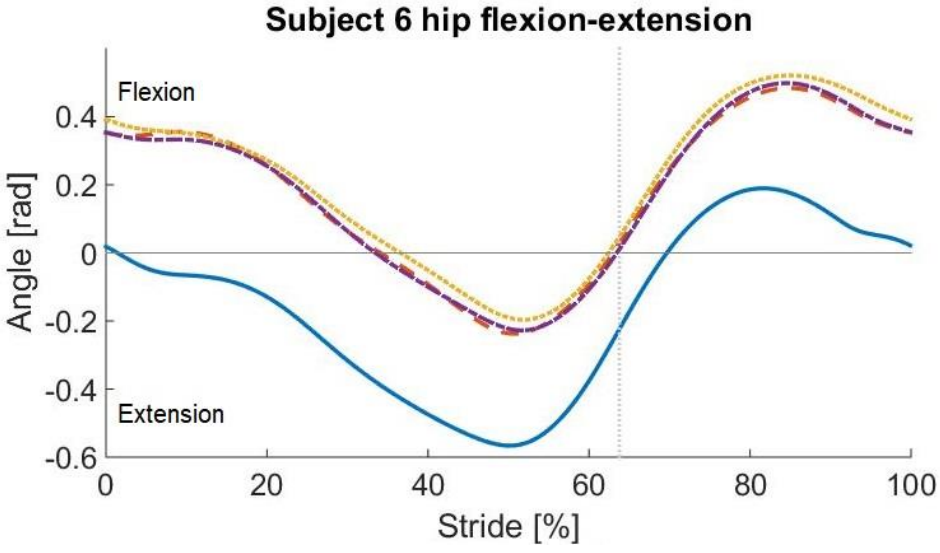

Fig. 18 Clear example of an offset in hip angle for the no-exo condition, found after processing motion capture data and performing inverse kinematics. The likely cause is a displacement of the pelvis marker cluster. The exoskeleton had to be removed for this last condition which increases the likelihood that marker clusters shift position.

Angular velocity and acceleration of the ankle before toe off was larger for the no exo condition (Fig. 10D), compared to the exoskeleton conditions. This can be explained by the increased inertia, due to the added mass, and the friction as already discussed in 4.1. The lower angular velocity caused the trend towards a decrease in plantarflexion. This result was not significant due to the small sample size, but Van Dijk et al. (2017) found similar reductions in ankle plantarflexion during their evaluation of the Achilles exoskeleton and also found that the effect was smaller for the support condition, from Fig. 10A it can be seen that indeed peak plantarflexion for the no support or ZI condition shows the largest deviation compared to normal walking.

Besides the ankle kinematics computed from marker data, there was also a recording of the ankle angle through encoders implemented in the Achilles exoskeleton. Angle and angular velocity from these encoders are plotted in figures 10C and 10F, what immediately stands out is that these recordings do not match the ankle angles that were computed through inverse kinematics. The mismatches are found to be largest during periods of high angular acceleration, during early and late stance. A possible explanation for this might be that because of the compliance of the shoes the distance between the foot shell (Fig. 5a) and the instep of the foot, on top of which the foot markers are placed, changes during these periods.

4.2.2 Kinetics

The encoder errors mentioned above may also explain the unwanted exoskeleton torque around 10% of the stride for all exoskeleton conditions, as well as the small negative and positive torque before and after toe off for the ZI condition (Fig. 10I) and the support torque patterns that are slightly different from the desired torque patterns. These unwanted torques might not have occurred at all or at least not as large as they are depicted in Fig. 10I, since this torque is computed by calculating the spring deflection, which is a function of the motor stroke and ankle angle, both measured by encoders (section 2.3.2 and Fig. 5a) and hence an incorrect ankle angle measurement will result in an incorrect recording of the spring deflection and exoskeleton torque.

Exoskeleton assistance was limited due to a maximum power output of 165W, as discussed in section 2.2.2, meaning peak torque was for the bang-bang condition was set to 0.4 N m kg^{-1}. This was sufficient to significantly reduce the metabolic cost of walking compared to no support, however, more substantial reductions may be achieved with more power and larger torques. When examining recent studies that use similar control strategies it can be found that many use larger average and peak torques and power, with peak torques up to 1.0 N m kg^{-1} (e.g. Mooney et al., 2014b; Jackson and Collins, 2015; and Zhang et al., 2017), resulting in metabolic reductions up to 24%. It should however be noted that maximizing exoskeleton torque, positive power and mechanical work does not necessarily equate to a further reduction of metabolic rate (Lee et al., 2016; Zhang et al., 2017).

4.3 Muscle activity

After processing raw EMG data it became apparent that some measurements were affected by either crosstalk or pressure or (cable-) movement artifacts. There was only a test performed whether each electrode provided a valid signal, not whether they were positioned correctly. This might have led to crosstalk in some cases. The pressure artifacts are mainly seen in the EMG data of the plantarflexors (GM, GL and SO) and can be explained by the fact that the shell parts of the Achilles exoskeleton were strapped tightly around the lower leg, squeezing the surface electrodes between the shell and the calf of the subject. Removing the exoskeleton for the normal walking condition led to a significantly lower EMG signal in some cases, Fig. 19 shows an example of this.

The EMG measurements of the muscles affected by these anomalies were not used to compute group averages. The same goes for the calculation of group means of muscle properties that were calculated using a function containing muscle activation, such as muscle fiber force (eq. 12). This is the reason why some muscle properties have a sample size of only four or five.

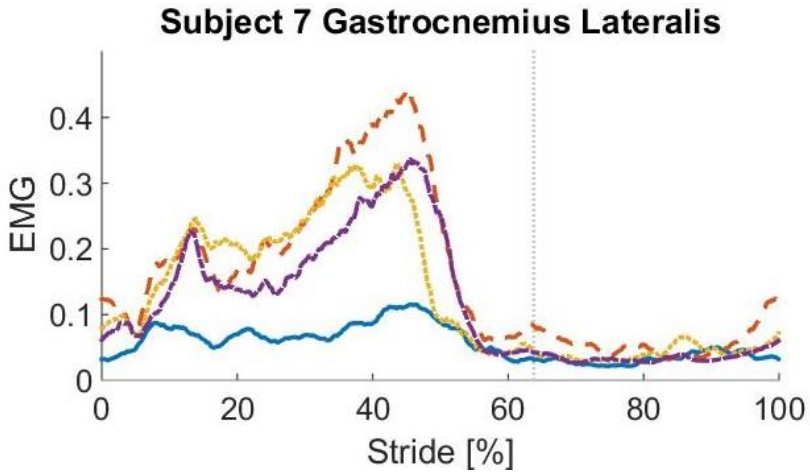

Fig. 19 Processed EMG of gastrocnemius lateralis shows a lower signal strength for subject 7 after the exoskeleton is removed. The shell parts of Achilles strapped around the calf, pressing the electrodes on the skin may have caused the signal to be stronger, compared to the condition without the exoskeleton.

4.4 Musculoskeletal Simulations

A consequence of the EMG anomalies and kinematic measurement errors discussed in 4.2 and 4.3 is that some data was rendered useless for performing simulations to compute muscle mechanics. Muscle properties such as fiber length and velocity were computed using kinematic data, therefore still a reasonable sample size could be used to compute these for the ankle plantarflexors that were affected by the EMG pressure artifacts. Other properties such as fiber force and work depend on fiber length, speed and muscle activity, for that reason the upper leg muscles, RF and BF, were affected the most since these suffered from both EMG measurement errors, as well as the errors in hip angle due to marker displacements seen in three subjects.

Results may have been affected by the fact that the musculoskeletal model and Achilles exoskeleton were not modelled as a perfect copy of reality. However the movements and reaction forces were taken from measured data and prescribed to the model, therefore the lack of inertial properties of the modelled exoskeleton may not have had any influence on the muscle mechanics, since the motion was fixed and the extra mass was accounted for in the reaction forces.

4.4.1 Muscle energetics

Table 6 shows the summed energy consumption per stride for the dorsi- and plantarflexors. As expected there was a significant increase for all exoskeleton conditions, this is in line with the total body energy consumption rate found through respiratory data. Converting the energy consumption to metabolic rate, by dividing by stride time (table 2) and multiplying by two, assuming muscles in both legs were affected the same, we find that metabolic rate increased by 0.35, 0.33 and 0.22 W kg^{-1} for the ZI, BB and VS conditions respectively. While whole-body metabolic rate increased by 1.31, 1.01 and 1.21 W kg^{-1}. A reason for this difference is that the increase is only partially due to ankle flexors, other muscles such as the ones in the upper legs and torso also have increased due to the added weight of the exoskeleton, which result in increased reaction forces. It is estimated that ankle flexors account for ~27% of the total energy consumption during walking (Umberger and Rubenson, 2011). Assuming all other muscles equally increase their energy expenditure with exoskeleton walking we find that the simulated whole-body metabolic rate for the baseline exoskeleton condition (ZI) increased by (0.35*100)/27 = 1.30 W kg^{-1}, which is more in line with the actual measurements. When assuming the support conditions only affected the plantar- and dorsiflexor muscles, one can simply subtract the difference between the no support and the support conditions, i.e. for BB 1.30 – (0.35-0.33) = 1.28 W kg^{-1} and for VS 1.30 – (0.35-0.22) = 1.17 W kg^{-1}. There are still some differences between measured and simulated metabolic rate, this may be due to the fact that each musculoskeletal model is not an exact replication of the corresponding subject and the assumption that these support conditions only affect ankle flexors might also be wrong. Collins et al. (2015) and Farris et al. (2014a) have both suggested that ankle exoskeletons

might also influence muscles in the upper leg. Reasoning behind this is that the plantarflexors gastrocnemius lateralis and medialis both also assist during knee flexion. A change in the muscle mechanics of these will therefore alter knee flexion and subsequently the mechanics of other muscles associated with knee flexion.

4.4.2 Muscle mechanics

Lower extremity kinematics were altered minimally, consequently it was found that changes in muscle fiber lengths and velocities, presented in tables 3-5 and figures 12-16, were also small between all conditions. This is a good sign, given that the muscles that were investigated already operate close to or at the optimal fiber length as can be seen in Fig. 15. The small differences imply that force producing capabilities remain the same and that mean and peak muscle force are largely dictated by the level of muscle activation (eq. 12). This explains, in most cases, where we see a significant increase in muscle activation we also see significant increases in force produced, work done and energy consumed.

One of the muscles that saw a somewhat larger change in muscle fiber velocity is the soleus. For this muscle the contraction velocity was lower for the no support and virtual spring support conditions (Fig. 16 & 20), on the force-velocity curve it can be seen that a slower contraction rate results in higher force producing capabilities, however, in this case it also means that power output, shown as the dashed line in Fig. 20, is lower compared to the other two conditions. Maximum power output is achieved at a shortening rate about a third of the maximum shortening velocity (V_0^M).

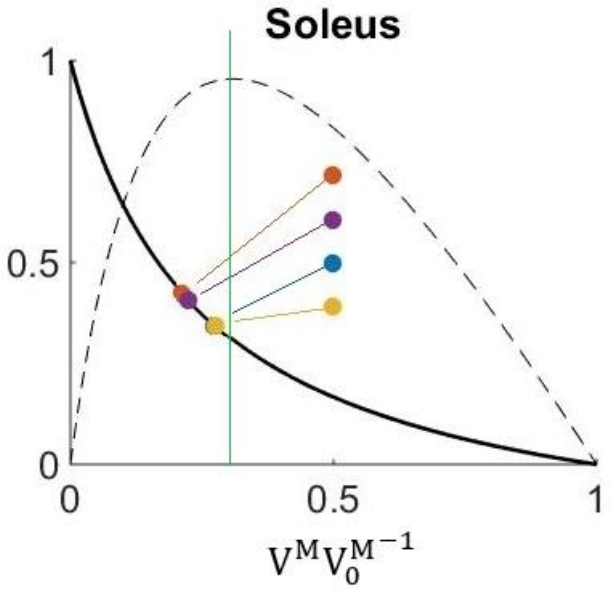

Fig. 20 Force-velocity curve for the soleus with the dashed line representing mechanical power output. Shortening velocity for maximum power output is approximately $\boldsymbol{V_0^M}$/3 (vertical green line). Although peak velocity for the ZI (orange) and VS (purple) conditions result in higher force producing capabilities it also means power output for these conditions is lower.

5

Conclusion

In this study two previously successful control methods were mimicked and implemented on the Achilles exoskeleton with the purpose of investigating possible changes to the human biomechanics to get a better understanding of how these supportive control methods make walking more energy efficient and how to possibly improve them. Walking experiments were performed to gain metabolic, kinematic, kinetic and EMG data. Due to an accumulation of EMG and kinematic measurement errors some of this data was rendered useless.

Processed data showed a significant increase of 39% in metabolic cost while wearing the exoskeleton in no support mode. One of the two support modes, bang-bang support, was able to reduce the metabolic rate by 6.3%, whereas the other support condition did not show a significant change compared to no support. Metabolic reductions of support conditions were limited due to a limited power output of the exoskeleton and might also have been affected by friction due to wear. Evaluation of kinematic data found that peak plantar- and dorsiflexion was reduced somewhat, likely because of added inertia by the exoskeleton. This effect was diminished by the bang-bang controller for peak plantarflexion. It was also found that the biological contribution to the ankle moment was reduced due to the exoskeleton torque and ankle power was consequently reduced for the bang-bang control method. Mean muscle activity, found through processing of EMG data, was shown to increase significantly for nearly all exoskeleton conditions and all muscles apart from gastrocnemius lateralis. Between no support and support conditions there was only a reduction found for the bang-bang and virtual spring conditions for soleus and tibialis anterior.

Apart from the analysis of gathered data there were also musculoskeletal simulations performed to get insight in the muscle mechanics. These simulations were performed in OpenSim and were driven by the collected experimental data. Conform to the small changes in kinematics there were also only small differences found in muscle fiber length and velocity, meaning force producing capabilities remained close to ideal for most muscles. The small changes in fiber length and velocity also meant that fiber force and work increased with the increased muscle activation. The increase of the summed energy consumption of the dorsi- and plantarflexors was found to be in line with the measured whole-body metabolic rate, validating the musculoskeletal model used.

The results suggest that providing net positive power before toe off is a more effective way at reducing the metabolic cost of walking compared to a passive control method that provides no net power and also that it may reduce any alterations to walking kinematics that may result from the added mass and inertia of an exoskeleton.

6

Recommendations

Future research done to find a better controller to control exoskeletons might start by performing simulations like the one done in this study and indeed a recent study by Dembia et al. (2017) have used such an approach. They used OpenSim to test seven hypothetical devices that could each provide a torque in one direction around either the hip (abduction, flexion or extension), knee (extension or flexion) or ankle (plantar- or dorsiflexion) to assist a musculoskeletal model during walking. Although results will not be as accurate as real life experiments, it requires less resources to setup such a simulation, basically a laptop or pc, a previously recorded dataset (this can be from any walking experiment) and the appropriate simulation software. Once a musculoskeletal model, including an exoskeleton, is set up in the simulation environment, one can test multiple control methods or tweak parameters in the same controller, such as activation timing and amount of torque, by applying the desired torque to the model. The controller can be tested in the lab, once the researcher is satisfied with the results of an optimized version found through simulations. A benefit of this, compared to using a custom exoskeleton in the lab, is reproducibility; data and scripts from such a simulation can be shared online to reproduce the results and others can extend upon the work.

This method, of trying out new (unconventional) controllers and optimizing them, might even yield unexpected outcomes, like the results found by Dembia et al. (2017), that would otherwise never have been found with physical modern-day exoskeletons. They for instance found that assisting hip abduction and flexion as well as knee flexion yielded higher metabolic reductions compared to assistance of the ankle, while nowadays the focus of many exoskeletons have been on assisting the latter. Again such a study has its limitation and might not give similar results in the real world, given the complexity of the human body and its behavior, but such results are interesting nonetheless and may lead to new and possibly better concepts.

When performing lab experiments it is recommended to gain experience with the equipment and actions to be performed, a lack of experience may lead to useless data, as was the case in this study. One should furthermore aim to recruit more subjects to get better, more significant results. The aim for this study was to test twelve subjects, but due to the exoskeleton breaking down twice the number of subjects completing all trials was only eight and, as discussed, it was later found that data from some of these eight was of no use because of measurement errors.

Appendices

Appendix A: Metabolic rate per individual

	Weight	Rest	No exo	No support	Bang-bang	Virtual spring
Subject	m [kg]	$\dot{E}$ [W kg^{-1}]	$\dot{E}$ [W kg^{-1}]	$\dot{E}$ [W kg^{-1}]	$\dot{E}$ [W kg^{-1}]	$\dot{E}$ [W kg^{-1}]
1	59	1.26	4.67	6.56	6.23	6.54
2	76	1.58	5.09	6.31	6.45	6.16
3	67	1.58	4.66	5.94	5.66	5.79
4	85	1.25	4.30	6.61	6.09	6.58
5	67	1.52	5.04	5.56	5.21	5.46
6	85	1.65	5.23	5.93	5.47	5.92
7	71	1.50	4.63	5.89	5.77	5.96
8	77	1.21	4.45	5.92	-	5.94
9	80	1.52	5.16	6.41	5.94	6.28
10	80	1.66	5.10	6.19	5.60	5.56
Mean	75.4	1.50	4.86	6.23	5.90	6.10
SD	9.1	0.16	0.33	0.29	0.34	0.36
NetMean		0	3.39	4.70	4.40	4.60
SD		0	0.20	0.38	0.45	0.51

Table 7 Weight and normalized metabolic rate for each subject. NetMean shows mean for net metabolic rate, i.e. resting rate subtracted from total metabolic rate. Results in grey were excluded because of technical problems with the Achilles exoskeleton. This order was not the order of measurements; 10 subjects were recruited and given a subject number before measurements started, the actual order of measurements is: Subject 1, 4, 5, 6, 7, 2, 3, 9, 10, 8.

Appendix B: Individual kinematics and kinetics

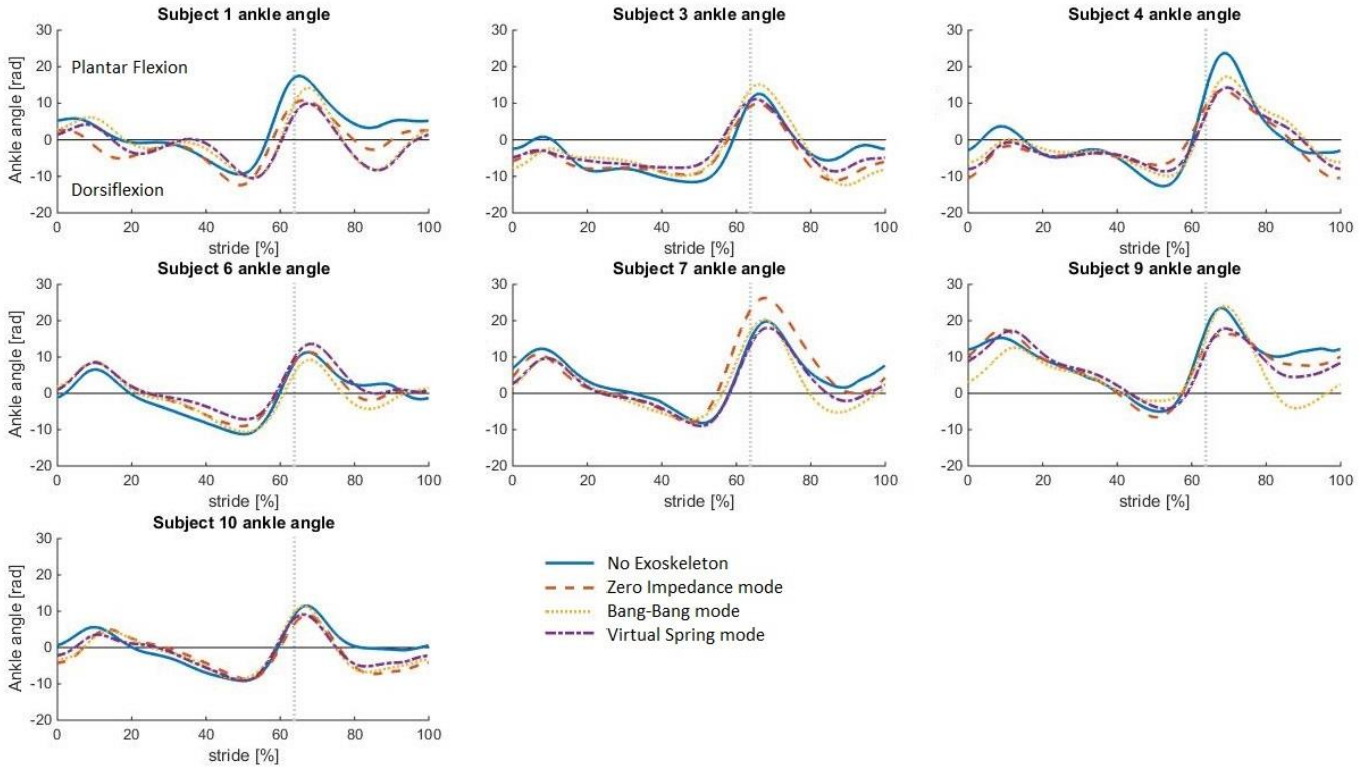

Fig. 21 Plots of mean ankle angle of each individual subject during the four walking conditions. Positive angle corresponds to dorsiflexion. Solid blue lines represent the no exoskeleton condition (NE), orange dashed lines represent walking with the exoskeleton in zero impedance mode (ZI), yellow dotted lines represent the bang bang condition (BB) and purple dash-dotted lines represent the virtual spring condition (VS). Data are normalized to stride cycle time (0-100%), with 0% representing heel strike and the grey dotted vertical lines representing the average toe off (63.8%).

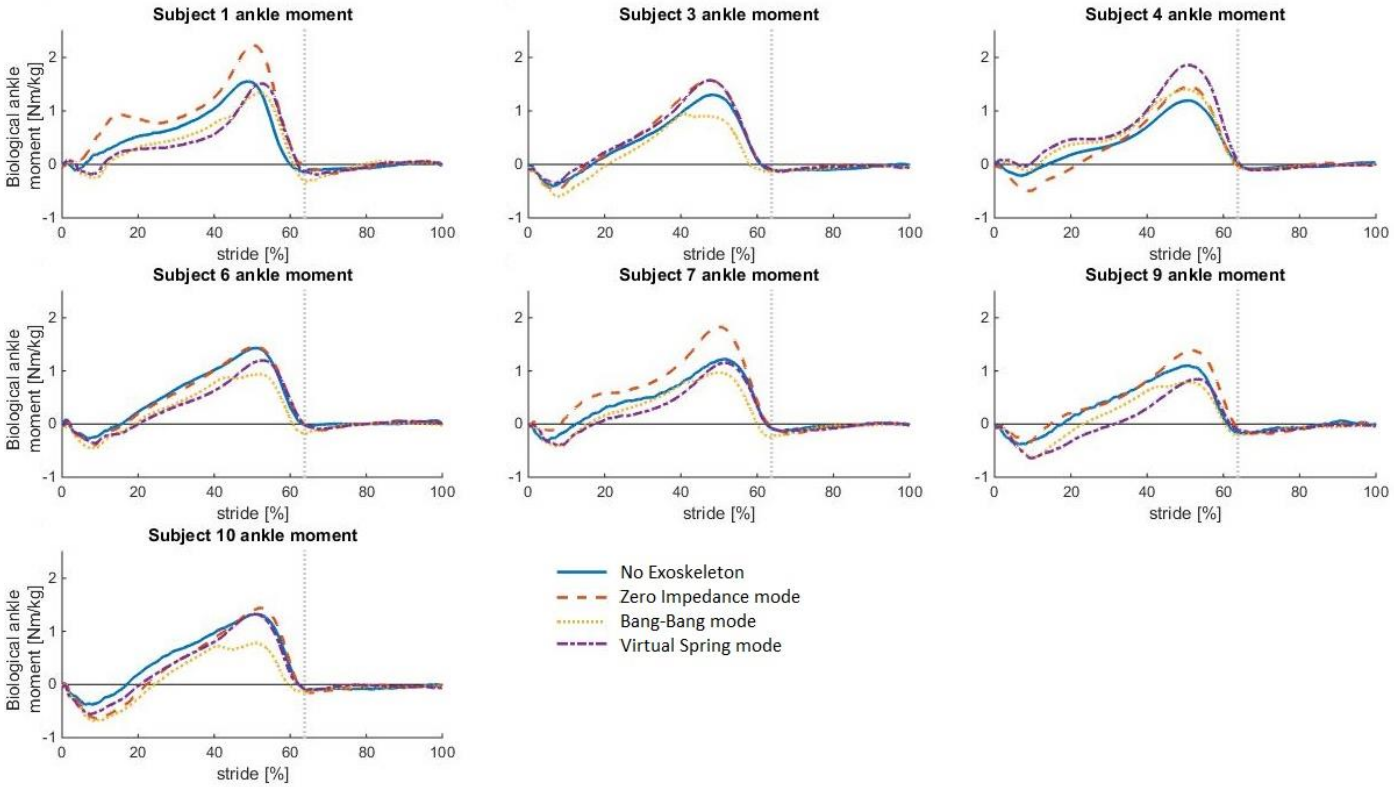

Fig. 22 Plots of mean normalized biological component of ankle moment of each individual subject during the four walking conditions. The biological component for the exoskeleton conditions was computed by subtracting exoskeleton torque from total ankle moment. Values were normalized to subject body mass. Solid blue lines represent the no exoskeleton condition (NE), orange dashed lines represent walking with the exoskeleton in zero impedance mode (ZI), yellow dotted lines represent the bang bang condition (BB) and purple dash-dotted lines represent the virtual spring condition (VS). Data are normalized to stride cycle time (0-100%), with 0% representing heel strike and the grey dotted vertical lines representing the average toe off (63.8%).

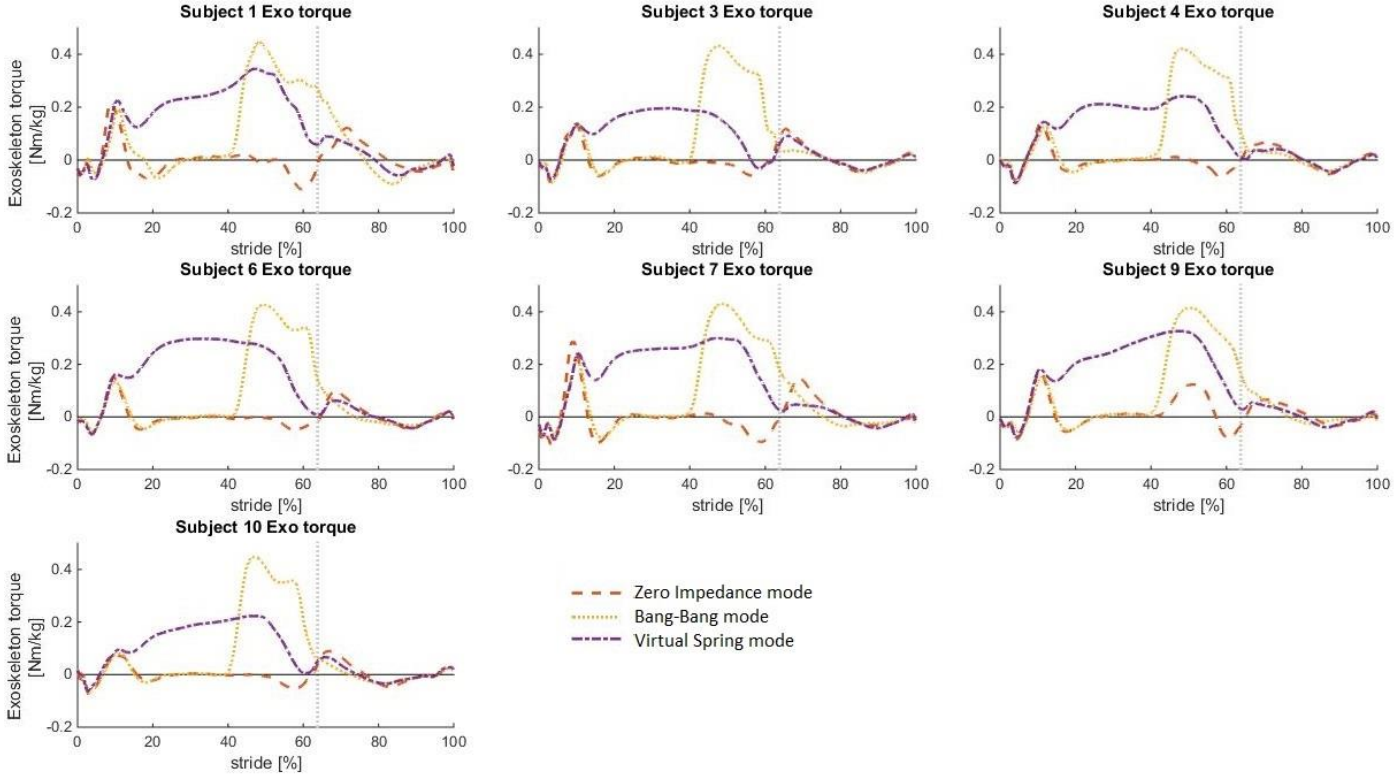

Fig. 23 Plots of mean normalized exoskeleton torque of each individual subject during the three exoskeleton walking conditions. Values were normalized to subject body mass. Solid blue lines represent the no exoskeleton condition (NE), orange dashed lines represent walking with the exoskeleton in zero impedance mode (ZI), yellow dotted lines represent the bang bang condition (BB) and purple dash-dotted lines represent the virtual spring condition (VS). Data are normalized to stride cycle time (0-100%), with 0% representing heel strike and the grey dotted vertical lines representing the average toe off (63.8%).

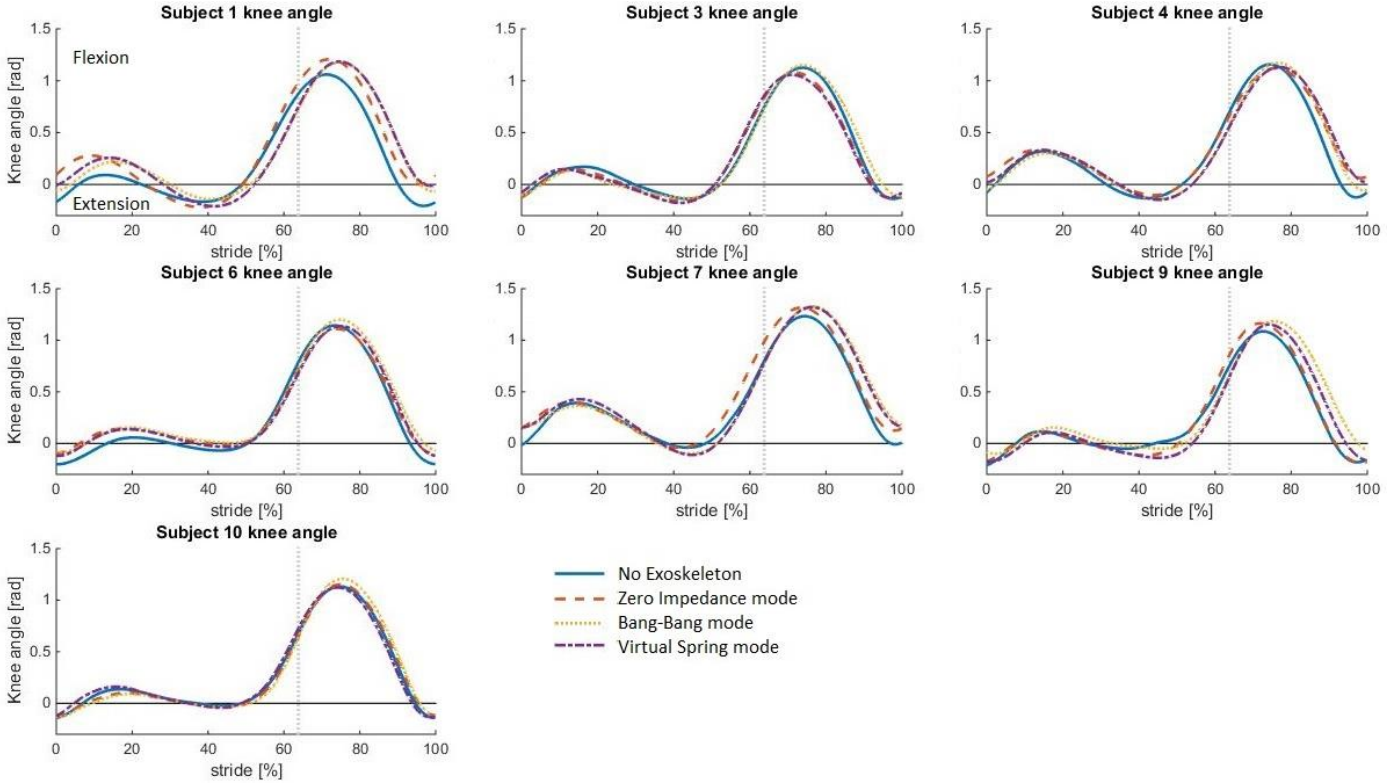

Fig. 24 Plots of mean knee angle of each individual subject during the four walking conditions. Positive angle corresponds to flexion. Solid blue lines represent the no exoskeleton condition (NE), orange dashed lines represent walking with the exoskeleton in zero impedance mode (ZI), yellow dotted lines represent the bang bang condition (BB) and purple dash-dotted lines represent the virtual spring condition (VS). Data are normalized to stride cycle time (0-100%), with 0% representing heel strike and the grey dotted vertical lines representing the average toe off (63.8%).

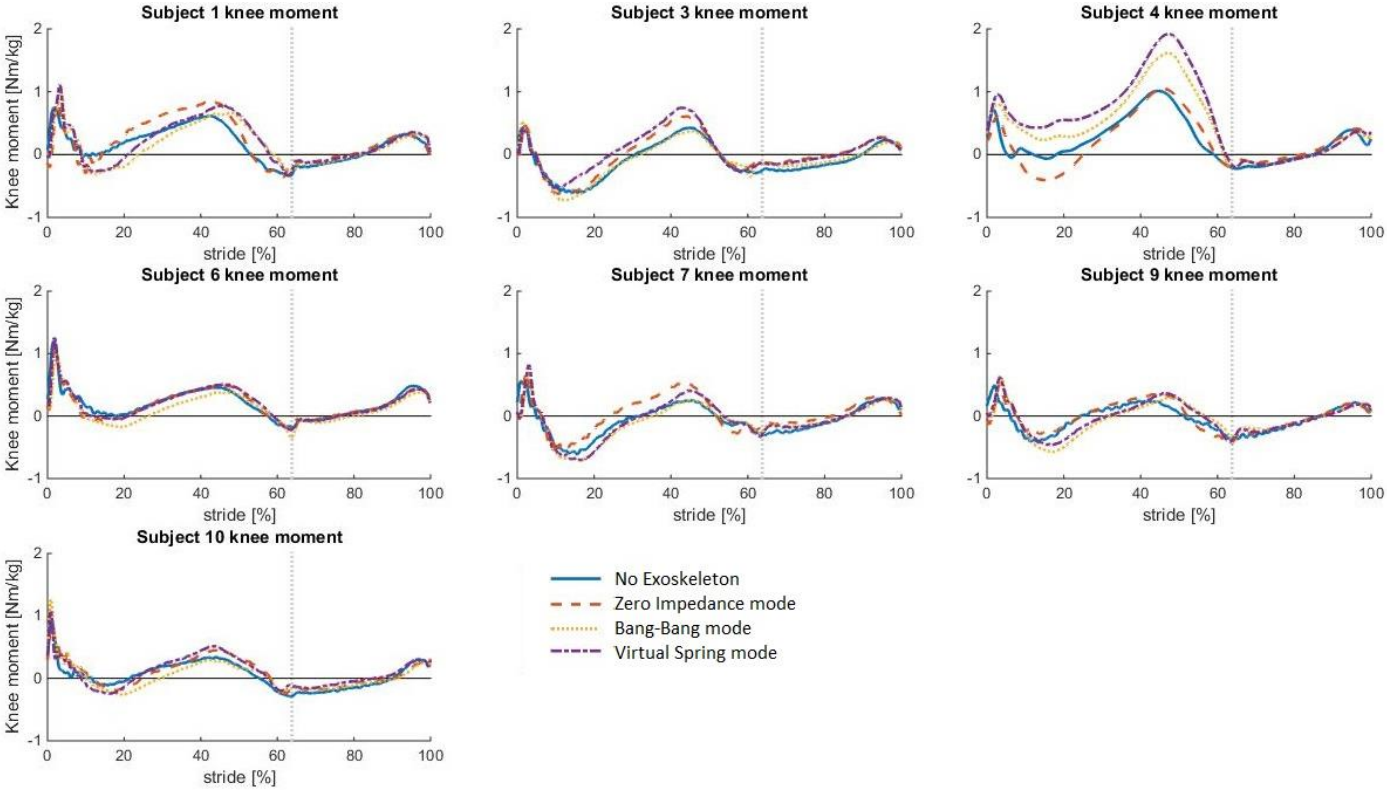

Fig. 25 Plots of mean normalized knee moment of each individual subject during the four walking conditions. Values were normalized to subject body mass. Solid blue lines represent the no exoskeleton condition (NE), orange dashed lines represent walking with the exoskeleton in zero impedance mode (ZI), yellow dotted lines represent the bang bang condition (BB) and purple dash-dotted lines represent the virtual spring condition (VS). Data are normalized to stride cycle time (0-100%), with 0% representing heel strike and the grey dotted vertical lines representing the average toe off (63.8%).

Bibliography

Alexander, R. M., & Bennet-Clark, H. C. (1977). Storage of elastic strain energy in muscle and other tissues. *Nature*, *265*(5590), 114-117.

Anderson, F. C., & Pandy, M. G. (1999). A dynamic optimization solution for vertical jumping in three dimensions. *Computer methods in biomechanics and biomedical engineering*, *2*(3), 201-231.

Arnold, E. M., Hamner, S. R., Seth, A., Millard, M., & Delp, S. L. (2013a). How muscle fiber lengths and velocities affect muscle force generation as humans walk and run at different speeds. *Journal of Experimental Biology*, *216*(11), 2150-2160.

Arnold, E. M., Hamner, S. R., Seth, A., Millard, M., & Delp, S. L. (2013b). How muscle fiber lengths and velocities affect muscle force generation as humans walk and run at different speeds. *Supplementary material* URL: https://simtk.org/frs/?group_id=769

Asbeck, A. T., Dyer, R. J., Larusson, A. F., & Walsh, C. J. (2013). Biologically-inspired soft exosuit. *Rehabilitation robotics (ICORR), 2013 IEEE international conference on* (pp. 1-8). IEEE.

Asbeck, A. T., De Rossi, S. M., Holt, K. G., & Walsh, C. J. (2015). A biologically inspired soft exosuit for walking assistance. *The International Journal of Robotics Research*, *34*(6), 744-762.

Banala, S. K., Kim, S. H., Agrawal, S. K., & Scholz, J. P. (2009). Robot assisted gait training with active leg exoskeleton (ALEX). *IEEE Transactions on Neural Systems and Rehabilitation Engineering*, *17*(1), 2-8.

Brockway, J. M. (1987). Derivation of formulae used to calculate energy expenditure in man. *Human nutrition. Clinical nutrition*, *41*(6), 463-471.

Brown, M., Fisher, J. S., & Salsich, G. (1999). Stiffness and muscle function with age and reduced muscle use. *Journal of orthopaedic research*, *17*(3), 409-414.

Browning, R.C., Modica, J.R., Kram, R., & Goswami, A., (2007). The effects of adding mass to the legs on the energetics and biomechanics of walking. Med Sci Sport. Exerc. 39, 515–25.

Cain, S. M., Gordon, K. E., & Ferris, D. P. (2007). Locomotor adaptation to a powered ankle-foot orthosis depends on control method. *Journal of Neuroengineering and Rehabilitation*, *4*(1), 48.

Collins, S. H., Wisse, M., & Ruina, A. (2001). A three-dimensional passive-dynamic walking robot with two legs and knees. *The International Journal of Robotics Research*, *20*(7), 607-615.

Collins, S. H., Wiggin, M. B., & Sawicki, G. S. (2015). Reducing the energy cost of human walking using an unpowered exoskeleton. *Nature*.

Constable, J. K., Barclay, C. J., & Gibbs, C. L. (1997). Energetics of lengthening in mouse and toad skeletal muscles. *The Journal of physiology*, *505*(1), 205-215.

Dembia, C. L., Silder, A., Uchida, T. K., Hicks, J. L., & Delp, S. L. (2017). Simulating ideal assistive devices to reduce the metabolic cost of walking with heavy loads. *PloS one*, *12*(7), e0180320.

De Leva, P. (1996). Adjustments to Zatsiorsky-Seluyanov's segment inertia parameters. *Journal of biomechanics*, *29*(9), 1223-1230.

Delp, S. L., Anderson, F. C., Arnold, A. S., Loan, P., Habib, A., John, C. T., ... & Thelen, D. G. (2007). OpenSim: open-source software to create and analyze dynamic simulations of movement. *IEEE transactions on biomedical engineering*, *54*(11), 1940-1950.

Delp, S. L., Loan, J. P., Hoy, M. G., Zajac, F. E., Topp, E. L., & Rosen, J. M. (1990). An interactive graphics-based model of the lower extremity to study orthopaedic surgical procedures. *IEEE Transactions on Biomedical engineering*, *37*(8), 757-767.

Ding, Y., Galiana, I., Asbeck, A. T., De Rossi, S. M. M., Bae, J., Santos, T. R. T., ... & Walsh, C. (2017). Biomechanical and physiological evaluation of multi-joint assistance with soft exosuits. *IEEE Transactions on Neural Systems and Rehabilitation Engineering*, *25*(2), 119-130.

Donelan, J. M., Kram, R., & Kuo, A. D. (2002). Mechanical work for step-to-step transitions is a major determinant of the metabolic cost of human walking.*Journal of Experimental Biology*, *205*(23), 3717-3727.

Dumas, R., Cheze, L., & Verriest, J. P. (2007). Adjustments to McConville et al. and Young et al. body segment inertial parameters. *Journal of biomechanics*, *40*(3), 543-553.

Eisenberg, E. V. A. N., Hill, T. L., & Chen, Y. D. (1980). Cross-bridge model of muscle contraction. Quantitative analysis. *Biophysical Journal*, *29*(2), 195-227.

EOVest – ESA telerobotics. URL: http://www.esa-telerobotics.net/gallery/Research/Haptic-robots-design-development/EOVest/16 - Accessed on March 29, 2017.

Farris, D. J., Hicks, J. L., Delp, S. L., & Sawicki, G. S. (2014a). Musculoskeletal modelling deconstructs the paradoxical effects of elastic ankle exoskeletons on plantar-flexor mechanics and energetics during hopping. *Journal of Experimental Biology*, *217*(22), 4018-4028.

Farris, D. J., Sawicki, G. S. & Hicks, J. L. (2014b). Estimate muscle dynamics during locomotion with elastic exoskeletons. [Video file] URL: https://youtu.be/wyujqyVX8rU

First-Order Activation Dynamics. (n.d.) *Opensim Documentation* URL: http://simtk-confluence.stanford.edu:8080/display/OpenSim/First-Order+Activation+Dynamics

Gait 2392 and 2354 Models. (n.d.) *OpenSim Documentation* URL: http://simtk-confluence.stanford.edu:8080/display/OpenSim/Gait+2392+and+2354+Models

Gordon, K. E., & Ferris, D. P. (2007). Learning to walk with a robotic ankle exoskeleton. *Journal of biomechanics*, *40*(12), 2636-2644.

Grabowski, A. M. & Herr, H. M. (2009) Leg exoskeleton reduces the metabolic cost of human hopping. *Journal of Applied Physiology, 107(3),* 670-678

Grimmer, M., Quinlivan, B. T., Lee, S., Malcolm, P., Rossi, D. M., Siviy, C., & Walsh, C. J. (2017). Comparison of Ankle Moment Inspired and Ankle Positive Power Inspired Controllers for a Multi-Articular Soft Exosuit for Walking Assistance. In *Wearable Robotics: Challenges and Trends* (pp. 337-341). Springer International Publishing.

Hill, A. V. (1938). The heat of shortening and the dynamic constants of muscle. *Proceedings of the Royal Society of London B: Biological Sciences*, *126*(843), 136-195.

Hill, C. (2015). Wearables–the future of biometric technology?. *Biometric Technology Today*, *2015*(8), 5-9.

How Inverse Kinematics Works. (n.d.) *OpenSim Documentation* URL: http://simtk-confluence.stanford.edu:8080/display/OpenSim/How+Inverse+Kinematics+Works

Jackson, R. W., & Collins, S. H. (2015). An experimental comparison of the relative benefits of work and torque assistance in ankle exoskeletons. *Journal of Applied Physiology*, jap-01133.

Jackson, R. W., & Collins, S. H. (2017) Heuristic-based online adaptation of ankle exoskeleton assistance using plantarflexor electromyography. URL: http://biomechatronics.cit.cmu.edu/publications.html

Jackson, R. W., Dembia, C. L., Delp, S. L., & Collins, S. H. (2017). Muscle–tendon mechanics explain unexpected effects of exoskeleton assistance on metabolic rate during walking. *Journal of Experimental Biology*, *220*(11), 2082-2095.

Kao, P. C., Lewis, C. L., & Ferris, D. P. (2010). Invariant ankle moment patterns when walking with and without a robotic ankle exoskeleton. *Journal of biomechanics*, *43*(2), 203-209.

Kuo, A. D., Donelan, J. M., & Ruina, A. (2005). Energetic consequences of walking like an inverted pendulum: step-to-step transitions. *Exercise and sport sciences reviews*, *33*(2), 88-97.

Lee, S., Crea, S., Malcolm, P., Galiana, I., Asbeck, A., & Walsh, C. (2016, May). Controlling negative and positive power at the ankle with a soft exosuit. In *Robotics and Automation (ICRA), 2016 IEEE International Conference on* (pp. 3509-3515). IEEE.

Lichtwark, G. A., & Wilson, A. M. (2005). A modified Hill muscle model that predicts muscle power output and efficiency during sinusoidal length changes. *Journal of Experimental Biology*, *208*(15), 2831-2843.

Lichtwark, G. A., & Wilson, A. M. (2007). Is Achilles tendon compliance optimised for maximum muscle efficiency during locomotion?. *Journal of biomechanics*, *40*(8), 1768-1775. [Supplementary material]

Liu, J., Fu, T. M., Cheng, Z., Hong, G., Zhou, T., Jin, L., & Lieber, C. M. (2015). Syringe-injectable electronics. *Nature nanotechnology*.

Lockheed Martin (n.d.) – FORTIS exoskeleton. URL: http://www.lockheedmartin.com/us/products/exoskeleton/industrial.html - Accessed on March 28, 2017.

Malcolm, P., Derave, W., Galle, S., & De Clercq, D., (2013). A simple exoskeleton that assists plantarflexion can reduce the metabolic cost of human walking. PLoS One 2013, 8:e56137

Mallwitz, M., Will, N., Teiwes, J., & Kirchner, E. A. (2015). The CAPIO active upper body exoskeleton and its application for teleoperation. In *Proc. of the 13th Symp. on Advanced Space Technologies in Robotics and Automation (ASTRA-2015)*.

McMahon, T. A. (1984). *Muscles, reflexes, and locomotion*. Princeton University Press.

Meijneke, C., van Dijk, W., & van der Kooij, H. (2014, August). Achilles: an autonomous lightweight ankle exoskeleton to provide push-off power. In *Biomedical Robotics and Biomechatronics (2014 5th IEEE RAS & EMBS International Conference on* (pp. 918-923). IEEE.

Millard, M., Uchida, T., Seth, A., & Delp, S. L. (2013). Flexing computational muscle: modeling and simulation of musculotendon dynamics. *Journal of biomechanical engineering*, *135*(2), 021005.

Mooney, L. M., Rouse, E. J., & Herr, H. M. (2014a). Autonomous exoskeleton reduces metabolic cost of human walking during load carriage. *J. Neuroeng. Rehabil*, *11*(5), 80.

Mooney, L. M., Rouse, E. J., & Herr, H. M. (2014b). Autonomous exoskeleton reduces metabolic cost of human walking. *Journal of neuroengineering and rehabilitation*, *11*(1), 151.

Mosher, R. S. (1967). *Handyman to hardiman* (No. 670088). SAE Technical Paper.

Rose, J., & Gamble, J. G. (Eds.). (2006). *Human walking*. Philadelphia: Lippincott Williams & Wilkins.

Ryschon, T. W., Fowler, M. D., Wysong, R. E., Anthony, A. R., & Balaban, R. S. (1997). Efficiency of human skeletal muscle in vivo: comparison of isometric, concentric, and eccentric muscle action. *Journal of applied physiology*, *83*(3), 867-874.

Sankai, Y. (2011). HAL: Hybrid assistive limb based on cybernics. In *Robotics Research* (pp. 25-34). Springer Berlin Heidelberg.

Sawicki, G. S., & Ferris, D. P. (2008). Mechanics and energetics of level walking with powered ankle exoskeletons. *Journal of Experimental Biology*,*211*(9), 1402-1413.

SENIAM, 2016 URL: http://www.seniam.org/

Thelen 2003 Muscle Model (n.d.) *OpenSim Documentation* URL: http://simtk-confluence.stanford.edu:8080

/display/OpenSim/Thelen+2003+Muscle+Model
Thelen, D. G. (2003). Adjustment of muscle mechanics model parameters to simulate dynamic contractions in older adults. *Transactions-American Society Of Mechanical Engineers Journal Of Biomechanical Engineering*, *125*(1), 70-77.
Thelen, D., Seth, A., Anderson, F.C., & Delp, S.L. URL: http://simtk-confluence.stanford.edu:8080/display/OpenSim/Gait+2392+and+2354+models Accessed on April 24, 2017
Umberger, B. R., & Rubenson, J. (2011). Understanding muscle energetics in locomotion: new modeling and experimental approaches. *Exercise and sport sciences reviews*, *39*(2), 59-67.
van Dijk, W. (2015). Human-Exoskeleton Interaction (doctoral thesis). *Retrieved from TU Delft repository* (doi:10.4233/uuid:8cf37c65-a48c-476e-8dcc-eb97c06c26d9)
van Dijk, W., Meijneke, C., & van der Kooij, H. (2017). Evaluation of the Achilles ankle exoskeleton. *IEEE Transactions on Neural Systems and Rehabilitation Engineering*, *25*(2), 151-160.
Veneman, J. F., Kruidhof, R., Hekman, E. E., Ekkelenkamp, R., Van Asseldonk, E. H., & Van Der Kooij, H. (2007). Design and evaluation of the LOPES exoskeleton robot for interactive gait rehabilitation. *IEEE Transactions on Neural Systems and Rehabilitation Engineering*, *15*(3), 379-386.
Vukobratovic, M., Hristic, D., & Stojiljkovic, Z. (1974). Development of active anthropomorphic exoskeletons. *Medical and Biological Engineering*, *12*(1), 66-80.
Vukobratovic, M., Borovac, B., Surla, D., & Stokic, D. (2012). *Biped locomotion: dynamics, stability, control and application* (Vol. 7). Springer Science & Business Media.
Wehner, M., Quinlivan, B., Aubin, P. M., Martinez-Villalpando, E., Baumann, M., Stirling, L., & Walsh, C. (2013). A lightweight soft exosuit for gait assistance. In *Robotics and Automation (ICRA), 2013 IEEE International Conference on* (pp. 3362-3369). IEEE.
Winters, J. M. (1995). An improved muscle-reflex actuator for use in large-scale neuromusculoskeletal models. *Annals of biomedical engineering*, *23*(4), 359-374.
Woledge, R. C., Curtin, N. A., & Homsher, E. (1985). Energetic aspects of muscle contraction. *Monographs of the physiological society*, *41*, 1-357.
Yagn, N. (1890). Apparatus for facilitating walking, running, and jumping. U.S. Patents 420 179 and 438 830.
Zahalak, G. I., & Ma, S. P. (1990). Muscle activation and contraction: constitutive relations based directly on cross-bridge kinetics. *Journal of biomechanical engineering*, *112*(1), 52-62.
Zajac, F. E. (1989). Muscle and tendon Properties models scaling and application to biomechanics and motor. *Critical reviews in biomedical engineering*, *17*(4), 359-411.
Zhang, J., Fiers, P., Witte, K. A., Jackson, R. W., Poggensee, K. L., Atkeson, C. G., & Collins, S. H. (2017). Human-in-the-loop optimization of exoskeleton assistance during walking. *Science*, *356*(6344), 1280-1284.